

DIPLOMA THESIS

**Simulation and performance analysis of a solar domestic hot water system controlled by weather forecast information**

**Author:**

Thomas Koller

**Student number:**

3092317

**Supervising tutors:**

Prof. Dr. Sergio Colle

Prof. Dr.-Ing. habil. Dr. h.c. Rudolf Schilling

July 18, 2012



## Declaration

I hereby confirm that I have written the present thesis independently and without illicit assistance from third parties and using solely the aids mentioned.

Florianópolis, 12.07.2012

---

Place, Date



---

Thomas Koller

# Abstract

Brazil is one of the few countries in the world which extensively uses electric shower heads to heat water for bathing. The national electrical system SIN (Sistema Interligado Nacional) has to set aside about 4 GW to support the electric energy demand between 6 p.m. and 9 p.m. Electric showers cause 43 % of this energy peak. The main objective of this work is to develop a solar domestic hot water system (SDHWS) that can guarantee to flatten the energy peak by energy from a solar collector and additionally an auxiliary heater in a backup tank, which only heats in the morning depending on the expected solar radiation of the current day. The developed SDHWS is designed for low-income residential homes in Brazil. Researched in an experimental study, the profile of the average hot water demand is known. The SDHWS is designed with the software TRNSYS by using typical meteorological year (TMY) data, which is a one-year data set of hourly solar radiation information. A parameter sensitivity analysis is done to study the influence of the shower head temperature, the water supply temperature, the insulation thickness, the tank volumes and the orientation of the tanks. Weather forecast data are generated by using the present-day as a prediction for the next day. This procedure is validated by the calculation of an hourly and daily root mean square deviation and the analysis of the results of the simulation of the SDHWS. Thus the developed SDHWS is independent in the manner that it does not need any connection to a weather station. The potential to reduce the energy peak in the critical hours in the evening is analysed. The thermodynamic performance of the developed SDHWS is analysed for different cities in Brazil and for different consumers, i. e. for an overload against the average hot water demand. The payback time for different prices of the SDHWS is calculated by considering the savings of money that can be achieved. The calculations are done for the actual electricity tariff and the electricity tariff which is planned for January 2014. Finally, based on the simulation with TRNSYS, a research facility is designed in CATIA V5 to give an impulse for further research.

# Resumo

O Brasil é um dos poucos países do mundo onde os chuveiros elétricos são utilizados como principal equipamento para o aquecimento de água pra banho. Dados do Sistema Interligado Nacional - SIN estimam uma potência reservada da ordem de 4 GW para suprir a demanda de energia elétrica no horário de pico compreendido entre as 18:00 e 21:00 horas. Estima-se ainda que os chuveiros elétricos respondam por aproximadamente 43% desse pico. O principal objetivo deste trabalho é desenvolver um sistema de aquecimento solar de água doméstico (SASAD) que elimine a demanda elétrica dos chuveiros no horário de pico. Tal sistema é composto por um coletor solar com reservatório térmico acoplado e um reservatório auxiliar contendo uma resistência elétrica em seu interior, a qual somente é acionada nas primeiras horas da manhã, dependendo da previsão de radiação solar para o corrente dia. O perfil de demanda de água quente considerado foi obtido através de um estudo experimental de escala que monitorou o consumo de água quente de 90 famílias de baixa renda do Brasil. O desempenho térmico do sistema é avaliado utilizando o software TRNSYS como ferramenta computacional de simulação e dados climáticos horários no formato TMY (Typical Meteorological Year). É realizada uma análise de sensibilidade de parâmetros no sentido de investigar a influência da temperatura da água do banho, temperatura da água fornecida pela rede de abastecimento, espessura do isolamento térmico do reservatório, volume dos reservatórios e sua orientação. Os dados de previsão climática utilizados são gerados assumindo que os dados de um presente dia são válidos como previsão para o dia seguinte. Esse procedimento é validado calculando o RMSD (Root Mean Square Deviation) horário e diário, e analisando os resultados da simulação do SASAD. Com isso o SASAD dispensa qualquer ligação com uma estação meteorológica. Por conseguinte o potencial de redução da demanda elétrica no horário de pico é analisado. O desempenho térmico do SASAD é avaliado para diferentes cidades do Brasil e para diferentes consumos diários de água quente. O tempo de retorno do investimento é calculado para diferentes preços de SASAD, considerando como ganho no fluxo de caixa a economia financeira decorrente da utilização do sistema. Os cálculos são realizados utilizando uma base tarifária de energia elétrica vigente para o presente ano e também outra prevista para entrar em vigor somente em janeiro de 2014. Finalmente, com base nos resultados obtidos, a bancada experimental para validação do sistema é projetada utilizando o software CATIA V5.

# Contents

Table of Figures . . . . .	IX
Table of Tables . . . . .	X
Glossary . . . . .	XI
<b>1 Introduction</b>	<b>1</b>
<b>2 Solar energy in Brazil</b>	<b>3</b>
2.1 The electric energy matrix . . . . .	4
2.2 Peak-hour problem . . . . .	5
2.2.1 Electric showers . . . . .	5
2.2.2 Load curve . . . . .	6
2.3 Solar energy potential and market development in Brazil . . . . .	8
2.3.1 Solar energy potential . . . . .	8
2.3.2 Market development . . . . .	9
<b>3 Theory</b>	<b>10</b>
3.1 Solar radiation . . . . .	10
3.1.1 Extraterrestrial solar irradiance . . . . .	10
3.1.2 Terrestrial solar irradiance . . . . .	11
3.1.3 Definitions . . . . .	12
3.2 Typical Meteorological Year (TMY) data . . . . .	13
3.3 Sky models . . . . .	13
3.3.1 Isotropic sky model . . . . .	13
3.3.2 Hay and Davis model . . . . .	14
3.3.3 Reindl model . . . . .	14
3.3.4 Perez model . . . . .	14
3.4 Flat plate collectors . . . . .	15
3.4.1 Efficiency curve . . . . .	16
3.4.2 Energy gain . . . . .	19
<b>4 Design of the solar domestic hot water system</b>	<b>20</b>
4.1 Basic description of the system . . . . .	20
4.2 The TRYNSYS Model . . . . .	21
4.2.1 Collector and tank . . . . .	22
4.2.2 Backup tank with heater and pump . . . . .	27
4.2.3 Hot water demand . . . . .	28

4.2.4	Definition of the solar fraction . . . . .	29
4.3	Algorithm to cut the energy peak . . . . .	29
4.4	Parameter sensitivity analysis . . . . .	32
4.4.1	Shower head temperature . . . . .	32
4.4.2	Water supply temperature . . . . .	33
4.4.3	Insulation thickness . . . . .	34
4.4.4	Tank volumes . . . . .	35
4.4.5	Orientation of the collector tank . . . . .	36
4.5	Weather forecast information . . . . .	37
4.5.1	Generation of weather forecast information . . . . .	37
4.5.2	Prediction uncertainties of the generated weather data . . . . .	38
<b>5</b>	<b>Results of the designed solar domestic hot water system</b>	<b>40</b>
5.1	Peak reduction . . . . .	40
5.2	Results for different consumers . . . . .	41
5.3	Results for different cities in Brazil . . . . .	46
5.4	The designed research facility . . . . .	50
5.5	Costing . . . . .	51
<b>6</b>	<b>Conclusion</b>	<b>54</b>
	<b>Bibliography</b>	<b>56</b>
<b>A</b>	<b>Parameters and dimensions of the developed SDHWS</b>	<b>58</b>
<b>B</b>	<b>TMY Typical Meteorological Year</b>	<b>61</b>
<b>C</b>	<b>Translation of Portuguese words used in this work</b>	<b>62</b>
<b>D</b>	<b>Technical drawing of the designed research facility</b>	<b>63</b>
D.1	Assembly . . . . .	63
D.2	L-parts . . . . .	68
D.3	Brackets . . . . .	80

# List of Figures

2.1	Annual average global horizontal solar radiation in Brazil [1412]. . . . .	3
2.2	Electric energy matrix of Brazil in the year 2010 [310]. . . . .	4
2.3	Typical Brazilian electric shower head. . . . .	5
2.4	The daily electric energy load curve of the residential sector in Brazil [708]. . . . .	7
2.5	Load curve for a typical day and a day when the Brazilian national team was playing football [CS10]. . . . .	8
2.6	Development of the installed SDHWS in Brazil [808]. . . . .	9
3.1	Cross section of the sun [Spi11]. . . . .	10
3.2	Solar spectrum of a blackbody and sunlight outside the atmosphere and at sea level [Spi11]. . . . .	12
3.3	Sketch of a typical glazed flat plate collector [1012]. . . . .	16
3.4	Normalized efficiency curves for different types of flat plate collectors. . . . .	18
4.1	Flowchart of the simulated SDHWS. . . . .	21
4.2	TRYNSYS model of the developed SDHWS. . . . .	22
4.3	Schematic view of the thermosiphon loop [Duf11]. . . . .	23
4.4	Concept of the plug-flow tank [Duf11]. . . . .	25
4.5	Distribution of the hot water demand per day [Sal04]. . . . .	29
4.6	Steps to calculate the minimal necessary backup tank set temperature $T_{set}$ . . . . .	31
4.7	Annual average solar fraction $\bar{f}_{sol}$ over different volume ratios $\chi$ for three simulated cases. . . . .	36
4.8	Results of a solar radiation forecast without uncertainties and a forecast by using the radiation of the present-day as a forecast for the next day. . . . .	38
5.1	Annual average peak energy reduction $\bar{P}_{red}$ and annual average solar fraction $\bar{f}_{sol}$ for different minimal admissible backup tank temperatures $T_{min,ad}$ . . . . .	41
5.2	Monthly average peak energy reduction $\bar{P}_{red,month}$ for different percentage of overloads $\Delta m$ . . . . .	42
5.3	Annual average solar fraction $\bar{f}_{sol}$ and annual average peak energy reduction $\bar{P}_{red}$ for different overloads $\Delta m$ of the developed SDHWS. . . . .	43
5.4	Annual average solar fraction $\bar{f}_{sol,ref}$ and annual average peak energy reduction $\bar{P}_{red,ref}$ for different overloads $\Delta m$ for the reference solar energy system. . . . .	44
5.5	Year fraction $y_o$ over energy fraction $x_o$ for different overloads $\Delta m$ of the developed SDHWS. . . . .	45

5.6	Year fraction $y_o$ over energy fraction $x_o$ for different overloads $\Delta m$ of the reference solar energy system. . . . .	46
5.7	Locations of the analyzed cities. . . . .	47
5.8	Annual average solar fraction $\overline{f}_{sol}$ of the same SDHWS for different cities. . . . .	49
5.9	Designed research facility. . . . .	50
5.10	Payback time for different initial costs. . . . .	52
B.1	Cutout of one day of a TMY text file . . . . .	61

# List of Tables

4.1	Analyzed parameters. . . . .	32
4.2	Comparison of three different shower head temperatures. . . . .	33
4.3	Thermodynamic performance of the SDHWS for four different water supply temperatures. . . . .	34
4.4	Comparison of three different insulation thicknesses. . . . .	35
5.1	Solar and auxiliary energy for different overloads . . . . .	43
5.2	Data and results of the analyzed cities. . . . .	48
A.1	Parameters of the solar collector and the collector tank. . . . .	58
A.2	Dimensions of the solar collector and the collector tank. . . . .	59
A.3	Parameters of the backup tank, the continuous-flow water heater and the pump of the heating loop. . . . .	60

# Glossary

## Latin letters

$A$	Area [ $m^2$ ]
$AM$	Air mass [-]
$\bar{C}$	Annual cost [ $R\$$ ]
$c_p$	Specific heat [ $\frac{kJ}{kgK}$ ]
$D$	Diameter [ $m$ ]
$E$	Energy [ $kJ$ ]
$ET$	Electricity tariff [ $R\$$ ]
$e$	Insulation thickness [ $m$ ]
$ex$	Specific exergy [ $\frac{kJ}{kg}$ ]
$F_R$	Heat removal factor [-]
$F_R(\tau\alpha)$	Intercept efficiency [-]
$f_{sol}$	Solar fraction [%]
$\bar{f}_{sol}$	Annual average solar fraction [%]
$g$	Gravitational constant [ $\frac{m^3}{kg s^2}$ ]
$h$	Height [ $m$ ]
$I$	Total incident solar radiation [ $\frac{W}{m^2}$ ]
$IC$	Initial cost [ $R\$$ ]
$IR$	Interest rate [ $R\$$ ]
$i$	Node [-]
$k$	Thermal conductivity [ $\frac{W}{mK}$ ]
$L$	Length [ $m$ ]
$\dot{M}$	Flowrate per unit area [ $\frac{kg}{m^2}$ ]
$m$	Mass [ $kg$ ]
$\dot{m}$	Mass flux [ $\frac{kg}{s}$ ]
$\Delta m$	Overload [%]
$N$	Number of segments [-]
$N_x$	Number of collector nodes [-]
$n$	Refractive index [-]
$P$	Pressure [ $Pa$ ]
$PT$	Payback time [ $a$ ]
$P_{red}$	Peak energy reduction [%]
$\bar{P}_{red}$	Annual average peak energy reduction [%]
$\bar{P}_{red,month}$	Monthly average peak energy reduction [%]

$Q$	Energy [ $kJ$ ]
$r$	Radius [ $m$ ]
$S_h$	Sunshine hours [-]
$\bar{S}$	Annual saving [ $R\$$ ]
$T$	Temperature [ $^{\circ}C$ ]
$t$	Simulation timestep [ $s$ ]
$U$	Overall energy loss coefficient [ $\frac{W}{m^2K}$ ]
$V$	Volume [ $m^3$ ]
$w_t$	Specific technical work [ $\frac{kJ}{kg}$ ]

## Greek letters

$\alpha$	Absorption coefficient [-]
$\beta$	Collector slope [ $^{\circ}$ ]
$\zeta$	Dimensionless size parameter [-]
$\eta$	Collector efficiency [-]
$\theta$	Incident angle of collector surface [ $^{\circ}$ ]
$\theta_z$	Zenith angle [ $^{\circ}$ ]
$\lambda$	Wavelength [ $\mu m$ ]
$\xi$	Friction head loss [-]
$\rho$	Density [ $\frac{kJ}{kg}$ ]
$\tau$	Transmission coefficient [-]
$\chi$	Volume ratio [-]

## Indices

<i>abs</i>	Absorber plate
<i>ad</i>	Admissible
<i>amb</i>	Ambient
<i>aux</i>	Auxiliary
<i>avg</i>	Average
<i>b</i>	Backup tank
<i>bm</i>	Beam radiation
<i>bottom</i>	Bottom of tank
<i>c</i>	Collector
<i>cold</i>	Water reservoir
<i>d</i>	Diffuse radiation
<i>elec</i>	Electric energy
$H_2O$	Water
<i>h</i>	Horizontal plane
<i>heat</i>	Heat
<i>in</i>	Incident radiation

<i>in</i>	Inlet
<i>ins</i>	Insulation
<i>L</i>	Losses
<i>load</i>	Load
<i>loop</i>	Backup heating loop
<i>m</i>	Mean
<i>max</i>	Maximum
<i>min</i>	Minimal
<i>n</i>	Normal surface to sun direction
<i>new</i>	New calculated
<i>o</i>	Extraterrestrial radiation
<i>out</i>	Outlet
<i>PUR</i>	Polyurethane hard foam
<i>p</i>	Pipe
<i>peak</i>	Peak hours
<i>r</i>	Return
<i>ref</i>	Reference
<i>replace</i>	Replacement
<i>set</i>	Set point
<i>sh</i>	Shower head
<i>sol</i>	Solar
<i>sup</i>	Supplied
<i>sur</i>	Surface
<i>T</i>	Tilted surface
<i>test</i>	Test conditions
<i>top</i>	Top of tank
<i>u</i>	Useful
<i>4h</i>	4 a.m.

# 1 Introduction

We live in a world where energy for our sakes became a matter of course. From the radio alarm in the morning and the ride to the fully air-conditioned office to switching off the bedside lamp in the evening, we constantly use technical equipment, which consumes energy. High-tech products evolve so rapidly that even the most enthused technology fan needs to invest much time to stay up-to-date. Smartphones, permanent internet connection and talking cars are taken for granted. The statement that we live in a highly developed society is obvious. But where comes the energy from that makes us all these tremendous advances? For the most part, we deplete the earth to generate energy, we burn coal, which was millions of years in the earth, we pump oil with a huge effort from huge depths in order to burn it and we create high-level radioactive waste for which we do not have any disposal sites. Only when the majority of our energy consumption, the foundation of our technological developments, is generated from the use of renewable energy sources, we are a highly developed society.

The present diploma thesis is the study of a solar domestic hot water system (SDHWS) which was done in a cooperation of the TUM (Technische Universität München) and the UFSC (Universidade Federal de Santa Catarina). The project was carried out by LEPTEN (Laboratórios de Engenharia de Processos de Conversão e Tecnologia de Energia) in the Lab-solar (Laboratório de Energia Solar) in Brazil. The research concerns of LEPTEN are solar energy, heat pipe, boiling heat transfer, energy conversion process, ethanol plants, petro-chemistry and wind energy. The heat pipe laboratory was founded in the frame of an international cooperation project by the German BMFT (Bundesministerium für Forschung und Technologie) and the Brazilian CNPq (Conselho Nacional de Desenvolvimento Científico e Tecnológico) with scientific support provided by Prof. Dr. Manfred Groll (IKE Institut für Kernenergetik und Energiesysteme/Universität Stuttgart) and Prof. Dr. Sergio Colle (Departamento de Engenharia Mecânica/UFSC). The solar energy laboratory was also founded in the frame of the German BMFT and the Brazilian CNPq with the scientific support provided by Prof. Dr. Erhard Raschke (IGMK Institut für Geophysik und Meteorologie/Universität zu Köln), Dr. Fritz Karsten (DWD Deutscher Wetterdienst Hamburg), Dr. Klaus Dehne (DWD Deutscher Wetterdienst Hamburg) and Prof. Dr. Sergio Colle (Departamento de Engenharia Mecânica/UFSC). Since the foundation of LEPTEN many professors and exchange students, supported by the DAAD (Deutscher Akademischer Austausch Dienst), are doing research in cooperation with LEPTEN and German universities. At this point I would like to encourage all students to strengthen the partnership between Brazil and Germany in the context of an exchange program.

The present work gives an overview of the solar energy potential in Brazil and how solar energy is integrated in the energy matrix until today. The electric load curve has a significant peak between 6 p.m. and 9 p.m. caused by the intensive use of electric shower heads, which requires to set aside about 4 GW just to provide enough energy during the peak hours. With a focus on this issue, meaning to avoid the use of electric energy during the peak hours, an intelligent SDHWS is developed in this work. The SDHWS is simulated with the software TRNSYS using typical meteorological year (TMY) data to obtain annual results of the thermodynamic performance. A parameter sensitivity analysis is done to optimize the thermodynamic performance of the SDHWS.

## 2 Solar energy in Brazil

Brazil is a country almost as big as Europe, but the population is about three times less than in Europe. The annual average global solar radiation is about twice as high as in Germany. The cities north of São Paulo have an annual solar radiation of about  $1800 \frac{kWh}{m^2a}$  up to more than  $2000 \frac{kWh}{m^2a}$ . Besides the high solar radiation, Brazil has a lot of space to install solar power plants. Figure 2.1 shows the annual average global solar radiation in Brazil.

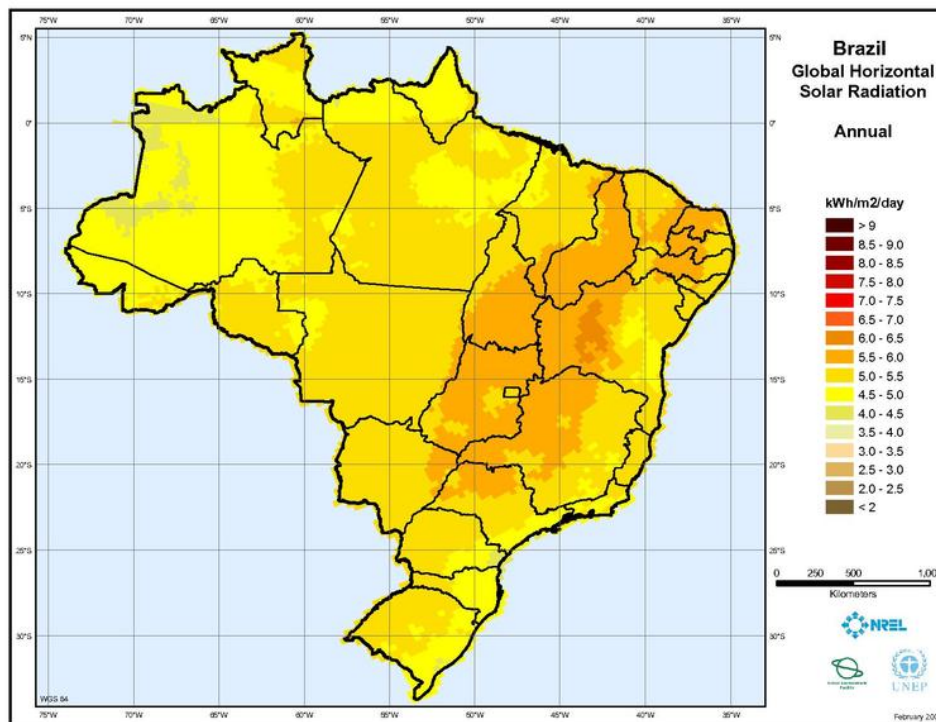


Figure 2.1: Annual average global horizontal solar radiation in Brazil [1412].

Caused by the high humidity in the coastal region, the solar radiation is lower there. The highest solar radiation appears in the countryside of Brazil, because the climate is very dry, so there is almost no absorption or scattering of the incident solar radiation. The fact that the countryside is scarcely populated and has the highest solar radiation leads to an optimal location for installing solar power plants.

The SDHWS developed in this work could be installed in any part of Brazil. The dimensioning is done for the city of Florianópolis in the state of Santa Catarina, which is in the south of Brazil. There the solar radiation is one of the lowest in the whole country and the

variation of the weather is one of the highest. In fact this weather scenario can be considered as a worst-case example.

### 2.1 The electric energy matrix

Brazil is a country which is already using many different renewable energy sources. The main energy source in Brazil is hydropower. Hydropower plants work without carbon dioxide emissions, but the potential for building new plants is limited. A huge amount of water has to be dammed up to build a new hydropower plant. This is a big human intervention in the nature and the people living in the affected region have to move away. In fact, it is quite difficult to get a concession to build a new hydropower plant. Nevertheless Brazil's electrical energy mainly comes from hydropower. Figure 2.2 shows the electric energy matrix of Brazil.

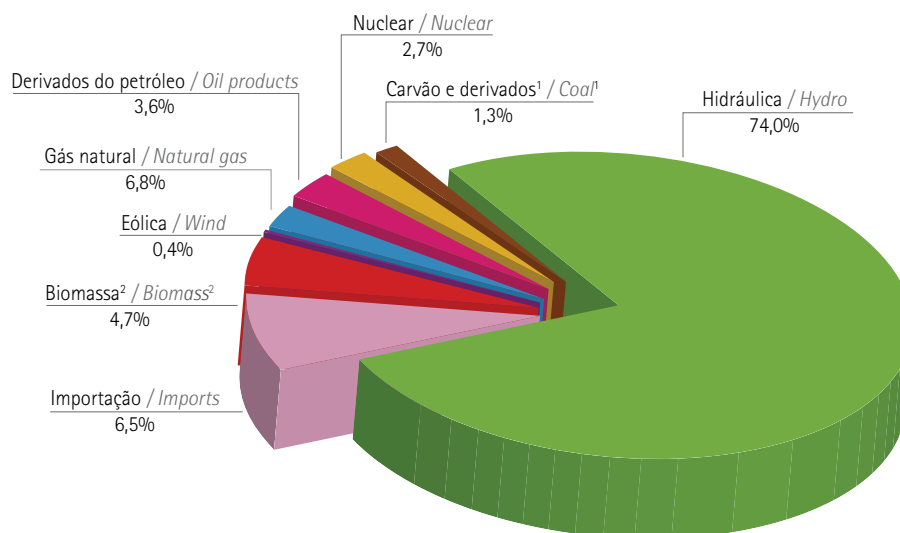


Figure 2.2: Electric energy matrix of Brazil in the year 2010 [310].

At the moment, Brazil does not use photovoltaic systems and almost no coal to produce electric energy, which is a big difference to the German energy matrix. Besides hydropower, Brazil is using even more renewable sources like wind and biomass. The energy matrix mainly consists of renewable sources, which is ideal. Due to the economic expansion, the energy demand of the country is growing. For this reason it will be necessary to provide more energy in the future. SDHWS can make a large contribution to the electric energy matrix. Subchapter 2.2 exhibits how SDHWS influence the electric energy matrix.

## 2.2 Peak-hour problem

### 2.2.1 Electric showers

The climate all over the country is warm throughout the whole year, which is why Brazilian houses do not have heating systems. There is no warm water circuit in Brazilian houses. Electric showers began to spread in Brazil in the 70's, caused by the oil crisis and the promotion of the use of electric equipments. During this time, Brazil started to construct hydroelectric power plants. Figure 2.3 shows a typical Brazilian electric shower head.



Figure 2.3: Typical Brazilian electric shower head.

The efficiency of the electric shower to convert electric energy to heat energy is nearly 100 %. Electricity is a very noble energy, its working capacity is 100 %. Thermodynamically speaking this means that it consists only of exergy. Water with a temperature of 39 °C has a very low working capacity. Its energy consists mainly of anergy, because the temperature difference to the environment, which is the working capacity, is low. The following calculations aim at obtaining a statement about the exergy losses of heating water with an electric shower head.

The calculations are the application of the second law of thermodynamics on energy conversions. The specific physical exergy  $ex$  of water with 39 °C is

$$ex = c_p \left[ T_{sh} - T_{amb} - T_{amb} \ln \left( \frac{T_{sh}}{T_{amb}} \right) \right] = 2.47 \frac{kJ}{kg} \quad (2.1)$$

The electric shower head can be considered as an adiabatic control room, where water is heated from 20 °C to 39 °C. The specific exergy loss  $ex_L$  of this heating process is

$$ex_L = T_{amb} \cdot c_p \ln \left( \frac{T_{sh}}{T_{amb}} \right) = 77.14 \frac{kJ}{kg} \quad (2.2)$$

The electric energy, which is supplied to the control room, is only exergy. According to the first law of thermodynamics, this specific technical work  $w_t$  is

$$w_t = c_p(T_{sh} - T_{amb}) = 79.61 \frac{kJ}{kg} \quad (2.3)$$

From these equations it can be concluded, that only

$$\frac{ex}{w_t} = 3\% \quad (2.4)$$

of the total supplied exergy is used to higher the exergy of the water, which means that an electric shower is a highly irreversible process. The following two irreversible processes are the reason for the exergy losses:

- The electric heating of the heating wire (Dissipative losses)
- Heat transfer from the hot heating wire to the cold water (Heat transfer with temperature difference)

An electric shower is a simple technical device which costs about US\$ 25 to US\$ 30 but the thermodynamic process is very bad, because nearly all the working capacity of the electric energy gets lost. There is no way to improve an electric shower. The only way to reduce the exergy loss while heating water is to use another technical device that is based on another thermodynamic process [BH09].

### 2.2.2 Load curve

There are about 30 Million electric showers installed in Brazil. They need a lot of electric energy, so they have a big influence on the energy demand. Figure 2.4 shows the typical, daily energy load curve in Brazil divided by consumers.

## 2.2 PEAK-HOUR PROBLEM

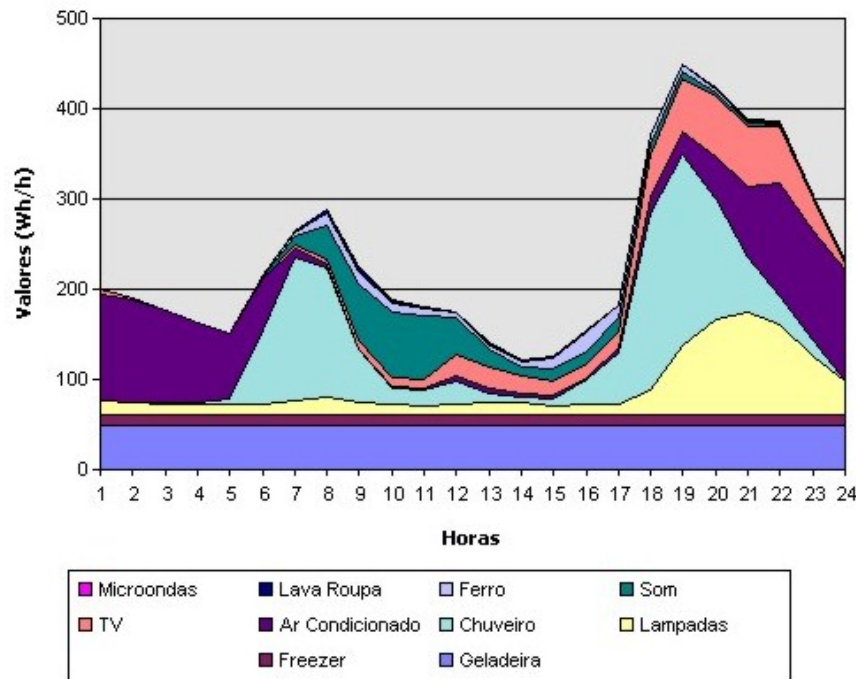


Figure 2.4: The daily electric energy load curve of the residential sector in Brazil [708].

There is an energy peak from 6 p.m. to 9 p.m. in the load curve. The analysis to gain this figure was done by the Brazilian company Eletrobras, hence the graphic is only available in Portuguese. Appendix C exhibits the translation of the Portuguese words in this figure. The energy peak is mainly induced by the electric showers (pt. chuveiros) because they consume 43 % of the electric energy needed during the peak hours. Brazilians like to take a hot shower when they come home from work. Due to the fact that closing times are similar everywhere, everybody takes a shower at the same time.

Figure 2.5 shows the energy demand for a regular day (06.06.2006) and the day when Brazil played against Croatia in the Football World Cup (13.06.2006). When the Brazilian national team plays football, employees are exempt from work. The graph (13.06.2006) shows that the energy demand during the peak hours from 6 p.m. to 9 p.m. decreased, because the employees came back from work earlier than usually and took a shower before the football game. The minimized peak exhibits that the energy during the peak hours of a regular day is caused largely by electric showers. The energy peak is a big problem for the grid stability, which is why it is important to find a solution to reduce the peak. Furthermore the national electrical system SIN (Sistema Interligado Nacional) has to set aside about 4 GW to support the electric energy for the peak hours.

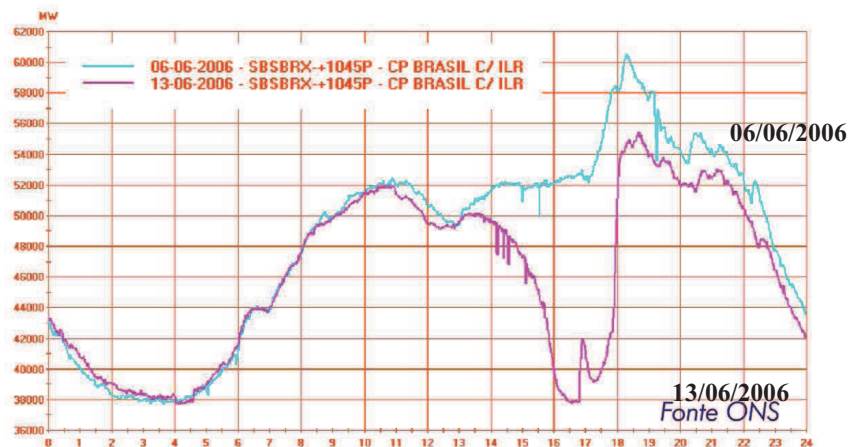


Figure 2.5: Load curve for a typical day and a day when the Brazilian national team was playing football [CS10].

## 2.3 Solar energy potential and market development in Brazil

### 2.3.1 Solar energy potential

The potential how much solar energy could be used with respect to the incident solar radiation is already shown in figure 2.1. Though, in this subsection potential means the possibility of using solar heaters by substituting the actual installed electrical showers in the residential sector.

The total amount of consumed electricity in Brazil was 509.2 TWh in the year 2010 [310]. This energy is divided into three sectors, the industrial sector, the residential sector and the commercial sector in which the residential sector is the second biggest. 24 % of the total amount of energy is consumed in the residential sector. The electric consumers are seen in figure 2.4. The electric showers consume 26 % of the total amount of energy of the residential sector. Finally this shows that about 6 % of the total electric energy consumed in Brazil is consumed by electric showers. This is equal to 30.55 TWh per year. In 2008 the installed solar energy was 650 GWh. This is only 2.1 % of the total energy consumed by electric showers.

According to a study of ABRAVA (Associação Brasileira de Refrigeração, Ar condicionado, Ventilação e Aquecimento) [808], the electric showers of a typical residential home consume 145 MWh per month. Hence the installed solar energy of 650 GWh is equal to 375.000 residential homes. Compared to the total amount of electric energy, consumed by electric showers, this leads to the theoretical possibility to install more than 17 million SDHWS just by substituting the electric showers. This calculation does not consider any selling conditions. It just shows the fundamental potential of installing SDHWS in Brazil.

### 2.3.2 Market development

The Brazilian solar market is still in its early stages, however it is developing positively. The new installed area of solar panels increases every year. Figure 2.6 shows the development of the new installed area and the accumulated area of solar collectors from the year 2001 to 2009.

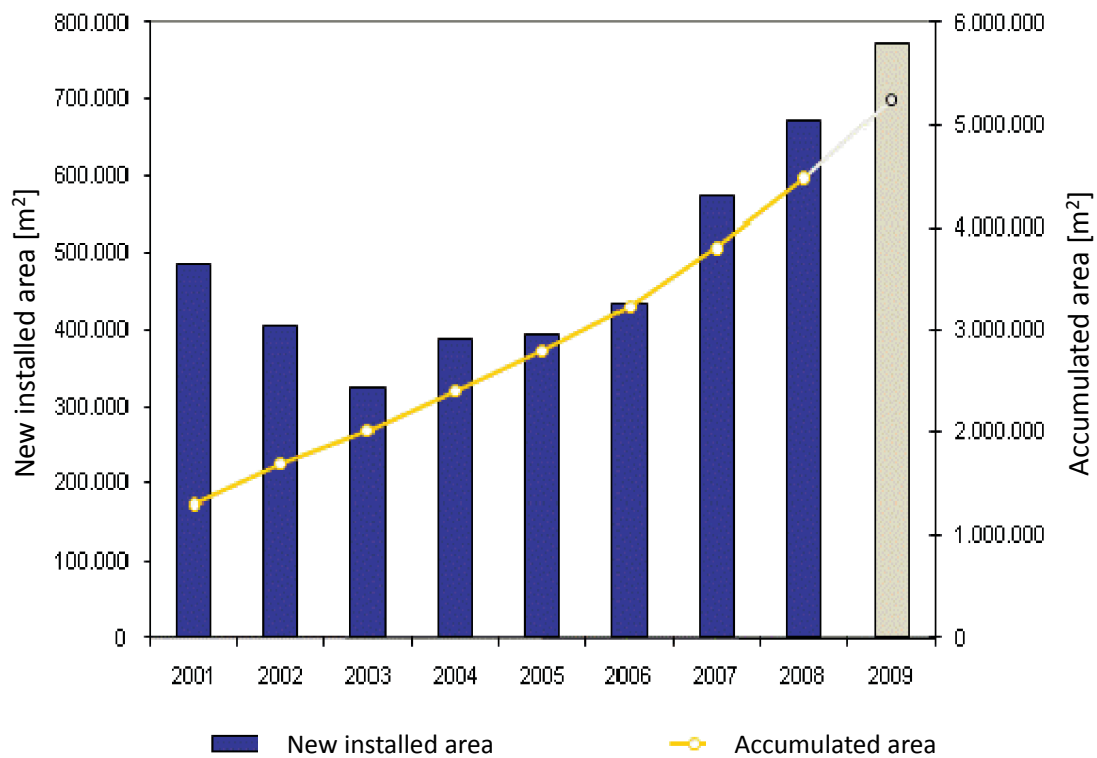


Figure 2.6: Development of the installed SDHWS in Brazil [808].

The increasing environmental awareness of the Brazilian population and the rising energy prices enhance the positive market development, although until today the main part of the SDHWS is installed in houses in the south of Brazil, because there the population is wealthier and therefore able to afford the investment to buy a SDHWS. The increase of the electricity tariff during the peak hours in January 2014 (section 5.5) will also support the positive development, because the annual saving of money due to the use of a SDHWS is becoming higher and the payback time becomes shorter. In addition, the increased demand of SDHWS lowers the price, which causes that more and more people are able to buy a SDHWS. Brazil is a huge country with about 200 million citizens. The theoretical potential to install a lot more SDHWS is enormous. Now it depends on the government, to support this development and on the companies to offer affordable SDHWS. The SDHWS has to be of a good quality and reliability, therefore it is important that universities do research in this area and exhibit the technical possibilities of the use of solar energy systems.

# 3 Theory

## 3.1 Solar radiation

The sun is the source of all radiation which reaches the earth. Its structure and characteristics determine the intensity and the spectral distribution. Figure 3.1 shows the cross section of the sun with the most important effects and types of radiation, also including rounded values of the core temperature, surface temperature and energy rate.

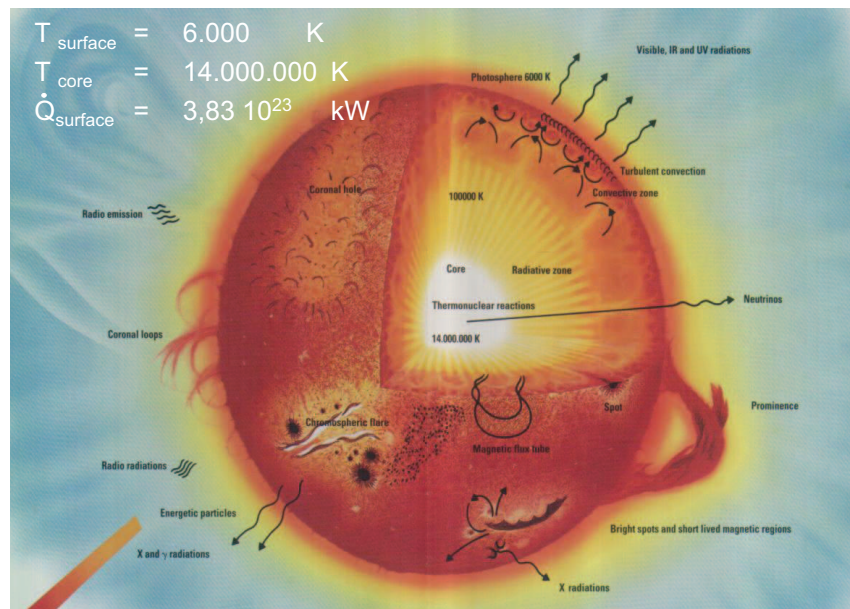


Figure 3.1: Cross section of the sun [Spi11].

The enormous energy is produced by thermonuclear reactions in the core. The average distance to the earth is  $150 \cdot 10^6$  km. Based on the light speed the radiation takes about eight minutes to arrive at the earth.

### 3.1.1 Extraterrestrial solar irradiance

Extraterrestrial solar radiation is the radiation outside the earth atmosphere. Due to the vacuum in outer space, the solar radiation can propagate there without any absorption or scattering. The solar constant is the energy rate per unit square meter of solar radiation arriving outside the atmosphere on an area perpendicular to the direction of the propagation direction. In the past, many measurements were done from balloons, aircrafts and spacecrafts to get the

most accurate value for the solar constant. Nowadays the World Radiation Center (WRC) accepts a value of  $1367 \frac{W}{m^2}$ . Due to the variation of the earth to sun distance and of the intensity of the sun the solar constant is not really a constant, but an average value with an uncertainty of about 1 % [DJ06].

#### 3.1.2 Terrestrial solar irradiance

Once the radiation enters the atmosphere, there are many different mechanisms which decrease the intensity of the solar irradiance. The short wave radiation is absorbed by  $O_2$  and  $O_3$  molecules, meanwhile the long wave radiation is absorbed by  $H_2O$  and  $CO_2$ . In consideration of designing a solar energy system, these effects reduce the usable solar radiation on the earth.

Besides the absorption of the solar radiation, there are two types of important scattering effects. The occurring scattering effect depends on the size of the particles in the air. The dimensionless size parameter  $\zeta$  is

$$\zeta = \frac{2\pi r}{\Lambda} \quad (3.1)$$

with the relative scattering wavelength  $\Lambda$ :

$$\Lambda = \frac{\Lambda_{in}}{n} \quad (3.2)$$

where  $\Lambda_{in}$  is the wavelength of the incident sunlight and  $n$  is the refractive index of the surrounding medium. Now the range of validity just depends of the dimensionless size parameter

- Rayleigh scattering theory ( $\zeta \ll 1$ )
- Mie scattering theory

Rayleigh scattering is a quasi-isotropic scattering, which occurs at non-absorbing, small and spherical particles. Mie scattering arises to non-absorbing and absorbing particles. In addition to the chemical properties, smaller particles scatter isotropically, while bigger particles scatter anisotropically. All absorptions and scattering phenomena described herein lead to a decrease of the solar radiation in the propagating direction, which can be characterized with the extinctions coefficient. The extinctions coefficient, which describes the attenuation of the solar radiation per unit meter in the direction of the solar light, is the sum of the attenuation through scattering and absorption. Knowing the value of the extinctions coefficient, it is possible to calculate the attenuation of the solar radiation per unit length.

Figure 3.2 shows the distribution of different spectra over the wavelength, including the blackbody spectrum at 5250 °C, the sunlight at the top of the atmosphere and the radiation at sea level.

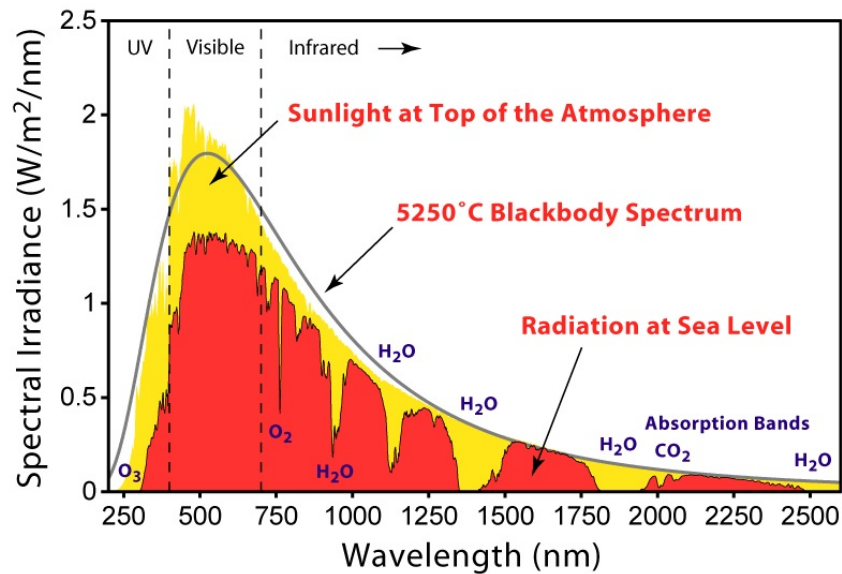


Figure 3.2: Solar spectrum of a blackbody and sunlight outside the atmosphere and at sea level [Spi11].

The sunlight at the top of the atmosphere has nearly the same spectrum as a blackbody at 5250 °C. The sun is often assumed to be a blackbody, in order to describe solar radiation theories and to do calculations. The solar radiation at sea level is different to the blackbody spectrum. Due to scattering and absorption, the spectral irradiance at certain wavelengths is reduced. The radiation absorbed around a wavelength of 1500 nm is the absorption due to the molecule  $CO_2$ . The absorption and reemission of this molecule at different wavelengths is one reason for the greenhouse effect.

### 3.1.3 Definitions

#### Beam radiation

Beam radiation  $I_{h,bm}$ , also called direct radiation, is the amount of electromagnetic radiation which passes through the atmosphere without any scattering or absorbing coming from the direction of the sun. The radiation is directed and short-wave.

#### Diffuse radiation

Diffuse radiation  $I_{h,d}$  is scattered or reflected electromagnetic radiation coming from the whole half space with a preferred direction from the sun. It is short-wave radiation.

#### Global radiation

Global radiation  $I_h$  is the sum of beam and diffuse radiation on a horizontal plane. It is short-wave radiation which is partly directed and undirected.

## 3.2 Typical Meteorological Year (TMY) data

TMY data are the basis of the simulation of the SDHWS. These data are representative for a local solar climate, e. g. Florianópolis. The data used are from the Solar and Wind Energy Resource Assessment (SWERA). Meteorological observations are done over many years for the region of interest. Just taking the yearly average of the data does not take into account the variability of the climate, hence another procedure is necessary. Thus, the monthly average radiation for each month is calculated as well as the average radiation of each month over the recorded period. Now the data for the month with a monthly average radiation that comes closest to the average of the recorded period is chosen as the TMY data for that month. This is repeated for each month and finally the months are added together to have a one-year sample of hourly data.

The big advantage of this procedure is that these data are real data with variability and not data that are processed or smoothed to generate an average climate data file. Appendix B exhibits a cutout of the used TMY text data file for Florianópolis. The TMY data are arranged by month, day and hour, which are the first three columns. Columns four to seven contain the solar radiation data in  $\frac{Wh}{m^2}$ , the global solar irradiance on a horizontal plane, the beam solar irradiance on a horizontal plane, the diffuse solar irradiance on a horizontal plane and the extraterrestrial solar irradiance on a horizontal plane. The last two columns contain the ambient temperature and the relative humidity.

## 3.3 Sky models

Sky models aim at computing the solar radiation on a tilted surface  $I_T$ , based on data of the solar radiation on a horizontal surface. The total solar irradiance is divided in beam and diffuse radiation, in which the beam radiation is modeled equal and the diffuse part makes the difference of the models discussed in the following.

For a given location (longitude, latitude) and a given time (date, time) the beam radiation on a tilted surface  $I_{T,bm}$  can be computed by geometrical relationships. The diffuse radiation on a tilted surface  $I_{T,d}$  is composed of an isotropic diffuse component, circumsolar diffuse component, horizon brightening component and a reflected component [LP06].

### 3.3.1 Isotropic sky model

The isotropic sky model is the simplest model. It assumes that the diffuse radiation is uniformly distributed over the half space and the ground reflection is diffuse. The circumsolar and the horizon brightening components are neglected. According to this model, the solar radiation on a tilted surface is

$$I_T = I_{h,bm}R_b + I_{h,d} \left( \frac{1 + \cos \beta}{2} \right) + I_h \rho \left( \frac{1 - \cos \beta}{2} \right) \quad (3.3)$$

where  $R_b$  is a geometric factor which takes into account the ratio of beam radiation on the horizontal surface and the tilted surface.

### 3.3.2 Hay and Davis model

The Hay and Davis model splits the diffuse radiation from the sky in isotropic diffuse radiation and circumsolar diffuse radiation, while the horizon brightening component is still assumed to be zero. Therefore, this model is more accurate than the isotropic one. The reflection from the ground is treated in the same way as in the isotropic sky model. According to this model, the solar radiation on a tilted surface is

$$I_T = (I_{h,bm} + I_{h,d}A)R_b + I_{h,d}(1 - A) \left( \frac{1 + \cos \beta}{2} \right) + I_h \rho \left( \frac{1 - \cos \beta}{2} \right) \quad (3.4)$$

where  $A$  is the anisotropy index, which is used to quantify the ratio of circumsolar diffuse radiation and isotropic diffuse radiation.  $A$  is the ratio of the direct extraterrestrial normal irradiance  $I_{bn}$  and the direct-normal solar irradiance  $I_{on}$ :

$$A = \frac{I_{bn}}{I_{on}} \quad (3.5)$$

### 3.3.3 Reindl model

The Reindl model is similar to the Hay and Davis model, though it also takes into account the horizon brightening component, hence the calculated diffuse radiation is slightly higher. The anisotropy index  $A$  is used in the same way as in the Hay and Davis model. According to this model, the solar radiation on a tilted surface is

$$I_T = (I_{h,bm} + I_{h,d}A)R_b + I_{h,d}(1 - A) \left( \frac{1 + \cos \beta}{2} \right) \cdot \left( 1 + \sqrt{\frac{I_{h,bm}}{I_h}} \sin^3 \left( \frac{\beta}{2} \right) \right) + I_h \rho \left( \frac{1 - \cos \beta}{2} \right) \quad (3.6)$$

### 3.3.4 Perez model

The Perez model is the most complex model. It takes more computational power to solve the equations but the result is the most accurate. Except for the reflected component, the other three components are calculated by using empirical coefficients. Therefore, to obtain the most precise results, this model should be favored. According to this model, the solar radiation on a tilted surface is

$$I_T = I_{h,bm}R_b + I_{h,d} \left[ (1 - F_1) \left( \frac{1 - \cos \beta}{2} \right) + F_1 \frac{a}{b} + F_2 \sin \beta \right] + I_h \rho \left( \frac{1 - \cos \beta}{2} \right) \quad (3.7)$$

where  $a$  and  $b$  are coefficients that take into account the incident angle of the sun on the tilted surface. The definitions of  $a$  and  $b$  are

$$a = \max(0^\circ, \cos \theta)$$

$$b = \max(\cos 85^\circ, \cos \theta_z)$$

$F_1$  and  $F_2$  are parameters that depend on the sky conditions such as the clearness  $\epsilon$  and brightness  $\delta$ . The definitions of  $\epsilon$  and  $\delta$  are

$$\epsilon = \frac{\frac{I_{h,d} + I_n}{I_{h,d}} + 5.535 \cdot 10^{-6} \theta_z^3}{1 + 5.535 \cdot 10^{-6} \theta_z^3}$$

$$\delta = AM \frac{I_{h,d}}{I_{on}}$$

where  $AM$  is the air mass and  $I_n$  is the global normal solar radiation.  $F_1$  and  $F_2$  are

$$F_1 = \max \left[ 0, \left( f_{11} + f_{12} \delta + \frac{\pi \theta_z}{180} f_{13} \right) \right]$$

$$F_2 = f_{12} + f_{22} \delta + \frac{\pi \theta_z}{180} f_{23}$$

where  $f_{11}, f_{12}, f_{13}, f_{21}, f_{22}$  and  $f_{23}$  are empirical coefficients which are derived from the statistical analyses for the different locations. The Perez model, as the most sophisticated model, is used in this work to do the simulations of the SDHWS.

## 3.4 Flat plate collectors

Flat plate collectors are solar thermal collectors which are used to heat up air or water. There are three different types of collectors that are mainly used:

- Unglazed collector
- Glazed collector
- Vacuum tube collector

Unglazed collectors are also called pool collectors. They have a low efficiency and the stagnation temperature is usually low, but the advantage is that they are simple. Glazed collectors have a higher efficiency and stagnation temperature. The protection glass with a high transmission coefficient  $\tau$  reduces the heat loss, i.e. the heat transfer coefficient to the environment. The manufacture is more sophisticated, because the collector has more technical details, there are more parts to be assembled and it is very important that the collector is watertight to avoid condensation on the inside of the protection glass. Vacuum tube collectors have the highest efficiency and stagnation temperature, but they are also the costliest collectors. Figure 3.3 shows a sketch of a typical glazed flat plate collector.

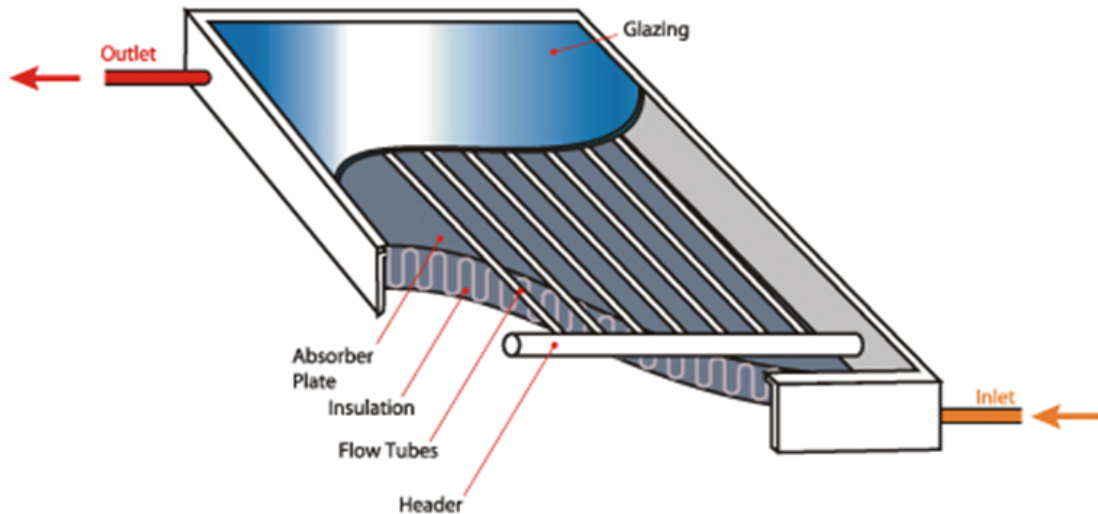


Figure 3.3: Sketch of a typical glazed flat plate collector [1012].

The main parts of the collector are the glazing on top, the absorber plate, the header and the flow tubes, the insulation of the backside and the connections of inlet and outlet. The insulation is usually a polyurethane foam which has a very low thermal conductivity and is cheap. The tubes could be made of copper, stainless steel or plastic, depending on the requirements and the costs. The array of the tubes could be harp or serpentine. Nowadays, the harp design is the most common array. The outlet temperature does not become as high as with the serpentine arrays, but the total energy gain is higher. The absorber plate is selectively coated, which means that the absorption coefficient  $\alpha(\lambda)$  and the emission coefficient  $\epsilon(\lambda)$  depend on the wavelength. The maximum of the solar radiation intensity is in the visible range, therefore the absorption coefficient in this range is high to maximize the energy gain. The maximum of the thermal radiation of the solar collector itself is in the infrared range, therefore the emission coefficient in this range is low to reduce the losses of gained energy. A good selective coating has an  $\alpha/\epsilon$  ratio of about 15 to 20.

#### 3.4.1 Efficiency curve

The efficiency of a solar collector changes during the day due to the variation of the incident solar radiation which changes the average temperature level of the solar collector. The energy loss and the energy gain depend on the temperature gradient to the environment. Hence, the collector efficiency depends on the temperature difference  $\Delta T$  from the absorber plate to the environment.

##### Collector efficiency by Hottel and Whillier

The efficiency curve according to Hottel and Whillier is a simple linear correlation of the collector efficiency and the temperature difference to the environment. The linear equation for the collector efficiency is

$$\eta = a_1 - a_2 \frac{(T_{ref} - T_{amb})}{I_T} \quad (3.8)$$

A collector test under constant and reproducible conditions is necessary to determine the unknown parameters in equation 3.8. The parameter  $a_1$  takes into account the optical losses, which are constant and always exist, even if the collector is at ambient temperature. Parameter  $a_2$  takes into account the thermal losses, which are correlated linear to the temperature difference to the ambient. The reference temperature  $T_{ref}$  should be a temperature that is easy to measure, in order to simplify the test. In the following, the reference temperature is chosen as the mean temperature of the collector  $T_m$ :

$$T_{ref} = T_m = \frac{T_{out} - T_{in}}{2} \quad (3.9)$$

where  $T_{in}$  and  $T_{out}$  are the temperatures of the inlet and the outlet of the collector. The parameters in equation 3.8 are the basic information of any solar collector. They have to be obtained to know the quality of a designed collector. A common way in the literature is to write equation 3.8 by using the parameter called heat removal factor. The definition of the heat removal factor  $F_R$  is

$$F_R = \frac{\text{Actual useful energy gain}}{\text{Useful energy gain if the collector was at the fluid inlet temperature}} \quad (3.10)$$

Now equation 3.8 can be reformulated:

$$\eta = F_R(\tau\alpha) - F_R U_L \frac{(\Delta T)}{I_T} \quad (3.11)$$

where the product  $F_R(\tau\alpha)$  is the optical efficiency,  $U_L$  is the overall energy loss coefficient and  $\Delta T = T_m - T_{amb}$ . Once the parameters are derived from a collector test, the efficiency curve can be generated. Figure 3.4 exhibits typical efficiency curves for different types of flat plate solar collectors.

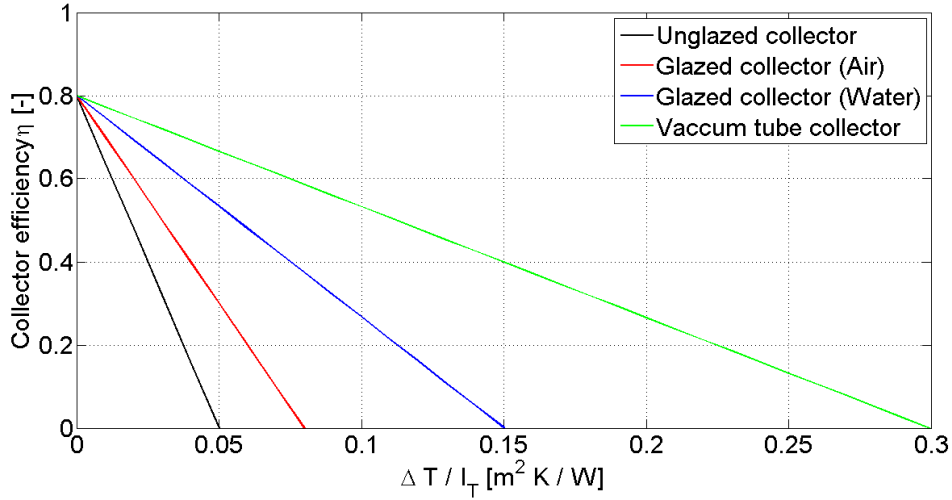


Figure 3.4: Normalized efficiency curves for different types of flat plate collectors.

The flatter the curve, the better is the collector in relation to the conversion of solar energy into thermal energy. All curves have their maximum at 0.8 efficiency for a temperature difference equal to zero. This means that 20 % are just optical losses caused by reflection of solar radiation and the transmission losses through the glass. The efficiency curve of the unglazed collector could start even higher, because the optical losses are smaller due to the missing glass on top. If  $\Delta T$  is greater than zero, thermal losses start to occur. The temperature of the collector for an efficiency of zero is called stagnation temperature. This means that all incident solar radiation are losses and there is no heat transfer to the fluid. The stagnation temperature of vacuum tube collectors can be quite high, which has to be taken into account while designing a solar energy system, because materials used have to withstand this temperature.

### Collector efficiency by ISO 9806

The collector efficiency according to Hottel und Whillier is linearly correlated to the temperature difference to the ambient, but the collector test shows that this is not exactly fulfilled. The heat transfer by conduction is linear, but the heat transfer by convection is non-linear. Therefore, the sum of both results in a non-linear efficiency curve. The efficiency curve according to the ISO standard ISO 9806 is

$$\eta = k_1 - k_2 \frac{\Delta T}{I_T} - k_3 \frac{(\Delta T)^2}{I_T} \quad (3.12)$$

where  $k_1$ ,  $k_2$  and  $k_3$  are parameters that have to be derived from the collector test. The test condition is specified in the ISO 9806 standard. The quadratic approximation of the efficiency curve results in a more accurate profile of the collector efficiency. The basic shape of the curve is shown in figure 3.4, but with this approximation it would be quadratic and not linear.

### 3.4.2 Energy gain

In steady state, the collector energy gain can be expressed by a simple energy balance. The useful solar radiation absorbed by the collector is equal to the difference of the incident solar radiation times the optical losses and the thermal losses to the surroundings by convection, conduction and infrared radiation. These losses can be represented by a product of the overall energy loss coefficient  $U$  times the difference between the mean absorber plate temperature  $T_{abs}$  and the ambient temperature  $T_{amb}$ :

$$Q_u = A_c [I_T(\tau\alpha) - U(T_{abs} - T_{amb})] \quad (3.13)$$

where  $(\tau\alpha)$  is the effective product of transmittance. The problem of this equation is the measurement or calculation of the mean absorber plate temperature. Equation 3.11 can be reformulated by using the definition for the efficiency:

$$\eta = \frac{Q_u}{A_c I_T} \quad (3.14)$$

where  $A_c I_T$  is the total amount of solar energy arriving on the tilted surface of the collector. Furthermore, the heat removal factor  $F_R$  is used now. Then the energy gain is

$$Q_u = A_c F_R [I_T(\tau\alpha) - U(T_m - T_{amb})] \quad (3.15)$$

Equation 3.15 applies only to a certain mass flow, because the heat removal factor depends on the mass flow. In practice, the heat removal factor is obtained for a special mass flow and afterwards this factor is converted to other mass flows by using simple correlations.

If the inlet and outlet temperature of the collector, as well as the mass flux are known, the energy gain can also be calculated by a simple energy balance around the collector. Then the energy gain is

$$Q_u = \dot{m} c_p (T_{out} - T_{in}) \quad (3.16)$$

## 4 Design of the solar domestic hot water system

The developed SDHWS is designed for typical Brazilian residential homes. It is a solution for the peak hour problem discussed in chapter 2.2. The system is a low-cost SDHWS which could be used in all states of Brazil because the study is done in Florianópolis, which has a low solar radiation with high variability, which are the worst conditions for a good thermodynamic performance of the SDHWS.

The main objectives considered while developing and designing the system are:

- Guarantee to cut the energy peak
- Guarantee to supply hot water all day
- Guarantee to supply hot water all year long
- Low-cost technology
- Cost reductions by reducing the collector area and volume of the tanks

First of all, the SDHWS was developed and designed in TRYNYSYS to study the thermodynamic performance. Then, a detailed parameter sensitivity analysis was done to study the influence on the gain of solar energy.

### 4.1 Basic description of the system

The basic components of the developed SDHWS are shown in the flowchart figure 4.1. The system consists of a circuit of natural circulation between the solar collector and the collector tank. In the following, this circuit is called thermosiphon loop. The output from the collector tank flows directly to the backup tank. The backup tank includes an auxiliary heater which guarantees to cut the energy peak and to provide hot water all day and all year long. Finally, the output of the backup tank is connected to the mixing valve which regulates the shower head temperature. This valve is a simple valve that is adjusted on a set point temperature. It has two inputs, one of which is connected directly to the cold water tank and the other one to the backup tank. The pressure in the cold water tank is higher than in the SDHWS, hence the collector tank is always filled completely. When the shower is used, the cold water tank replaces the drained-out water in the collector tank.

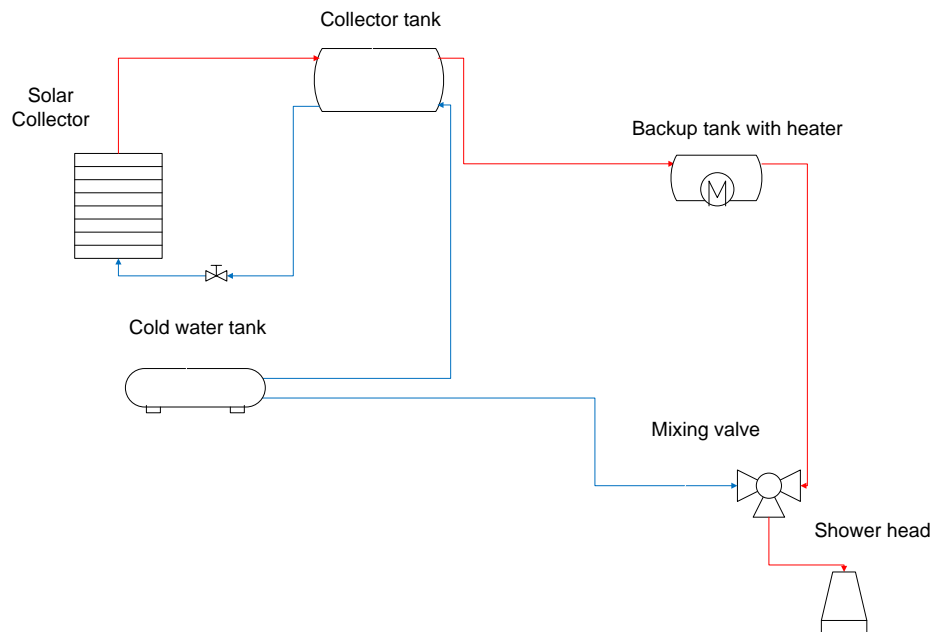


Figure 4.1: Flowchart of the simulated SDHWS.

The average temperature of the collector tank is the key parameter to reach a high solar fraction. This temperature should be as low as possible to reach the highest temperature gradient between the water and the absorber inside the flat plate collector. Therefore, the auxiliary heater is installed in the backup tank. This way, the average temperature of the collector tank is not influenced by the auxiliary heater. In this constellation, the solar collector and its collector tank are acting as a pre-heater and the auxiliary heater of the backup tank is only used for days with low solar radiation, when the solar collector cannot provide enough energy. The innovation of this SDHWS is the control of the auxiliary heater in the backup tank. Chapter 4.3 explains in detail how this regulation works. The results show that it is possible to heat the backup tank in the morning and guarantee hot water during the peak hours, regardless of whether the solar radiation is high or low.

## 4.2 The TRYNSYS Model

The thermodynamic performance of the developed SDHWS was simulated with the software TRYNSYS. TRYNSYS is a simulation program for the transient simulation of thermal systems, especially for solar energy systems. This program has been used by engineers and researchers for thirty years and has been continually enhanced.

Figure 4.2 shows the TRNSYS model of the developed SDHWS, including the collector, the tanks, the mixing valve and the shower head. The data readers which print and save the results are not shown in this figure. Furthermore, it shows the interface which allows to use MATLAB

to interact with TRNSYS to enhance the thermodynamic performance by controlling the set point temperature of the auxiliary heater of the backup tank.

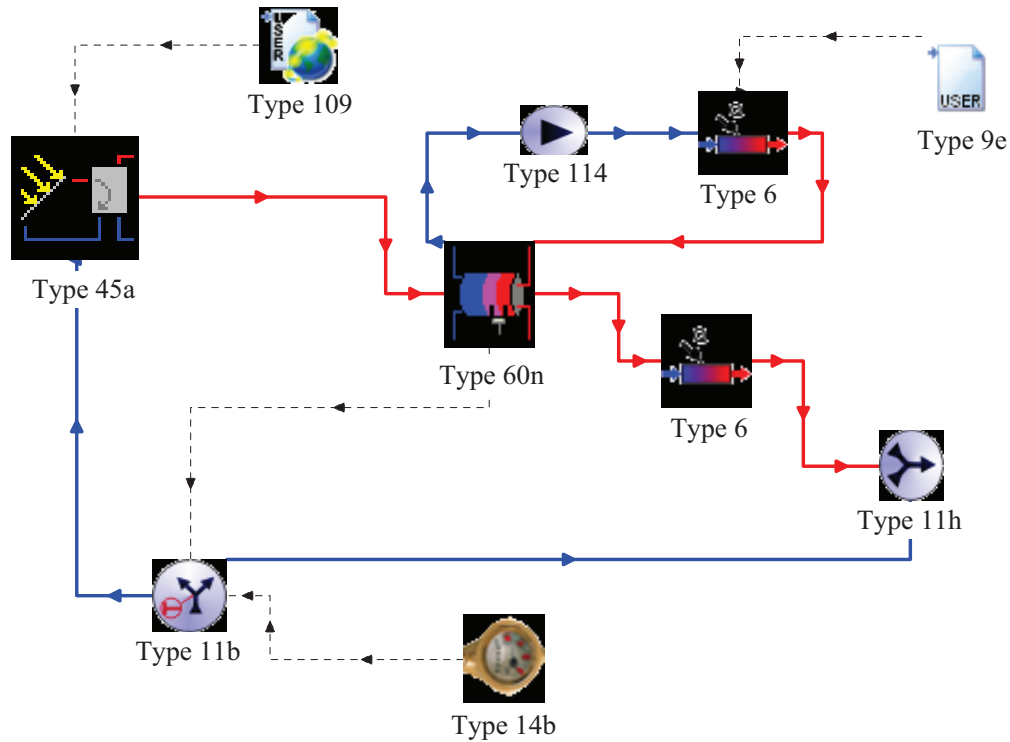


Figure 4.2: TRYNSYS model of the developed SDHWS.

The graphical user interface consists of modules which represent the components of the SDHWS. Between these modules, the user has to insert connections that represent the interactions between the components. These interactions can be physical connections or connections to transfer information. The following subchapters give a detailed description of the used modules, which are called types in TRNSYS.

### 4.2.1 Collector and tank

The thermal solar collector and its storage tank are represented by type 45a, which is a thermosiphon collector with integral storage. All used parameters are shown in table A.1. The dimensions are shown in table A.2.

#### Thermosiphon calculations

Figure 4.3 exhibits a schematic view of the solar collector and the collector tank. The position of the auxiliary heater is not specified in table A.2 because the heater is turned off.

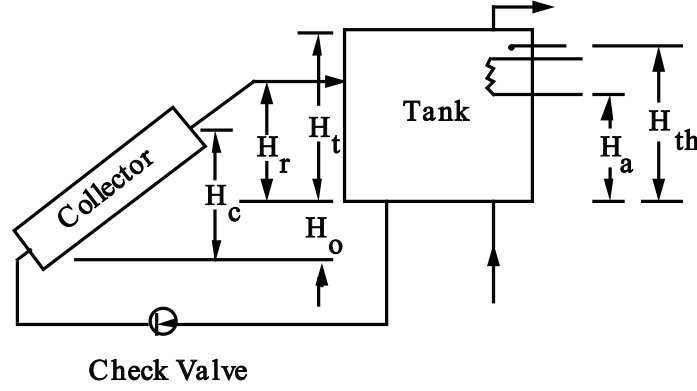


Figure 4.3: Schematic view of the thermosiphon loop [Duf11].

The first step of the solution is to calculate the temperature distribution around the loop using the mass flux  $\dot{m}$  of the previous time step. The connecting pipes between the storage tank and the collector are modeled as one node. According to equation 4.1, the temperature drop of the pipe can be calculated by using the temperature at the bottom of the tank as the pipe inlet temperature  $T_{pi}$ . The thermal capacitance of the pipe is neglected.

$$T_{p,out} = T_{amb} + (T_{p,in} - T_{amb}) \cdot \exp\left(-\frac{(U_p A_{sur})}{\dot{m} c_p}\right) \quad (4.1)$$

To model the thermal performance of the collector, the Hottel-Whillier equation is used. Applying this equation, the temperature at the midpoint of any node  $i$   $T_{c,i}$  can be calculated:

$$T_{c,i} = T_{amb} + \frac{I_T F_R(\tau\alpha)}{F_R U_L} + \left(T_{c,in} - T_{amb} - \frac{I_T F_R(\tau\alpha)}{F_R U_L}\right) \cdot \exp\left[\frac{F' U_L}{\dot{M} \cdot C_p} \cdot \frac{(i-1/2)}{N_x}\right] \quad (4.2)$$

where the collector parameter  $F' U_L$  is calculated by using the value of  $F_R(\tau\alpha)$  and the collector flow rate per unit area at test conditions  $\dot{M}_{test}$ :

$$F' U_L = -\dot{M}_{test} \cdot c_p \ln\left(1 - \frac{F_R U_L}{\dot{M}_{test} c_p}\right) \quad (4.3)$$

Since  $(\tau\alpha)$  depends on the angle of incidence, the next step is the determination of the effects of the angle of incidence.  $F_R(\tau\alpha)_n$  is known from the collector test, the multiplication with the incident angle modifier  $K_{\tau\alpha}$  leads to  $F_R(\tau\alpha)$ . Equation 4.4 gives a general expression to calculate the incident angle modifier  $K_{\tau\alpha}$ :

$$K_{\tau\alpha} = 1 - b_0 \left(\frac{1}{\cos\Theta} - 1\right) \quad (4.4)$$

It shows that for a value of  $b_0 = 0.163$  and for angles  $\Theta < 60^\circ$ , this equation is a useful approximation to account for angle of incidence effects. The new entering temperature of the storage tank is calculated by applying equation 4.1 again. Finally, the new temperature profile of the tank is evaluated by applying the equations of the storage tank (subchapter 4.2.1).

The density of the water depends on its temperature. Now, by knowing the temperature distribution, it is possible to calculate the pressure drop for each segment  $\Delta P_i$  caused by height difference and friction losses:

$$\Delta P_i = \rho_i g \Delta h_i + \rho_i g \xi_i \quad (4.5)$$

where  $\xi_i$  is the friction head loss in the piping. This factor depends on the geometrical characteristics and has to be calculated for each segment of the loop. For more details about the calculations of this factor see the TRYNSYS manual [Duf11] or professional literature about fluid mechanics [Ide96]. Ultimately, at any instant of time the sum of the pressure changes around the loop has to be zero:

$$\sum_{i=1}^{i=N} \rho_i \Delta h_i = \sum_{i=1}^{i=N} \rho_i \xi_i \quad (4.6)$$

At the first onset, equation 4.6 will not be satisfied, because the used mass flux  $\dot{m}$  was the mass flux of the previous time step. Using an iterative numerical solution, the TRNSYS thermosiphon algorithm finds the mass flux that satisfies the set of equations.

### Storage tank calculations

The collector tank is represented by type 38, which is a plug-flow tank [Duf11]. This model uses variably sized fluid segments depending on the simulation time step, the magnitude of the collector and the load flow rate. Hence the big advantage is that the temperature stratification can be modeled with small fluid segments in the temperature gradient zone without the use of small time steps. This component is most suitable for a high degree of stratification which is important to model the thermosiphon loop.

Figure 4.4 shows the concept of this component. Here the tank is initially divided into four volume segments. The figure exhibits the initial configuration, the condition after a volume of liquid from the heat source has entered, the condition after a volume of liquid from the load has entered and, finally, the state of equilibrium that results.

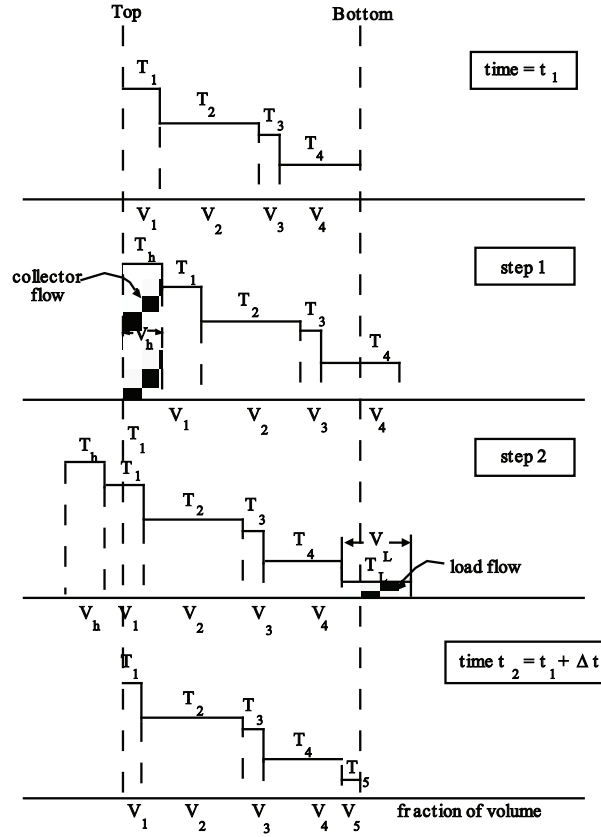


Figure 4.4: Concept of the plug-flow tank [Duf11].

This example assumes that the temperature of the heat source is higher than the temperature at the top of the tank  $T_{heat} > T_1$  as well as the temperature of the load is lower than the temperature at the bottom of the tank  $T_{load} < T_4$ . In step 1, a volume of liquid from the heat source  $V_{heat}$  equal to  $\frac{\dot{m}_{heat}\Delta t}{\rho}$  enters at the top of the tank and shifts the profile. In step 2, a volume of liquid from the load  $V_{load}$  equal to  $\frac{\dot{m}_{load}\Delta t}{\rho}$  enters and shifts the profile to the other direction. The net shift of the profile is  $\frac{(\dot{m}_{heat} - \dot{m}_{load})\Delta t}{\rho}$ . As seen in figure 4.4, the part of the volume of liquid that falls outside the bound is returned to the heat source or to the load. Depending on the volume ratio  $\frac{V_{heat}}{V_{load}}$ , two cases can be distinguished:

If  $V_{heat} < V_{load}$ , then the temperature at the bottom of the tank is equal to the load temperature  $T_{bottom} = T_{load}$ . The temperature at the top of the tank has to be calculated as

$$T_{top} = \frac{V_{heat}T_{heat} + \sum_{i=1}^{k-1} T_i V_i + a T_k V_k}{V_{load}} \quad (4.7)$$

where  $a$  and  $k$  must satisfy

$$0 \leq a \leq 1$$

$$V_{heat} + \sum_{i=1}^{k-1} V_i + aV_k = V_{load}$$

If  $V_{heat} > V_{load}$ , then the temperature at the top of the tank is equal to the heat source temperature  $T_{top} = T_{heat}$ . The temperature at the bottom of the tank has to be calculated as

$$T_{bottom} = \frac{V_{load}T_{load} + \sum_{i=k+1}^N T_i V_i + aT_k V_k}{V_{heat}} \quad (4.8)$$

where a and k must satisfy

$$0 \leq a \leq 1$$

$$V_{load} + \sum_{i=k+1}^N V_i + aV_k = V_{heat}$$

Resulting from this calculation, the temperature of the border segments changes. The new temperature profile has to be evaluated. There are time-dependent storage losses from the tank as well as conduction between the segments. The new temperature profile is calculated by solving the differential equation 4.9 for each segment of the tank:

$$\rho c_p V_i \frac{dT_i}{dt} = -(UA)_i(T_i - T_{amb}) + (k_{H_2O}A)_{i-1} \frac{T_{i-1} - T_i}{\Delta h_{i-1}} - (kA)_i \frac{T_i - T_{i+1}}{\Delta h_{i+1}} \quad (4.9)$$

where  $\Delta h_{i-1}$  is the distance between the midpoint of segment  $i - 1$  and  $i$ , and  $\Delta h_{i+1}$  is the distance between the midpoint of segment  $i$  and  $i + 1$ .  $(kA)$  is the thermal conductivity times the cross section. Since these differential equations are coupled, they have to be solved by successive substitution.

Finally, the total loss from the storage tank can be calculated as

$$\dot{Q}_{amb} = \sum_{i=1}^N (UA)_i(T_i - T_{amb}) \quad (4.10)$$

The energy input to the tank from the heat source is

$$\dot{Q}_{in} = \dot{m}_{heat} c_p (T_{heat} - T_{bottom}) \quad (4.11)$$

The energy supplied to the load is

$$\dot{Q}_{sup} = \dot{m}_{load} c_p (T_{top} - T_{load}) \quad (4.12)$$

### Overall loss conductance of the tank

The overall loss conductance of the cylindrical tank is calculated by using the Péclet equations for stationary heat conduction. The resistance against the lateral surface, the surface of the bottom and the surface of the top are added by using the principle of superposition. The external thermal resistance due to convection is neglected. The thermal resistance of the tank itself is also neglected, because the thermal conductivity of iron is about 1000 times higher than the insulation.

The ratio of height to diameter for all tanks used in this work is  $\frac{h}{D} = 2$ . Hence, the diameter can be calculated by just using the volume of the tank:

$$D = \left( \frac{2V}{\pi} \right)^{\frac{1}{3}} \quad (4.13)$$

Using the principle of superposition, the overall loss conductance  $UA$  is

$$UA = k_{ins}\pi \left( \frac{4D}{\ln\left(\frac{D+2e}{D}\right)} + \frac{D^2}{2e} \right) \quad (4.14)$$

where  $k_{ins}$  is the thermal conductivity of the insulation and  $e$  the thickness of the insulation. The reference plane  $A$  is the lateral surface area of the tank.

#### 4.2.2 Backup tank with heater and pump

The backup tank with an internal auxiliary heater is represented by type 60n which is a stratified fluid storage tank with internal heat exchangers. The internal heat exchanger of this tank could not be used to control the transient heating periods, because the set point temperature is an initial value that cannot be changed by time. From a thermodynamic point of view, a loop with a pump and a heat exchanger is equal as far as the losses are set to be zero. This heating loop is represented by type 114, which is a pump and type 6, which is a continuous-flow water heater. Now it is possible to change the set point temperature of the continuous-flow water heater each day, because this set point temperature is not an initial value anymore. This temperature is controlled by type 9, which is a data reader. This component reads the set point temperature for each day. The calculation of this temperature is based on an algorithm programmed in MATLAB, see chapter 4.3. Table A.3 exhibits the used parameters of the tank, the heater and the pump. The fluid properties are the same as shown in table A.1.

#### Backup tank

As said before, the backup tank is represented by type 60n, which is a stratified fluid storage tank. This tank is the most detailed storage tank available in the standard TRNSYS library. It is possible to model up to 100 stratification levels. Since the tank is installed horizontally, the stratification is very low, therefore the tank is modeled as fully mixed.

Since the tank is modeled as fully mixed, the position of the inlets and outlets is not important, although they do have to be specified. The two inlets are put at the top and the two outlets are put at the bottom. The change of the internal energy only depends on the energy

fluxes of the four inlets and outlets plus the losses over the surface of the tank. The differential equation for the temperature is

$$mc_p \frac{dT_i}{dt} = (UA) \cdot (T_{amb} - T_{avg}) + \dot{m}_{in} c_p T_{in} - \dot{m}_{out} c_p T_{out} + \dot{m}_{in,aux} c_p T_{in,aux} - \dot{m}_{out,aux} c_p T_{out,aux} \quad (4.15)$$

where  $\dot{m}_{in}$  is the hot mass flux coming from the collector storage tank and  $\dot{m}_{out}$  is the hot mass flux going to the shower head. Based on the continuity equation, these two mass fluxes have to be equal, because the two fluxes connected to the heating loop are equal as well. The mass flux  $\dot{m}_{out}$ , which is going to the shower head, depends on the hot water demand, more precisely on the temperature of the backup tank  $T_{avg}$  and the quantity of requested water. There is no temperature distribution in the tank, because the tank is modeled as fully mixed, therefore the average temperature  $T_{avg}$  is the tank temperature and does not have to be calculated. The mass fluxes  $\dot{m}_{in,aux}$  and  $\dot{m}_{out,aux}$  are controlled by the heating regulation of the connected loop. The overall loss conductance of the tank ( $UA$ ) is calculated by equation 4.14.

### The backup heating loop

The backup heating loop consists of type 114 and type 6, which are a constant speed pump and a continuous-flow water heater. There is no heating loop in the real system thus the pump and the heater are modeled without losses.

The heating period is controlled by the pump by switching the pump ON or OFF. The continuous-flow water heater is controlled by a set point temperature. It heats with the maximum heating rate as long as the fluid temperature is lower than the set point temperature. This temperature is calculated for each day (see subchapter 4.3).

### 4.2.3 Hot water demand

The hot water demand is an input which is determined in advance. The dimensions of the SDHWS depend largely on the daily average amount of required hot water. To model the reality, it would be necessary to simulate a lot of different hot water demand profiles. Obviously, this would be too time-consuming and furthermore it is not necessary. The most important aspect is that the daily average of hot water consumption is correct. In addition, the distribution during the day should represent the peak of hot water demand during the peak hours. In Florianópolis, Brazil, an experimental study was conducted to establish a daily average hot water demand profile.

In this study, the energy consumption of the electric shower heads of 90 low-income homes was recorded. The cold water temperature was estimated, because it was not possible to install thermometers in all these households. The efficiency of an electrical shower head is nearly 100 %, therefore a simple energy balance allows to calculate the heated mass flux:

$$\dot{m}_{demand} = \frac{\dot{Q}_{heat}}{c_p \Delta T} \quad (4.16)$$

The volume of heated water was calculated for each hour and for each household. Figure 4.5 shows the derived average distribution of hot water demand per day of the observed households.

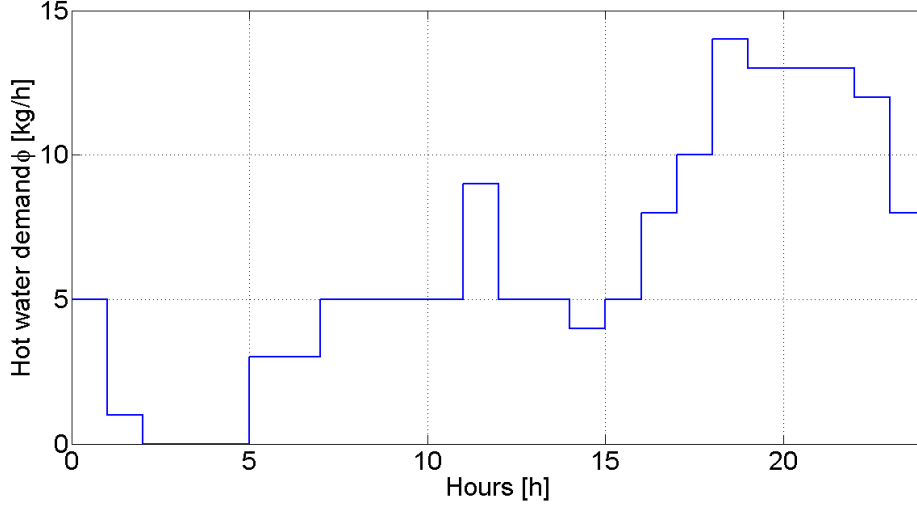


Figure 4.5: Distribution of the hot water demand per day [Sal04].

#### 4.2.4 Definition of the solar fraction

The solar fraction  $f_{sol}$  is defined as the amount of solar energy the SDHWS provides divided by the amount of solar energy plus the amount of electric energy which is still consumed:

$$f_{sol} = \frac{Q_{sol}}{Q_{sol} + Q_{aux,1} + Q_{aux,2}} \quad (4.17)$$

where  $Q_{sol}$  is the gained solar energy:

$$Q_{sol} = \dot{m}_{load} c_p (T_{top} - T_{cold}) \quad (4.18)$$

where  $m_{load}$  is the mass flux from the collector tank to the backup tank.  $T_{top}$  is the temperature at the top of the collector tank and  $T_{cold}$  is the replacement temperature of the collector tank which is the temperature of the water reservoir of the building.  $Q_{aux,1}$  is the auxiliary energy consumed by the continuous-flow water heater of the backup heating loop and  $Q_{aux,2}$  is the auxiliary energy consumed by the second continuous-flow water heater before the shower head (figure 4.2). According to this definition the solar fraction can have values between zero and one.

### 4.3 Algorithm to cut the energy peak

The main objectives of this work is to avoid to use electrical energy during the peak hours, regardless of whether the solar radiation is high or low, but there are more specifications to

fulfull: The developed SDHWS should be able to provide enough hot water all day long, although the backup tank is only heated between 4 a.m. and 6 a.m. According to this guideline, an algorithm was developed to calculate the minimal necessary backup tank set temperature  $T_{set}$  to heat up during the heating period in the morning to provide enough hot water for the rest of the day. This temperature depends on the expected solar radiation for the considered day. The minimal daily temperature of the backup tank appears at 4 a.m.  $T_{4h}$ , because this is right before the next heating period.  $T_{4h}$  should be at least higher than 39 °C, which is the required temperature for the shower head. However, a temperature margin is necessary to consider uncertainties in the calculations and weather forecast information (section 4.5). The temperature margin is a design variable and must be determined in advance. In the following, the minimal admissible backup tank temperature is set to  $T_{min,ad} = 43$  °C. Therefore, the temperature margin to consider uncertainties is 4 °C.

First of all, the SDHWS is simulated in TRNSYS with an arbitrary temperature  $T_{set}$ . This leads to a temperature  $T_{4h}$  which is not equal to  $T_{min,ad}$ . The temperature difference between these two temperatures  $\Delta T$  calculated with MATLAB for each day is

$$\Delta T = T_{min,ad} - T_{4h} \quad (4.19)$$

Now this temperature difference is added to the temperature  $T_{set}$  the day before. If N represents one day and runs from 1 to 365, the equation to calculate the minimal necessary backup tank set temperature  $T_{set,new}$  is

$$T_{set,new}^N = T_{set}^N + (T_{min,ad} - T_{4h}^{N+1}) \quad (4.20)$$

Now, after the second simulation with TRNSYS, the temperature  $T_{4h}$  is still not exactly  $T_{min,ad}$ , because the heat losses have changed due to the different temperatures levels of the SDHWS, but it is already closer than before. This iteration proceeding of calculating new minimal necessary backup tank set temperatures  $T_{set,new}$  for each day with equation 4.20 and simulating the system in TRNSYS can be repeated many times, but after three times the values  $T_{4h}$  for each day are already close to the minimal admissible backup tank temperature  $T_{min,ad}$ .

Figure 4.6 shows the temperature distribution of the backup tank and the shower head for a period of 10 days. The figure shows three steps of the process to calculate the minimal necessary backup tank set temperatures  $T_{set}^N$ . Step 1 shows the temperature distribution after the simulation in TRNSYS with arbitrary temperatures  $T_{set}^N$ . This leads to temperatures  $T_{4h}^{N+1}$ , which are not equal to  $T_{min,ad}$ . After calculating new minimal necessary backup tank set temperatures  $T_{set,new}^N$  with equation 4.20, the system is simulated again. This leads to a temperature distribution as seen in step 2. This procedure is repeated and the result is shown in the third graph. The temperatures  $T_{4h}^{N+1}$  are now close to the minimal admissible backup tank temperature  $T_{min,ad} = 43$  °C, which is shown as a dashed line.

### 4.3 ALGORITHM TO CUT THE ENERGY PEAK

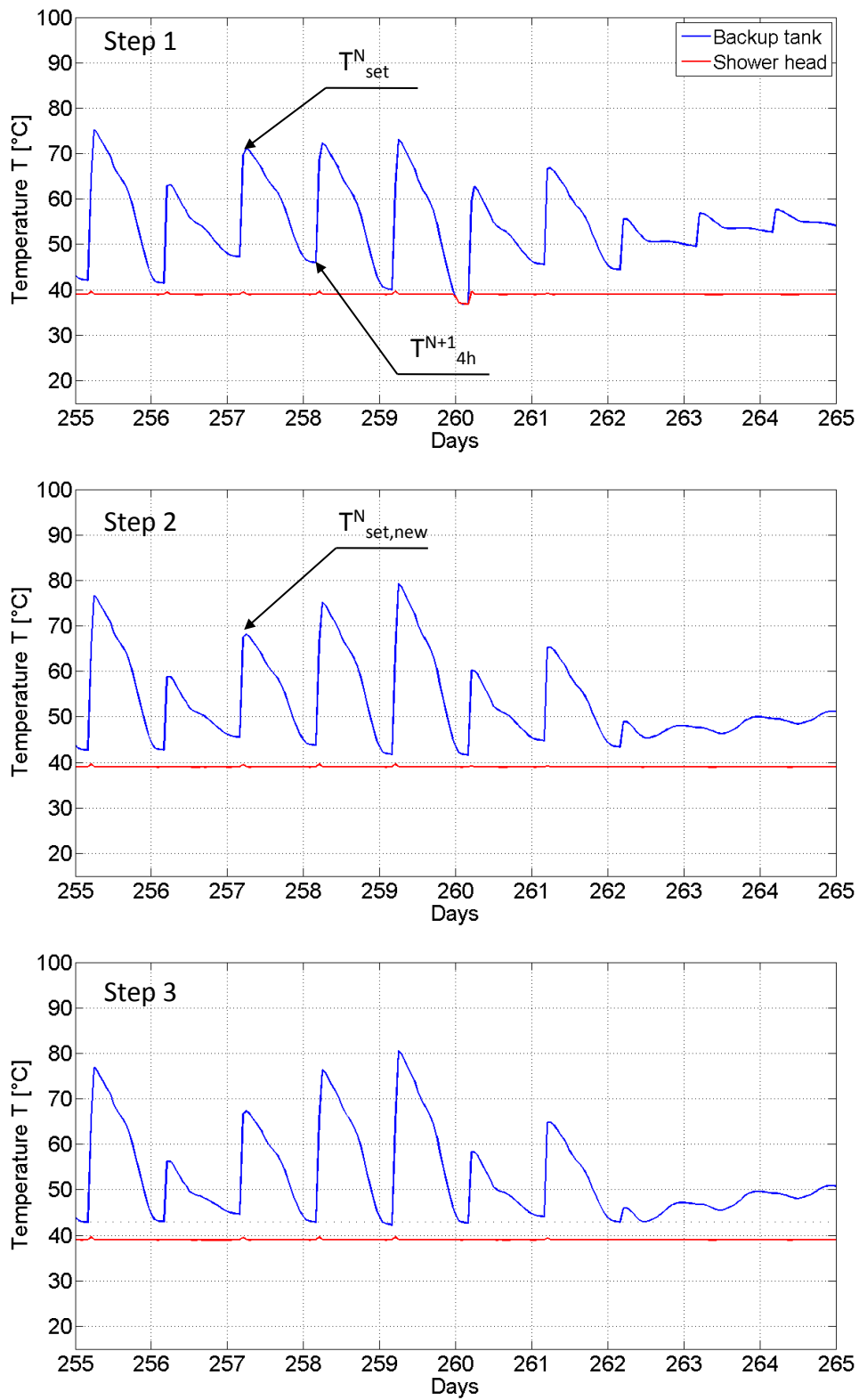


Figure 4.6: Steps to calculate the minimal necessary backup tank set temperature  $T_{set}$ .

The simulation was done in TRNSYS by using TMY data for the weather information. Therefore, it is possible to use solar radiation data for the next day to calculate the minimal necessary backup tank set temperature  $T_{set}$  for the present-day. Obviously, this is only possible for a real system, if weather forecast data are available. Section 4.5 discusses this problem and gives a solution of how weather forecast information can be generated in an easy way.

## 4.4 Parameter sensitivity analysis

The following subsections discuss how the variation of different parameters influences the gain of solar energy and the temperature levels of the SDHWS. Table 4.1 shows the values for the analyzed parameters for the subsections where they are considered fixed values.

Table 4.1: Analyzed parameters.

Label	Symbol	Value	Unit
Shower head temperature	$T_{sh}$	39	°C
Water supply temperature	$T_{cold}$	20	°C
Insulation thickness of backup tank	$e_b$	0.1	<i>m</i>
Insulation thickness of collector tank	$e_c$	0.05	<i>m</i>
Volume of collector tank	$V_c$	130	<i>l</i>
Volume of backup tank	$V_b$	70	<i>l</i>
Tank orientation		<i>horizontal</i>	–

### 4.4.1 Shower head temperature

The influence of the shower head temperature  $T_{sh}$  on the annual solar fraction  $\bar{f}_{sol}$  is analyzed without changing other parameters. The minimal admissible backup tank temperature should be changed correlated to the shower head temperature to maintain the temperature margin to consider uncertainties, however this has been neglected in this analysis to focus just on the shower head temperature. Table 4.2 exhibits the gained solar energy  $Q_{sol}$ , the consumed auxiliary energy  $Q_{aux,1}$  and the annual solar fraction  $\bar{f}_{sol}$  for three different shower head temperatures  $T_{sh}$ .

The shower head temperature is inversely correlated to the annual average solar fraction. The lower the shower head temperature the less auxiliary energy is needed to heat the water in

the morning. The reduced use of auxiliary energy in the days with low solar radiation increases the annual average solar fraction. On the other hand, the lower the shower head temperature the lower the gain of solar energy in days with high solar radiation, because the necessary energy to heat the water is lower. In sum, this results in a decreased annual solar fraction. The reduced demand of auxiliary energy is the dominant effect.

Table 4.2: Comparison of three different shower head temperatures.

$T_{sh} [^{\circ}\text{C}]$	$Q_{sol} [kWh]$	$Q_{aux,1} [kWh]$	$\bar{f}_{sol} [\%]$
38	858.44	383.92	69.10
39	886.58	423.47	67.67
40	913.61	463.89	66.32

#### 4.4.2 Water supply temperature

The water supply temperature has a big influence on the thermodynamic performance of the SDHWS. The lower this temperature the more energy is necessary to heat up the water. In Brazil the supply water does not come directly from the water supply pipe. The water is stored in huge tanks on top of the houses, because the water supply pipes are often without water. If there were no water tanks installed, Brazilian houses were without water quiet often. As a result the water supply temperature in Brazil is the temperature of the water tank on top of the house.

The National Renewable Energy Laboratory developed an algorithm for mains water temperature [BJ]. It comes to the conclusion that the mains water temperature is the ambient temperature plus 3.3 °C, while the ambient temperature varies roughly with an annual sinusoid. The uncertainties of this algorithm are quite high. Hence for this work the water supply temperature is set constant to the annual average ambient temperature of the considered city. This assumption can be seen as a worst case consideration.

The influence of the water supply temperature on the solar fraction is analyzed for the city of Florianópolis. The developed SDHWS was simulated for four different water supply temperatures. Table 4.3 shows the gained solar energy  $Q_{sol}$ , the necessary electric energy  $Q_{aux,1}$  and the annual average solar fraction  $\bar{f}_{sol}$  for the four water supply temperatures.

Table 4.3: Thermodynamic performance of the SDHWS for four different water supply temperatures.

$T_{cold} [^{\circ}\text{C}]$	$Q_{sol} [kWh]$	$Q_{aux,1} [kWh]$	$\bar{f}_{sol} [\%]$
20	886.58	432.47	67.67
22	802.78	374.86	68.17
24	719.81	325.69	68.85
26	637.22	276.02	69.78

Due to the reduced energy demand of a higher water supply temperature, the gained solar energy and the necessary electric energy are lower. In proportion the auxiliary energy is reduced even more. As a result of both, the annual average solar fraction is only slightly affected by the change of the water supply temperature. In the following, the water supply temperature is assumed to be  $T_{cold} = 20^{\circ}\text{C}$  for the city of Florianópolis.

### 4.4.3 Insulation thickness

The collector tank and the backup tank are insulated to minimize the energy losses. The insulation material used is polyurethane hard foam (PUR), which has a thermal conductivity of  $k_{PUR} = 0.02 - 0.03 \frac{\text{W}}{\text{mK}}$ . For the analysis, a value of  $k_{PUR} = 0.023 \frac{\text{W}}{\text{mK}}$  is used. The thinner the insulation thickness, the lower the material costs. Hence, the insulation thickness should be as thin as possible with respect to the energy losses, which become higher with a thin insulation. A cost analysis of the insulation thickness against the material costs, with the result that a thickness of about 0.1 m is the optimum balance of these contrary objectives, is described in detail in the paper of Colle and Abreu [CS01]. Nevertheless, in this work three different cases for two different collectors are analyzed. The main parameters of the two analyzed collectors can be found in subsection 4.4.4. The differences in the annual average solar fraction  $\bar{f}_{sol}$  are shown in table 4.4.

Table 4.4: Comparison of three different insulation thicknesses.

$e_c[m]$	$e_b[m]$	$\bar{f}_{sol,glazed}[\%]$	$\bar{f}_{sol,unglazed}[\%]$
0.05	0.05	94.63	67.06
0.05	0.1	96.02	70.35
0.1	0.1	97.11	72.01

The analysis exhibits that the insulation of the backup tank is more important than the insulation of the collector tank. The backup tank has a higher average temperature level, therefore the energy losses are higher because the temperature gradient to the environment is higher. To reduce the energy losses, it is necessary to have a good insulation, especially of the backup tank.

#### 4.4.4 Tank volumes

The developed SDHWS consists of two tanks. The total volume of these two tanks is defined to  $V_{total} = 200l$ , thus here only the volume ratio  $\chi = \frac{V_b}{V_c}$  is varied. The volume ratio is varied between  $\chi = 0.33$  and  $\chi = 3$ . The simulation is done for two different collectors:

- Unglazed collector:  $F_R(\tau\alpha)_n = 0.73$  and  $F_R U_L = 19.30 \frac{W}{m^2K}$
- Glazed collector:  $F_R(\tau\alpha)_n = 0.67$  and  $F_R U_L = 5.74 \frac{W}{m^2K}$

The SDHWS using the unglazed collector was simulated for an area of  $A_c = 2m^2$  and  $A_c = 4m^2$ . Figure 4.7 shows the results for the three simulated cases.

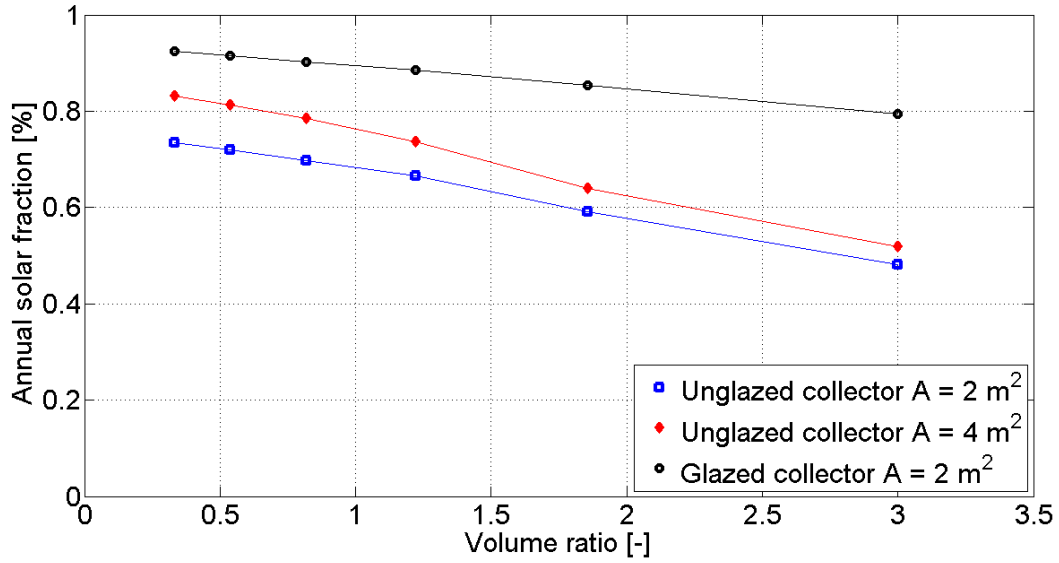


Figure 4.7: Annual average solar fraction  $\bar{f}_{sol}$  over different volume ratios  $\chi$  for three simulated cases.

It is true for all three simulated cases that the smaller the volume ratio the higher the annual average solar fraction. In other words, the backup tank should be as small as possible. On the other hand, the volume of the backup tank has to have a minimum volume, because the storable energy has to be sufficient to provide enough hot water for one day, even for winter days with the lowest solar radiation. Obviously, the temperature limit is the boiling temperature which is 100 °C. For this reason, the minimum volume of the backup tank is  $V_b = 70l$ , which results in a minimal necessary backup tank set temperature  $T_{set}$  of less than 90 °C on the days with the lowest solar radiation.

#### 4.4.5 Orientation of the collector tank

The tank orientation is a parameter that influences the stratification of the tank. The thermosiphon enables a higher energy gain when the level of stratification is higher. For this SDHWS, the orientation was already fixed before doing the parameter sensitivity analysis. The tank is installed horizontally, because this way the assembling and handling is a lot easier. The assembling of a research facility does not have to be easy, but with regard to a real system, it should be as easy as possible.

Nevertheless, a comparison of the equal SDHWS with different orientations of the collector tank is done. For both SDHWS, an equal height to diameter ratio of the tank is chosen, hence the SDHWS with the vertically orientated tank has a much higher level of stratification. The difference in the annual average solar fraction is

- horizontally orientated tank:  $\bar{f}_{sol} = 67.67\%$
- vertically orientated tank:  $\bar{f}_{sol} = 72.58\%$

## 4.5 Weather forecast information

The analysis and design of the SDHWS in the prior sections was done by using TMY data. It was possible to use solar radiation data from the next day to calculate the minimal necessary backup tank set temperature  $T_{set}$  for the present-day. This is not possible in a real SDHWS. Therefore, it is necessary to have weather forecast information, which however present uncertainties, even if they are based on a smart prediction algorithm. Furthermore, it is quite complicated to get good numerical data from official meteorological stations and, besides, the developed SDHWS should not need an internet connection to get data. It should be an independent SDHWS for low-income homes, even though this means that the weather forecast information used is generated in a different way.

### 4.5.1 Generation of weather forecast information

The idea is to use the incident solar radiation of the present-day as a prediction for the next day. In general, the weather is not changing rapidly. The climate is a slow changing process. To examine this method, the TMY data of Florianópolis is used to calculate  $T_{set}$ . However the simulation is done by using a modified TMY data file. The modified data are shifted exactly one day. The result is equal to a real system that uses the radiation of the present-day as a prediction for the next day. The above graph in figure 4.8 shows the temperature distribution of the backup tank  $T_b$  and the distribution of the global solar radiation  $I_h$  simulated with the regular TMY data file, which corresponds to a weather prediction without uncertainties. On the other hand, the lower graph exhibits the result of the simulation with the modified TMY data file, which corresponds to a weather prediction with uncertainties that uses the solar radiation of the present-day as a prediction for the next day. The shown time period of ten days and the parameters used are equal to those in figure 4.6.

A high positive temperature gradient in the distribution of the backup tank temperature represents the auxiliary energy input in the morning. The temperature of the backup tank is inversely correlated with the global solar radiation. On days with low solar radiation,  $T_{set}$  is high. On days with high solar radiation,  $T_{set}$  is low. If the solar radiation is really high, the auxiliary heater of the backup tank does not need to heat, because the temperature at 4 a.m. is still higher than  $T_{set}$ .

The bottom graph shows the result for the simulation with the modified TMY data, which means, for a solar radiation forecast by using the present-day as a forecast for the next day. Two cases must be distinguished. If the solar radiation is underrated, the temperature at 4 a.m. is higher than the minimal admissible backup tank temperature  $T_{min,ad}$ . This results in a reduced gain of solar energy, but there are no problems in respect to the guarantee to take a hot shower. This can be seen on days 255 and 259. If the solar radiation is overrated, the temperature of the backup tank can go below the shower head temperature  $T_{sh} = 39^\circ\text{C}$ . On these days it is necessary to use electric energy during the day to provide hot water to take a shower. Day 257 is an example for this situation. On the rest of the days with overrated solar radiation the temperature margin of 4 °C to consider uncertainties was sufficient to prevent the backup tank temperature from falling below the shower head temperature. This can be seen on days 256 and 258.

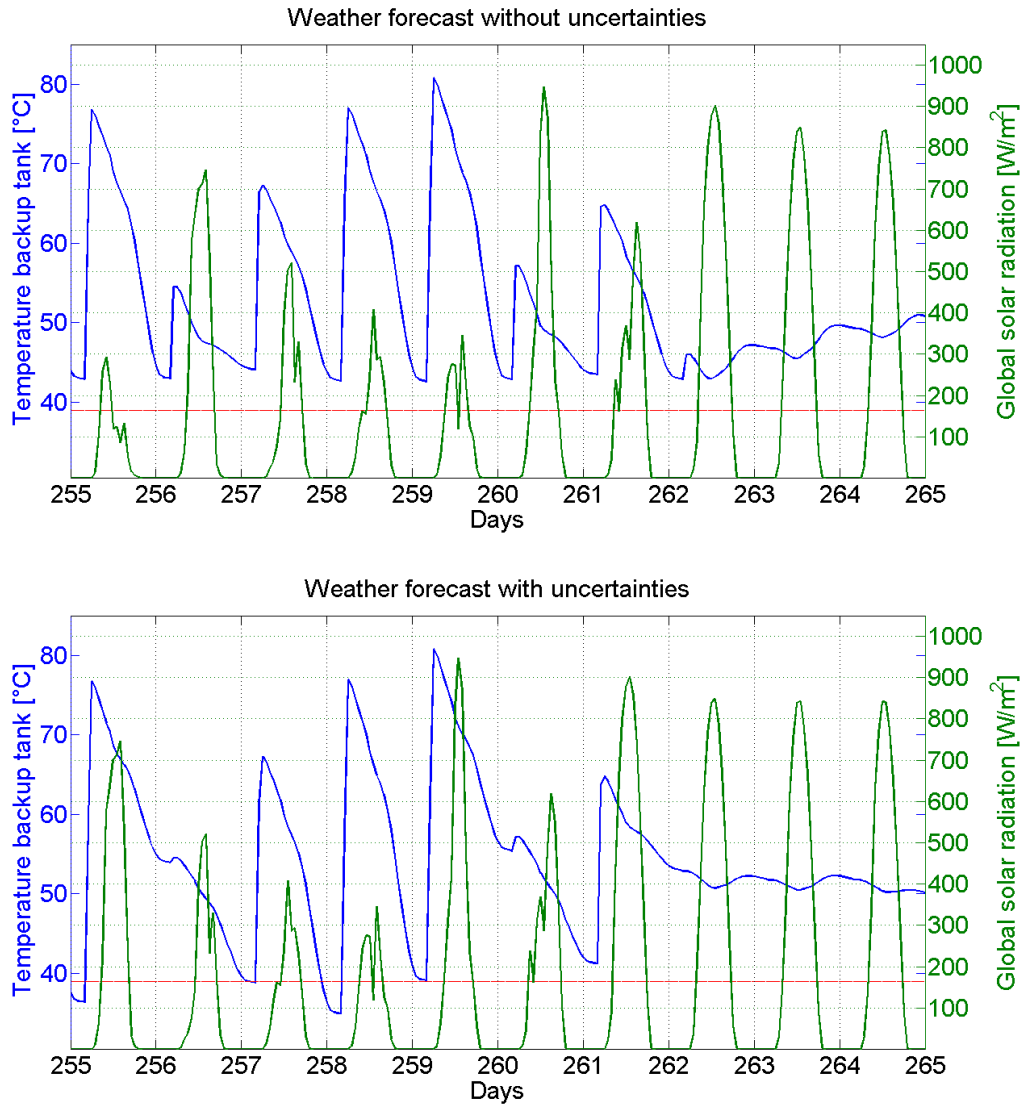


Figure 4.8: Results of a solar radiation forecast without uncertainties and a forecast by using the radiation of the present-day as a forecast for the next day.

### 4.5.2 Prediction uncertainties of the generated weather data

The uncertainties of the TMY data in comparison to the modified TMY data can be calculated, which actually represents the uncertainty of using the solar radiation of the present-day as a prediction for the next day. The TMY data is a dataset of hourly values for one year (Appendix B). As a consequence the most obvious is to calculate an hourly root mean square deviation  $RMSD_{hour}$ . The hourly root mean square deviation for the TMY data of Florianopolis is

$$RMSD_{hour} = \sqrt{\frac{1}{S_h} \sum_1^{S_h} (I_h^N - I_h^{N+1})^2} = 226.6 \frac{W}{m^2} \quad (4.21)$$

where  $S_h$  are the sunshine hours. This means that only hours with a total incident solar radiation  $I_h$  greater than zero are considered in the deviation calculation.  $N$  is the running index of the sunshine hours.

To calculate the arriving energy per day  $E_{day}$ , the incident global solar radiation  $I_h$  has to be integrated for each day. Using the integrated values it is possible to calculate a daily root mean square deviation. The daily root mean square deviation  $RMSD_{day}$  for the TMY data of Florianopolis is

$$RMSD_{day} = \sqrt{\frac{1}{365} \sum_1^{365} (E_{day}^N - E_{day}^{N+1})^2} = 1204.3 \frac{Wh}{m^2} \quad (4.22)$$

To get a qualitative statement of these values, it is necessary to calculate a deviation expressed as a percentage. Each of these two deviations is normalized to the annual average of the considered values. The normalized root mean square deviations are:

- $RMSD_{hour} = 66.84\%$
- $RMSD_{day} = 26.19\%$

$RMSD_{hour}$  is very high in comparison to  $RMSD_{day}$ . The only problem of weather uncertainties in respect to the developed SDHWS is that the minimal necessary backup tank set temperature  $T_{set}$  which is calculated for each day, depends on the expected solar radiation. The energy gap between the arriving solar energy and the energy that is needed to supply hot water has to be provided by the auxiliary heater of the backup tank. The deviation of the distribution of the expected solar radiation has a small influence, because the calculated temperature  $T_{set}$  depends on the amount of energy that is expected for the whole day. Therefore, the  $RMSD_{day}$  should be as low as possible, whereas the  $RMSD_{hour}$  may be higher. For this SDHWS, this method of generating weather forecast information by using the present-day as a prediction for the next day is a good alternative to using information from meteorological stations.

# 5 Results of the designed solar domestic hot water system

This chapter exhibits detailed results of the performance simulation of the SDHWS designed in chapter 4. The simulation is done by using the solar radiation of the present-day as a prediction for the next day as described in section 4.5. The results of interest are the solar fraction, the peak reduction potential, the performance for different consumers and the performance in different cities of Brazil. The simulation in TRYNSYS is done with a simulation time step of  $t = 360s$ .

The results of the developed SDHWS are compared with a reference solar energy system using the same solar collector but no backup tank. The collector tank has a volume  $V_{c,ref} = 200l$ , which is the sum of the volume of the collector tank and the backup tank of the developed SDHWS. The parameters and dimensions remain unchanged. The simulation using the TMY data of the city of Florianópolis results in an annual average solar fraction  $\bar{f}_{sol,ref} = 83.41\%$  and an annual average peak reduction  $\bar{P}_{red,ref} = 85.38\%$ .

## 5.1 Peak reduction

The main objective of this work is to develop a SDHWS that cuts the energy peak and that shifts the energy necessary during the peak hours to the morning hours. The developed SDHWS operates perfectly, if the forecast of the solar radiation for the next day has no uncertainties. There is no need for using electric energy during the peak hours, which can be seen in the above graph of figure 4.8. The temperature of the backup tank, which is the source of heat entering the shower head, never drops below the shower head temperature.

If there are uncertainties in the predicted solar radiation, the SDHWS does not work perfectly. The temperature of the backup tank can drop below the shower head temperature, if the predicted solar radiation was overrated. Therefore, it is necessary to use electric energy during the peak hours to take a hot shower. This can be seen in the graph of figure 4.8 below, which represents a system where the solar radiation of the present-day is used as a prediction for the next day. To get a representative statement, it is necessary to consider one year, which is the whole TMY dataset.

Whether the backup tank temperature falls below the shower head temperature depends on the temperature margin between the minimal admissible backup tank temperature and the shower head temperature  $\Delta T = T_{min,ad} - T_{sh}$ . If this temperature margin is big, the solar radiation can be overrated even more and the backup tank temperature still does not drop below the shower head temperature. Most importantly, the backup tank temperature does not fall below the shower head temperature during the peak hours, because if this happens,

electric energy is needed during the peak hours. If the temperature of the backup tank drops below the shower head temperature after the peak hours, this is not so bad, because the grid utilization is low at night and therefore the use of electric energy is no problem.

Figure 5.1 shows the annual average peak energy reduction  $\bar{P}_{red}$  and the annual average solar fraction  $\bar{f}_{sol}$  for different minimal admissible backup tank temperatures  $T_{min,ad}$ . The peak energy reduction is the energy needed during the peak hours that can be provided by the SDHWS divided by the total necessary energy needed during the peak hours, if an electric shower head was used.

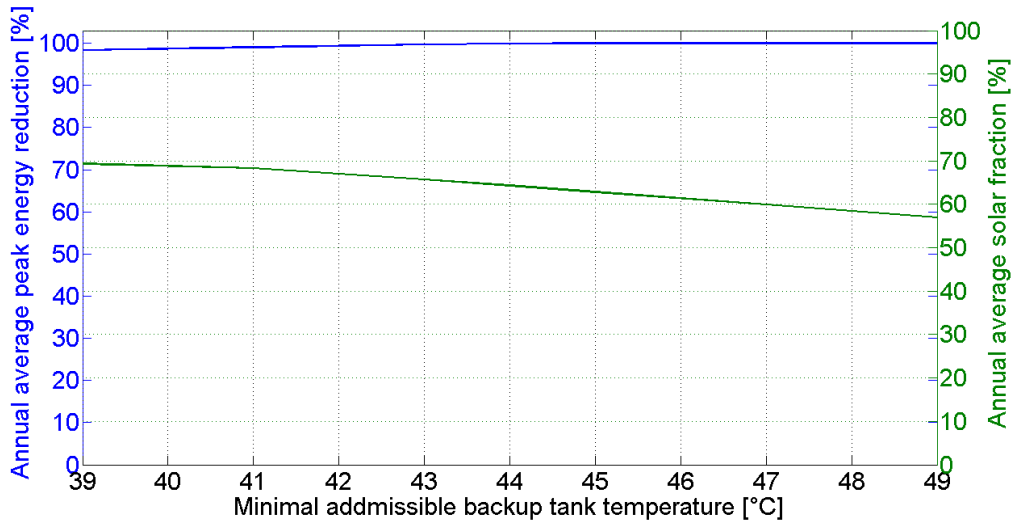


Figure 5.1: Annual average peak energy reduction  $\bar{P}_{red}$  and annual average solar fraction  $\bar{f}_{sol}$  for different minimal admissible backup tank temperatures  $T_{min,ad}$ .

$\bar{f}_{sol}$  is inversely correlated to  $T_{min,ad}$ , because a higher level of the backup tank temperature reduces the gain of solar energy. Starting from a temperature  $T_{min,ad} = 43^\circ\text{C}$ , the gain of a higher  $\bar{P}_{red}$  is minimal in comparison to the lower  $\bar{f}_{sol}$ . In the following, a temperature  $T_{min,ad} = 43^\circ\text{C}$  is selected. This is a good compromise of a high peak energy reduction and a high solar fraction. For this temperature, the annual average peak energy reduction is  $\bar{P}_{red} = 99.83\%$ . This means that from the total annual amount of electric energy which is needed during the peak hours without the SDHWS  $Q_{peak,total} = 322.9\text{kWh}$  now by using the SDHWS less than  $Q_{peak} = 1\text{kWh}$  is needed during the peak hours.

## 5.2 Results for different consumers

The hot water demand (subsection 4.2.3) is a fixed input for the simulation of the developed SDHWS. This hot water demand is an average consumption profile of low-income homes which was derived by an experimental study. The calculation of the minimal necessary backup tank set temperature  $T_{set}$  could be based on different hot water demands to optimize the thermodynamic performance. To derive the hot water demand of a home where a SDHWS is to be

installed, this household would have to be observed over a considerable period of time. It is far too expensive to install the measuring instruments and do the observation just to derive the hot water demand, which actually would just be an average profile again.

The distribution of the hot water demand has a small influence on the performance of the SDHWS because for the calculation of  $T_{set}$ , mainly the total daily demand of hot water is important. Hence the impact of a percentage overload on the hot water demand profile is analyzed. This means that the minimal necessary backup tank set temperature  $T_{set}$  is calculated for the average hot water demand, but the simulation is done for a higher hot water demand. The results are analyzed for each month and an overload of up to 100 %. Figure 5.2 shows the monthly average peak energy reduction  $\bar{P}_{red,month}$  for different percentages of overloads  $\Delta m$

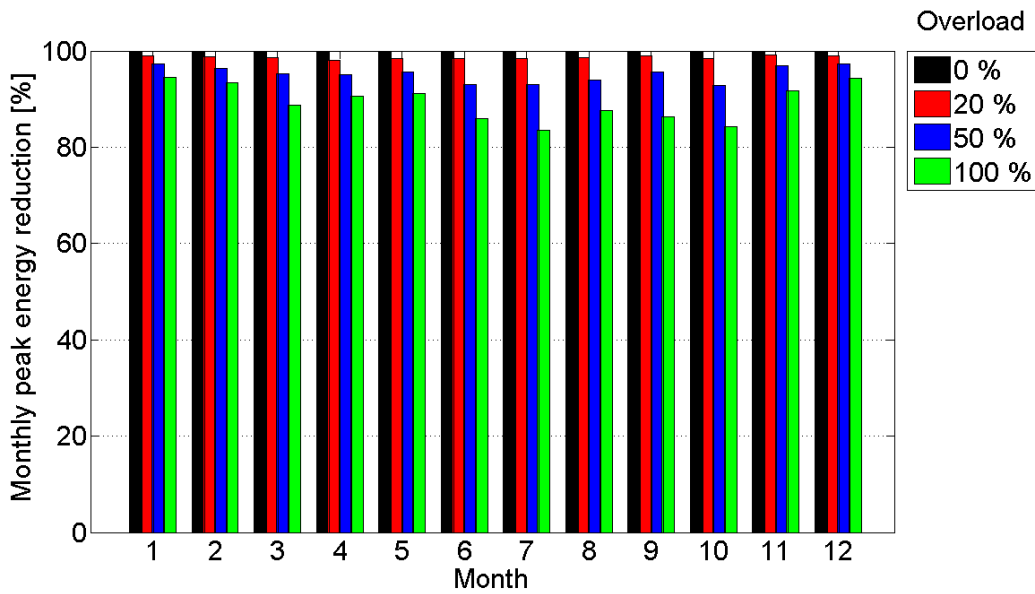


Figure 5.2: Monthly average peak energy reduction  $\bar{P}_{red,month}$  for different percentage of overloads  $\Delta m$ .

Up to an overload  $\Delta m = 20\%$ , the impact is negligible, because the monthly average peak energy reduction never goes below  $\bar{P}_{red,month} = 98\%$ . For a higher  $\Delta m$ , the  $\bar{P}_{red,month}$  becomes lower, because the required hot water demand and the expected hot water demand are too far apart. The  $\bar{P}_{red,month}$  is lower in the winter months, because the solar radiation is lower and therefore the correct control of the auxiliary heater is more important.

The monthly results give information about how the SDHWS works when the average radiation is lower or higher, meaning how the SDHWS works in winter and summer. In the following, the annual average results are analyzed. Figure 5.3 exhibits the annual average solar fraction and the annual average peak reduction  $\bar{P}_{red}$  for different overloads for the developed SDHWS.

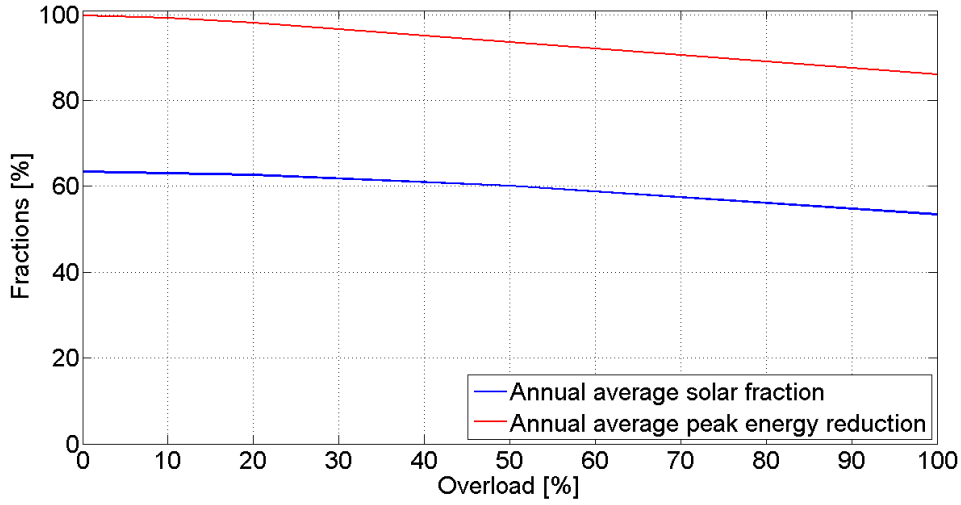


Figure 5.3: Annual average solar fraction  $\bar{f}_{sol}$  and annual average peak energy reduction  $\bar{P}_{red}$  for different overloads  $\Delta m$  of the developed SDHWS.

The  $\bar{f}_{sol}$  and  $\bar{P}_{red}$  are correlated inversely to the overload, in which the solar fraction is less influenced than the peak energy reduction. Both parameters do not regress considerable. Since  $\bar{P}_{red}$  regresses with a higher overload,  $\bar{P}_{red} = 86.1\%$  still applies for a doubled overload. The solar fraction  $\bar{f}_{sol}$  is defined in equation 4.17. Due to the increased hot water demand, the input of cold water to the SDHWS is greater too, therefore the gain of solar energy  $Q_{sol}$  increases, which increases the annual average solar fraction. In contrast, the  $\bar{f}_{sol}$  is reduced due to the higher demand of auxiliary energy. The higher demand of auxiliary energy is the dominant effect influencing the annual average solar fraction. Table 5.1 exhibits the gained solar energy  $Q_{sol}$ , the consumed auxiliary energy of the continuous-flow water heater of the backup loop  $Q_{aux,1}$  and the consumed auxiliary energy of the continuous-flow water heater before the shower head  $Q_{aux,2}$  for different overloads  $\Delta m$ .

Table 5.1: Solar and auxiliary energy for different overloads

$\Delta m$ [%]	$Q_{sol}$ [kWh]	$Q_{aux,1}$ [kWh]	$Q_{aux,2}$ [kWh]
0	833	467	14
50	1153	667	98
100	1350	878	300

This result shows that the developed SDHWS is stable to overloads of the hot water demand and the solar fraction, as well as the peak reduction are not regressing strongly. The main part

of  $Q_{aux,2}$  is does not appear during the peak hours. It is necessary at night between 9 p.m. and 4 a.m. Figure 5.4 exhibits the annual average solar fraction and the annual average peak reduction for different overloads for the reference solar energy system with only one tank of  $V_{c,ref} = 200l$ .

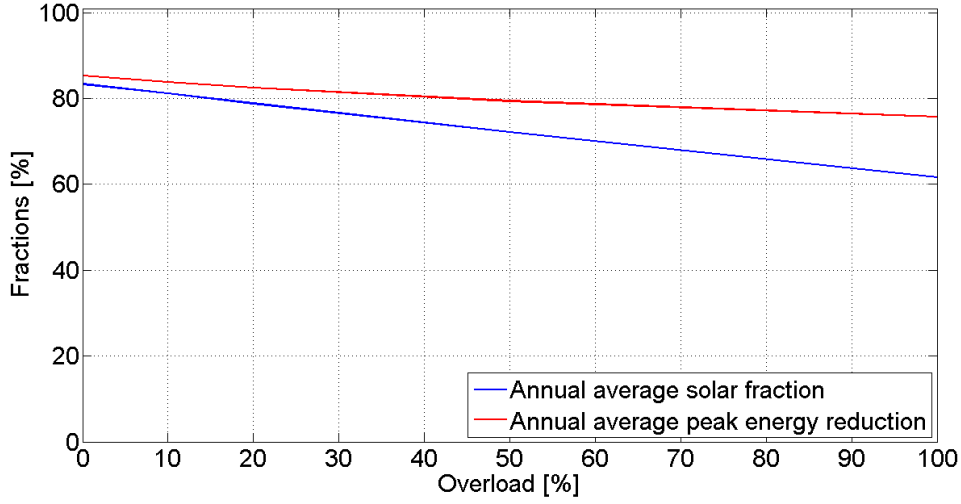


Figure 5.4: Annual average solar fraction  $\bar{f}_{sol,ref}$  and annual average peak energy reduction  $\bar{P}_{red,ref}$  for different overloads  $\Delta m$  for the reference solar energy system.

The  $\bar{P}_{red,ref}$  is nearly constant up to an overload  $\Delta m = 100\%$ . The need of electric energy appears in the days with low solar radiation. The peak energy reduction is a variable normalized to the total energy necessary during the peak hours therefore it does not change due to a higher hot water demand. The  $\bar{f}_{sol,ref}$  regresses due to an higher overload. This shows that the gained of solar energy increased less than the auxiliary energy. The solar fraction could be increased with a greater collector area or a higher collector efficiency.

The days of the year when it is necessary to use electric energy during the peak hours are analyzed in respect to how much electric energy is needed. The energy fraction is defined as the electric energy that is needed during the peak hours divided by the electric energy that would be necessary if the whole amount of water was heated by an electric shower:

$$x_o = \frac{Q_{peak,elec}}{Q_{peak,total}} \quad (5.1)$$

The energy fraction is the inverse peak reduction  $x_o = P_{red}^{-1}$ . The year fraction  $y_0$  is defined as the accumulated days of the year, which have a higher energy fraction. Figure 5.5 exhibits the results for different percentage overloads  $\Delta m$ .

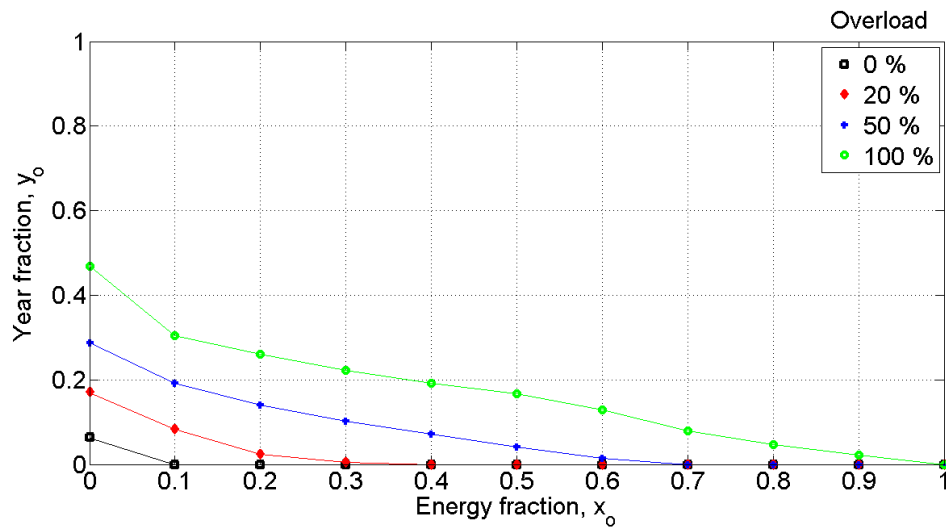


Figure 5.5: Year fraction  $y_o$  over energy fraction  $x_o$  for different overloads  $\Delta m$  of the developed SDHWS.

The result in figure 5.5 indicates for example that 30 % of the days per year require more than 10 % of the total amount of electricity, which would be necessary without the SDHWS during the peak hours for an percentage overload of 100 %.

The energy fraction gives information on how much electric energy is needed during the peak hours for the days that require electric energy, due to an overrated solar radiation. The observation of the results shows that on many days electric energy is required during the peak hours, but just a little percentage of the amount that would be necessary without the SDHWS. This can be concluded from the quick flattening of the curves. In summary, the results show that an overload of hot water demand lowers the peak energy reduction, but the main part of the energy required during the peak hours can still be supported by the SDHWS.

Figure 5.6 shows the year fraction over the energy fraction for different overloads for the reference solar energy system. These results show the big advantage of the developed SDHWS. The curves of the reference solar energy system are not flattening down to zero. This means that there are days that need the total amount of electric energy during the peak hours. This is a huge problem for the national electric system (SIN), which has to provide the electric energy during the peak hours (section 2.2). The developed SDHWS can guarantee to flatten the energy peak. On days with overrated solar radiation the peak reduction decreases. This appears local, according to the local climate and the local overrated solar radiation. As a result, the SIN is not affected.

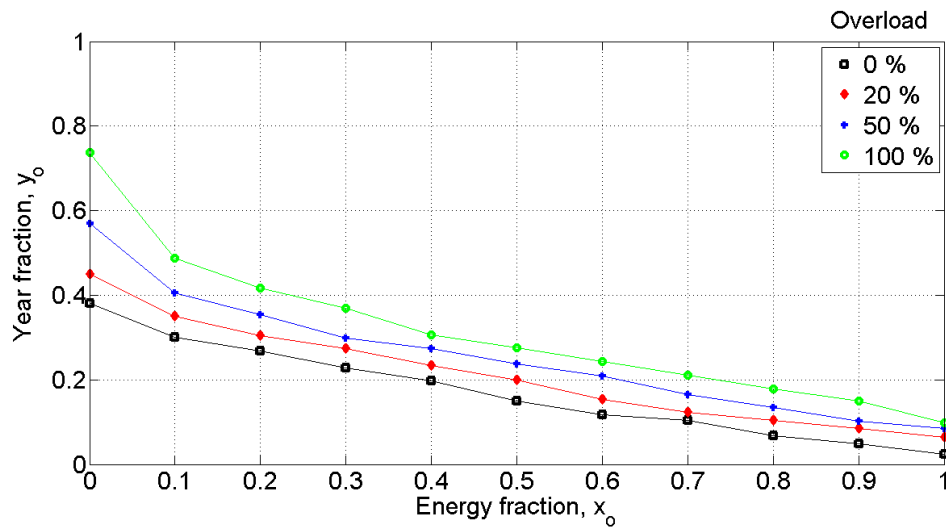


Figure 5.6: Year fraction  $y_o$  over energy fraction  $x_o$  for different overloads  $\Delta m$  of the reference solar energy system.

### 5.3 Results for different cities in Brazil

The developed SDHWS is simulated by using TMY data for different cities all over Brazil. The water supply temperature is set equal to the annual average ambient temperature. The result of interest is the annual average solar fraction  $\bar{f}_{sol}$ . Figure 5.7 shows the locations of the selected cities to analyze. Table 5.2 exhibits  $\bar{f}_{sol}$ , which is the result of the TRNSYS simulation, as well as the latitude, the longitude, the average ambient temperature  $\bar{T}_{amb}$  and the annual amount of solar radiation per square meter in those cities.

### 5.3 RESULTS FOR DIFFERENT CITIES IN BRAZIL

---

The cities are divided into coastline cities and countryside cities, because first the climate depends on the distance from the sea and second the colonization is a lot higher in coastal regions. Therefore, it is important that the developed SDHWS has a good performance in coastline cities. Curitiba has the lowest solar radiation of all analyzed cities, because it is a city in the south with a low average ambient temperature and a high precipitation rate. However, Curitiba still has a higher solar radiation than any German city. The average amount of solar radiation per year in Germany is 900 to 1200  $\frac{kWh}{m^2a}$  whereas in Curitiba it is 1521  $\frac{kWh}{m^2a}$ .

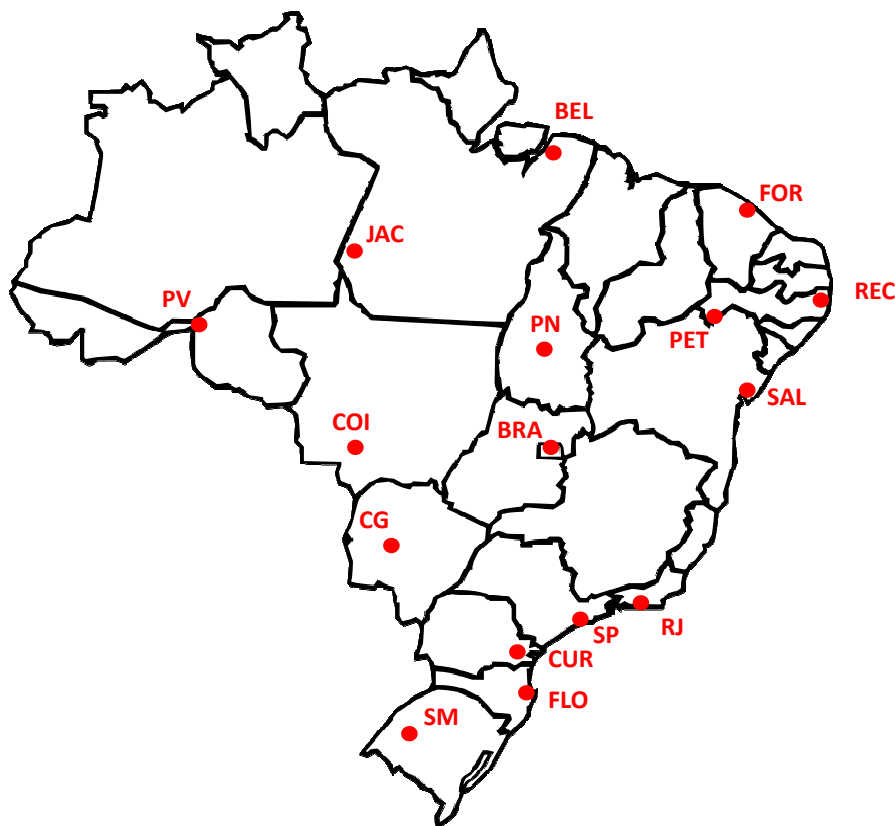


Figure 5.7: Locations of the analyzed cities.

Table 5.2: Data and results of the analyzed cities.

<b>Coastline cities</b>	<b>Latitude [°]</b>	<b>Longitude [°]</b>	$\bar{T}_{amb}$ [°C]	<b>Radiation</b> [ $\frac{kWh}{m^2a}$ ]	$\bar{f}_{sol}$ [%]
Florianópolis (FLO)	S 27.60	W 48.55	20.7	1647	64.69
Curitiba (CUR)	S 25.43	W 49.27	17.2	1521	51.62
São Paulo (SP)	S 23.54	W 46.64	19.5	1679	60.86
Rio de Janeiro (RJ)	S 22.90	W 43.21	24.0	1843	78.84
Salvador (SAL)	S 12.97	W 38.51	25.9	1926	80.03
Recife (REC)	S 8.05	W 34.88	27.1	1980	90.03
Fortaleza (FOR)	S 3.72	W 38.54	27.2	2010	86.48
Belém (BEL)	S 1.46	W 48.50	26.5	1856	79.61
<b>Countryside cities</b>					
Santa Maria (SM)	S 29.68	W 53.80	19.5	1626	58.74
Campo Grande (CG)	S 20.44	W 54.65	24.0	1928	84.78
Cuiabá (CUI)	S 15.60	W 56.09	26.7	1949	90.55
Brasília (BRA)	S 14.24	W 51.93	21.3	1963	78.12
Porto Nacional (PN)	S 10.71	W 48.41	27.1	2078	91.08
Petrolina (PET)	S 9.39	W 40.51	26.8	2076	89.65
Porto Velho (PV)	S 8.76	W 63.90	26.3	1860	83.02
Jacareacanga (JAC)	S 6.28	W 57.65	25.9	1814	79.30

São Paulo, the economic capital of Brazil has a similar solar radiation as Florianópolis, whereas all cities north from São Paulo have a higher solar radiation, regardless of whether they are located in the countryside or the coastal regions. Rio de Janeiro is close to São Paulo, but it already has a significantly higher solar radiation. In fact, it presents similar conditions as Sal-

### 5.3 RESULTS FOR DIFFERENT CITIES IN BRAZIL

vador. Heading up north, the solar radiation only lowers in the cities of the Amazon region, like Belém, because there is less beam radiation due to the high humidity. All cities in the countryside, except Santa Maria, which is far in the south, have a high solar radiation. The climate in the interior of Brazil is comparable to the climate in the desert in the north of Africa. The DESERTEC-Africa organization considers cities with a higher radiation than  $2000 \frac{kWh}{m^2 a}$  as suitable for their project. From the sixteen considered cities in this work, three cities have a higher radiation than  $2000 \frac{kWh}{m^2 a}$  and five are quite close to that value. In fact, Brazil has really good conditions to install solar energy systems.

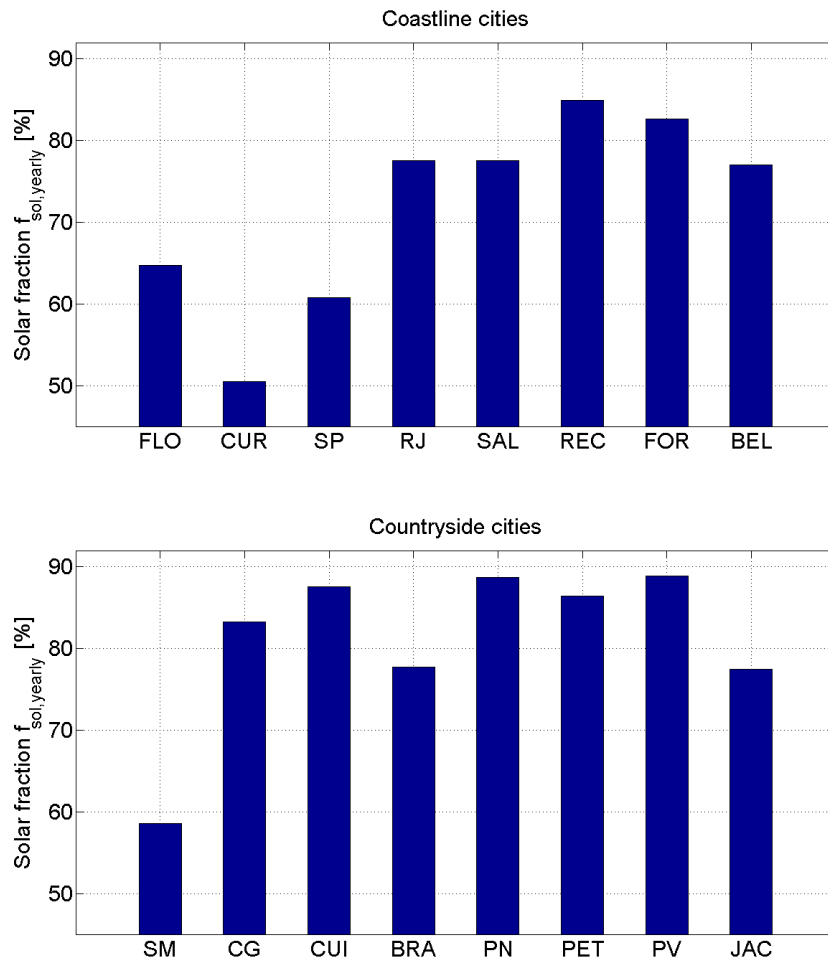


Figure 5.8: Annual average solar fraction  $\bar{f}_{sol}$  of the same SDHWS for different cities.

Figure 5.8 exhibits  $\bar{f}_{sol}$  for the considered cities.  $\bar{f}_{sol}$  is correlated with the intensity of the solar radiation. Almost all analyzed cities reach a higher  $\bar{f}_{sol}$  than Florianópolis, thus these results acknowledge that this work, which mainly analyzes the performance of the SDHWS in Florianópolis, is a worst case study. The conditions for installing SDHWS are really good all over Brazil. The market for SDHWS in the countryside is small, because these regions are less populated. However, this analysis shows that the conditions in the interior for installing solar

energy systems are good, and precisely because the countryside is sparsely populated, the possibilities to install solar power plants are perfect. Until today, only one solar power plant has been mounted in Brazil. It was established by MPX, which is a company of Eike Batista, the wealthiest person of Brazil. The plant is located in Tauá, a city with a high solar radiation close to Fortaleza, Recife and Petrolina.

### 5.4 The designed research facility

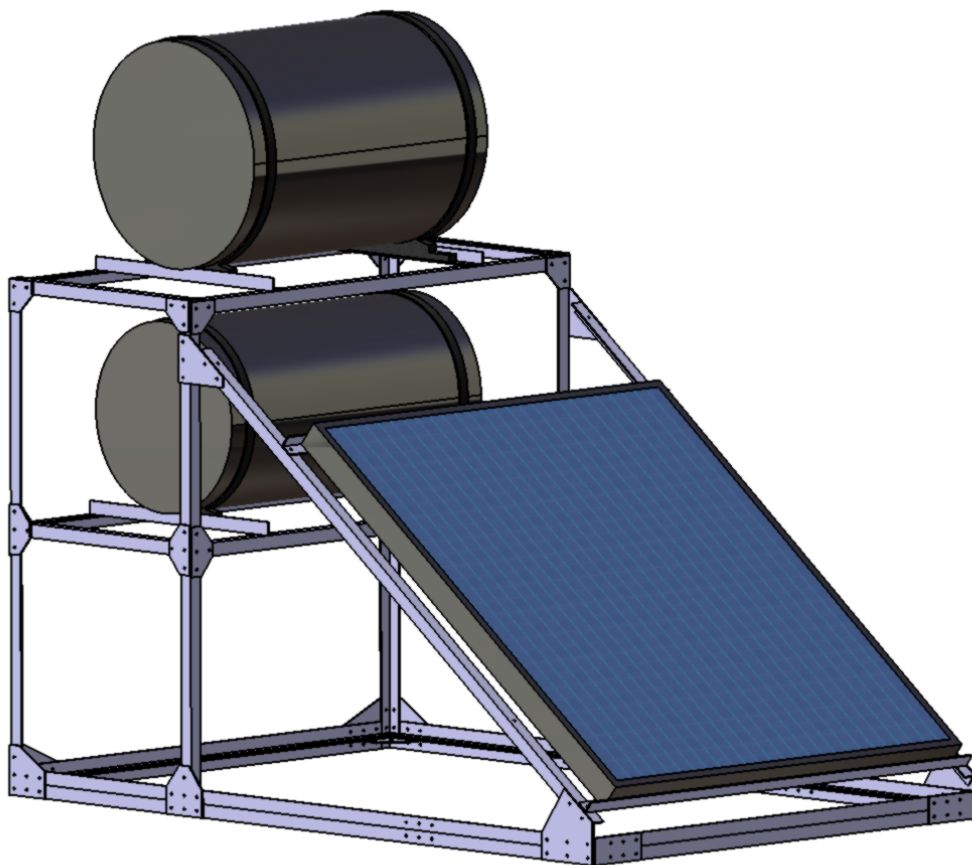


Figure 5.9: Designed research facility.

Based on the results of the performance analysis of the simulation in TRYSYS, a research facility was designed in CATIA V5, which is shown in figure 5.9. The main objective was to make it simple. Hence, the framework only consists of L-sections and brackets to connect the parts just with screws. There is no need of welding. The collector tank is installed higher than the solar collector to run the thermosiphon loop. The backup tank is lower than the collector tank to avoid having to use a pump. The pressure of the water supply system of the building is

sufficient to refill the collector tank. The technical drawings which contain all technical details as well as the assembly drawings can be found in appendix D. The designed research facility is a template to continue this work by doing experimental studies.

## 5.5 Costing

The costing calculations of this section aim at deriving the payback time for different costs of the SDHWS and different electricity tariffs. Currently, the electricity price in Brazil is the same all day long, though this will change in January 2014. The energy peak between 6 p.m. and 9 p.m. (figure 2.4) is a problem for the grid stability, therefore the new electricity tariff should support the shift of the energy peak.

For this work, a regular electricity tariff of  $ET = 0.4 \frac{R\$}{kWh}$  is assumed. Approved by ANEEL (Agência Nacional de Energia Elétrica) in January 2014, the electricity tariff will be five times higher during the peak hours and three times higher one hour before and one hour after the peak hours. The fixed electricity tariff and the variable electricity tariff of the future are compared in the following.

### Case 1: Fixed electricity tariff

The annual amount of energy that is needed to fulfill the hot water demand (figure 4.5) is  $E_{total} = 1310.4 kWh$ . The annual average solar fraction of the developed SDHWS for the city of Florianópolis is  $\bar{f}_{sol} = 64.69\%$ . Thus, the electric energy that is still needed even when the SDHWS is used is  $E_{elec} = 462.7 kWh$ , from which  $E_{peak,1} = 0.37 kWh$  is needed during the peak hours and  $E_{peak,2} = 0.75 kWh$  is needed in the two hours from 5 p.m. to 6 p.m. and from 9 p.m. to 10 p.m. The electric energy that would be needed during these time frames without the use of the SDHWS are  $E_{elec,1} = 322.9 kWh$  and  $E_{elec,2} = 185.6 kWh$ .

The annual saving of money  $\bar{S}_1$  is calculated by subtracting the electricity costs, which still occur while using the SDHWS from the electricity costs without using the SDHWS:

$$\bar{S}_1 = (E_{total} - E_{elec}) \cdot ET = R\$339.08 \quad (5.2)$$

### Case 2: Increased electricity tariff during the peak hours

The calculations are based on the same amounts of energy as in Case 1, whereas now the increased electricity tariff during the peak hours is considered. The annual cost for electricity when the SDHWS is not used,  $\bar{C}_1$  is

$$\bar{C}_1 = (E_{total} - E_{elec,1} - E_{elec,2}) \cdot ET + E_{elec,1} \cdot 5ET + E_{elec,2} \cdot 3ET = R\$1189.28 \quad (5.3)$$

The annual cost for electricity when the SDHWS is used,  $\bar{C}_2$  is

$$\bar{C}_2 = (E_{elec} - E_{peak,1} - E_{peak,2}) \cdot ET + E_{peak,1} \cdot 5ET + E_{peak,2} \cdot 3ET = R\$186.26 \quad (5.4)$$

Thus, the annual saving of money  $\bar{S}_2$  is

$$\bar{S}_2 = \bar{C}_1 - \bar{C}_2 = R\$1003.02 \quad (5.5)$$

$\bar{S}_1$  and  $\bar{S}_2$  are the annual savings of money, calculated for the two considered cases. This is the amount of money that can be saved when the developed SDHWS is used. Hence, depending on the savings and the price of the SDHWS, the payback time can be calculated. The payback time is calculated by considering the time value of money. This means that the sum of the savings has to be even higher than the money that is invested to buy the SDHWS, so that the SDHWS is paid off, because the money invested to buy the SDHWS will not earn any interest. The missed interest must also be covered by the savings, thus the payback time is

$$\sum_{i=1}^{PT} \frac{S}{(1 + IR)^{PT}} = IC \quad (5.6)$$

where PT is the payback time. The interest rate is  $IR = 0.08$  and IC are the initial costs, i. e. the price of the SDHWS. This implicit equation is solved for various ICs. Figure 5.10 shows the results for Case 1 and Case 2.

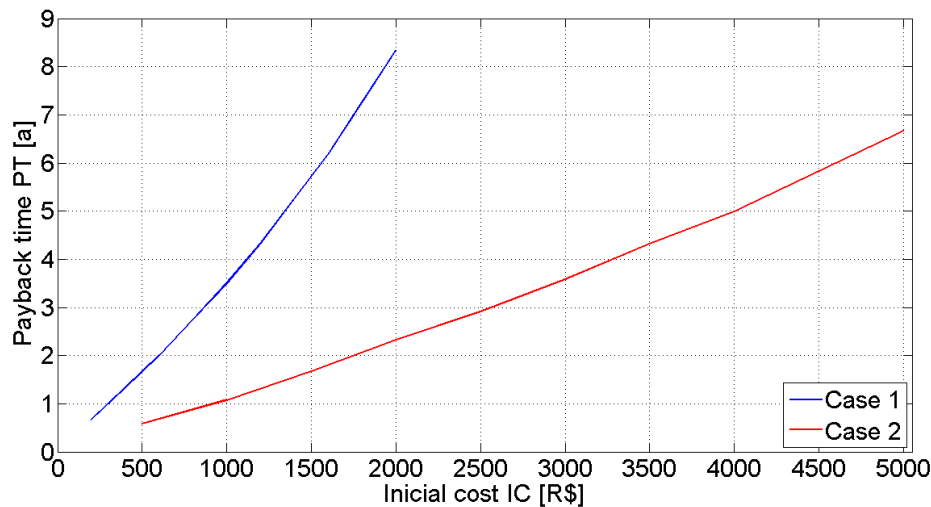


Figure 5.10: Payback time for different initial costs.

The Case 1 scenario, which represents the actual electricity tariff situation, requires a low price of the SDHWS to achieve a short payback time. The developed SDHWS is designed to cut the energy peak therefore it consists of two tanks to guarantee no usage of electricity during the peak hours. The price for such a SDHWS will be about R\$ 2000, which results in a bearable payback time of 2.4 years for case 2. This SDHWS is designed to cut the energy peak, therefore this system has no advantage in respect to higher annual savings in the case 1 scenario. From the point of view of an investor, a SDHWS designed for a case 1 scenario does not need to cut the energy peak, because the electricity tariff is the same all day long. It just needs to have a high annual average solar fraction to increase the annual savings of money. Such a system just

needs one tank, so the price goes down. It would be conceivable that a simple SDHWS which does not guarantee to cut the energy peak costs about R\$ 1000, which results with respect to case 1 in a payback time of 3.5 years.

The comparison of  $\bar{S}_1$  and  $\bar{S}_2$  exhibits the savings in electricity costs for a consumer that uses the SDHWS before January 2014 and after January 2014. In contrast, the electricity costs for a consumer that uses an electric shower are going to increase more than six times due to the change of the electricity tariff. This enormous increase of electricity costs are not realizable, therefore according to my opinion ANEEL has to lower the regular electricity tariff to implement a five times higher electricity tariff during the peak hours. As a result the costs for electricity for a consumer who uses an electric shower head would just increase a little, but the consumer could save a lot if he uses a SDHWS. Finally, this comparison shows that when the electricity tariff is going to change in January 2014, a SDHWS which guarantees to cut the energy peak, can be paid off quite fast, because the electricity costs during the peak hours will increase strongly.

## 6 Conclusion

The present work is the development of a solar domestic hot water system controlled by weather forecast information, which can guarantee to minimize the energy peak from 6 p.m. to 9 p.m. The energy peak is caused to about 43 % by the intensive use of electric shower heads. The widespread use of the developed SDHWS can provide a significant contribution to flatten the energy peak and therefore stabilize the national electrical system SIN (Sistema Interligado Nacional) as well as minimize the power, which is set aside just to provide enough electric energy during the peak hours.

The results of the simulation with the transient simulation software TRYNYSYS of the SDHWS using TMY data for the city of Florianópolis exhibit that the annual average peak energy reduction for an average consumer is 99.8 %. In other words, the developed SDHWS guarantees to go by without almost any electric energy during the peak hours. The energy is provided by the SDHWS by making use of the incident solar radiation with a thermosiphon solar energy system. On days with low solar radiation, the backup tank is heated in the morning when the demand of electric energy is low. This is controlled by self-generated weather forecast information. The well insulated backup tank stores this energy until the peak hours. The further analysis of an percentage overload on the average hot water demand shows that for an overload of 100 % the peak energy reduction still is 86.1 %. This shows that the developed SDHWS is stable against different consumer profiles.

The SDHWS was simulated with TMY data of 16 different cities all over Brazil. The criterion of the annual average solar fraction was used to compare the results. The analysis shows that the high solar radiation all over Brazil results in a high annual average solar fraction in the analyzed cities. Brazil has a high solar radiation, up to more than  $2000 \frac{kWh}{m^2 a}$ , which is approximately twice the maximum solar radiation in Germany. The intelligent algorithm which controls the auxiliary heating of the backup tank, based on the self-generated weather forecast data, makes the SDHWS suitable to all cities of Brazil, i. e. to different solar radiation climates.

The annuals saving of money using the SDHWS in comparison to the use of a common electric shower head were calculated. The calculations were done for the actual and the planned electricity tariff from January 2014, which will be higher during the peak hours. Based on the annual savings of money, the payback time was calculated for different costs of the SDHWS. The results show that for the planned electricity tariff in January 2014, the annual savings of money using the developed SDHWS become a lot higher, because the saving caused by avoiding to use electricity during the peak hours are significant. The resulting short payback time could convince many people to invest in a SDHWS, which guarantees to minimize the use of electric energy during the peak hours all year long.

## Conclusion

---

Further researches, based on the simulation done in this work, should be made. The corresponding research facility has already been designed and is a template to start experimental studies. The TRYNSYS model of the SDHWS has to be validated by experiments. Furthermore, the distribution of the water supply temperature should be derived from experiments. The Brazilian water supply pipes are not reliable, therefore huge water reservoirs are installed in all houses. The temperature of the water reservoir depends on the location where it is mounted, i.e. if the location is sunny or shady. The annual average solar fraction is hardly influenced of the water supply temperature, whereas the absolute values of gained solar energy and necessary electric energy are strongly influenced.

The present work was the first step to implement a SDHWS in the Brazilian energy matrix. Electric showers are an obsolete technology and this work showed the possibilities to replace them by a SDHWS. The LEPTEN of the Universidade Federal de Santa Catarina has the possibilities to continue this research project. The installation of a research facility to do experimental studies will be the next step.

# Bibliography

- [1012] *GoGreen Heat Solutions*. <http://gogreenheatsolutions.co.za/project-type/solar-water-heating/flat-plate-collector>, 2012.
- [1412] *Geographic information system*. National renewable energy laboratory (NREL), 2012.
- [310] *Brazilian Energy Balance, Final Report*. Ministério de Minas e Energia - MME e Empresa de Pesquisa Energética - EPE, 2010.
- [708] *Pesquisa de posse de equipamentos e hábitos de uso*. PROCEL, 2008.
- [808] *O mercado de aquecimento solar e as perspectivas para Brasil*. ABRAVA, 2008.
- [BH09] Kapelac S. Baehr H. *Thermodynamik*. Springer, 2009.
- [BJ] Christensen C. Burch J. *Towards development of an algorithm for mains water temperature*. National renewable energy laboratory (NREL).
- [CS01] Abreu S. Colle S. *Optimization of the Auxiliary Heating and Water Storage Insulation of a Low Cost Domestic Hot Water Heating System with an Electric Shower*. ISES Solar World Congress, 2001.
- [CS10] Starke A. Colle S. *Uma análise de sistemas de aquecimento solar de água para uso doméstico no Brasil*. Congresso Brasileiro de Energia Solar, 2010.
- [DJ06] Beckman W. Duffie J. *Solar Engineering of Thermal Processes*. John Wiley & Sons, Inc, 2006.
- [Duf11] M. Duffy. *TRNSYS 17, Mathematical Reference*. <http://sel.me.wisc.edu/trnsys/>, 2011.
- [Ide96] I. Idelchik. *Handbook of Hydraulic Resistance*. Begell House, 1996.
- [Kra12] M. Kratzenberg. *Previsão da radiação solar com redes neurais wavelet e sua aplicação na redução da potência dos chuveiros elétricos no horário de pico com um sistema inteligente de aquecimento solar*. Universidade Federal de Santa Catarina, PhD thesis, 2012.
- [LP06] Manz H. Loutzenhiser P. *Empirical validation of models to compute solar irradiance on inclined surfaces for building energy simulation*. Science Direct, 2006.

- 
- [Pas11] L. Passos. *Um estudo sobre os impactos técnicos e econômicos da agregação do aquecimento solar de água nos domicílios brasileiros*. Universidade Federal de Santa Catarina, Master Thesis, 2011.
- [PE06] Martins F. Pereira E. *Atlas Brasileiro de Energia Solar*. 2006.
- [PW09] Kopitz J. Polifke W. *Wärmeübertragung: Grundlagen, analytische und numerische Methoden*. Pearson Studium, 2009.
- [Sal04] J. Salazar. *Economia de energia e redução do pico da curva de demanda para consumidores de baixa renda por agregação de energia solar térmica*. Dissertação da Universidade Federal de Santa Catarina, Engenharia Mecânica, 2004.
- [Spi11] M. Spinnler. *Solar Engineering*. Technische Universität München, Department of thermodynamics, Lecture documents, 2011.

# A Parameters and dimensions of the developed SDHWS

Table A.1: Parameters of the solar collector and the collector tank.

<b>Label</b>	<b>Symbol</b>	<b>Value</b>	<b>Unit</b>
Intercept efficiency	$F_R(\tau\alpha)_n$	0.73	–
Efficiency slope	$F_R U_L$	19.3	$\frac{W}{m^2 K}$
Tested flow rate	$\dot{M}_{test}$	60	$\frac{kg}{hm^2}$
Incidence angle modifier constant	$b_0$	0.163	–
Number of collector nodes	$N_x$	20	–
Pipe loss coefficient	$U_p$	0.56	$\frac{W}{m^2 K}$
Specific heat of water	$c_p$	4.19	$\frac{kJ}{kgK}$
Fluid density	$\rho_{H_2O}$	1000	$\frac{kg}{m^3}$
Thermal conductivity	$k_{H_2O}$	0.56	$\frac{W}{mK}$

Table A.2: Dimensions of the solar collector and the collector tank.

<b>Label</b>	<b>Symbol</b>	<b>Value</b>	<b>Unit</b>
Collector area	$A_c$	2.025	$m^2$
Collector slope	$\beta$	37.6	$^\circ C$
Number of parallel collector risers	$NR$	<i>Formel</i>	–
Riser diameter	$D_{riser}$	0.0142	$m$
Header diameter	$D_{header}$	0.027	$m$
Header length	$L_{header}$	1.46	$m$
Collector inlet to outlet distance	$H_c$	0.85	$m$
Collector inlet to tank outlet distance	$H_o$	0.85	$m$
Collector inlet diameter	$D_{in}$	0.015	$m$
Length of collector inlet	$L_{in}$	1.52	$m$
Number of inlet bends	$NB_{in}$	4	–
Collector outlet diameter	$D_{out}$	0.019	$m$
Length of collector outlet	$L_{out}$	0.32	$m$
Number of outlet bends	$NB_{out}$	4	–
Tank volume	$V_c$	130	$l$
Tank diameter	$D_c$	0.44	$m$
Height of collector return	$H_r$	0.26	$m$

Table A.3: Parameters of the backup tank, the continuous-flow water heater and the pump of the heating loop.

<b>Label</b>	<b>Symbol</b>	<b>Value</b>	<b>Unit</b>
Tank volume	$V_b$	70	[l]
Tank diameter	$D_b$	0.35	<i>m</i>
Flow rate	$\dot{m}_{loop}$	0.56	$\frac{kg}{s}$
Maximum heating rate	$\dot{Q}_{max}$	2000	<i>W</i>

## B TMY Typical Meteorological Year

```

<userdefined>
<longitude> 48.5
<latitude> -27.6
<gmt> -3
<interval> 1
<firsttime> 1
<var> IGLOB_H <col> 4 <interp> 0 <add> 0 <mult> 1 <samp> -1 !...to get radiation in W/m²
<var> IBEAM_H <col> 5 <interp> 0 <add> 0 <mult> 1 <samp> -1 !...to get radiation in W/m²
<var> IDIFF_H <col> 6 <interp> 0 <add> 0 <mult> 1 <samp> -1 !...to get radiation in W/m²
<var> TAMB <col> 8 <interp> 2 <add> 0 <mult> 1 <samp> 0 !...to get °C
<var> RHUM <col> 9 <interp> 1 <add> 0 <mult> 1 <samp> 0 !...to get rel. hum. in %
<var> udef1 <col> 7 <interp> 0 <add> 0 <mult> 1 <samp> -1 !...to get ... in ...
<data>
1 1 1 0 0 0 0 23.47 74.23
1 1 2 0 0 0 0 22.98 77.41
1 1 3 0 0 0 0 22.42 80.63
1 1 4 0 0 0 0 22 83.3
1 1 5 0 0 0 0 21.71 84.96
1 1 6 11.57 1.47 11.2 49.26 21.48 86.01
1 1 7 144.13 347.4 61.5 322.69 22.92 80.98
1 1 8 388.9 638 122.83 617.93 25.39 73.13
1 1 9 563.1 557.27 225.37 888.57 27.07 59.87
1 1 10 684.87 422.53 345.73 1116.17 28.87 52.57
1 1 11 779.97 344.8 450.97 1285.22 29.09 53.21
1 1 12 839.47 266.43 560.2 1384.18 27.27 60.2
1 1 13 788.47 190.5 572.67 1406.33 26.51 61.36
1 1 14 878.7 353.17 519.5 1350.15 26.36 59.05
1 1 15 768.67 326.67 446.93 1219.47 26.47 56.97
1 1 16 428.27 77.47 355.13 1023.19 25.04 60
1 1 17 245.53 1.33 238.5 774.69 23.74 64.8
1 1 18 93.93 0 92.3 490.91 22.76 69.51
1 1 19 38.13 0 36.73 191.19 22.2 71.43
1 1 20 1.47 0.5 0.97 2.85 21.91 72.45
1 1 21 0 0 0 0 21.79 73.25
1 1 22 0 0 0 0 21.74 73.2
1 1 23 0 0 0 0 21.87 72.24
1 1 24 0 0 0 0 21.79 72.13
1 2 1 0 0 0 0 21.49 73.09
1 2 2 0 0 0 0 21.87 70.62
. . . . .
. . . . .
. . . . .

```

Figure B.1: Cutout of one day of a TMY text file

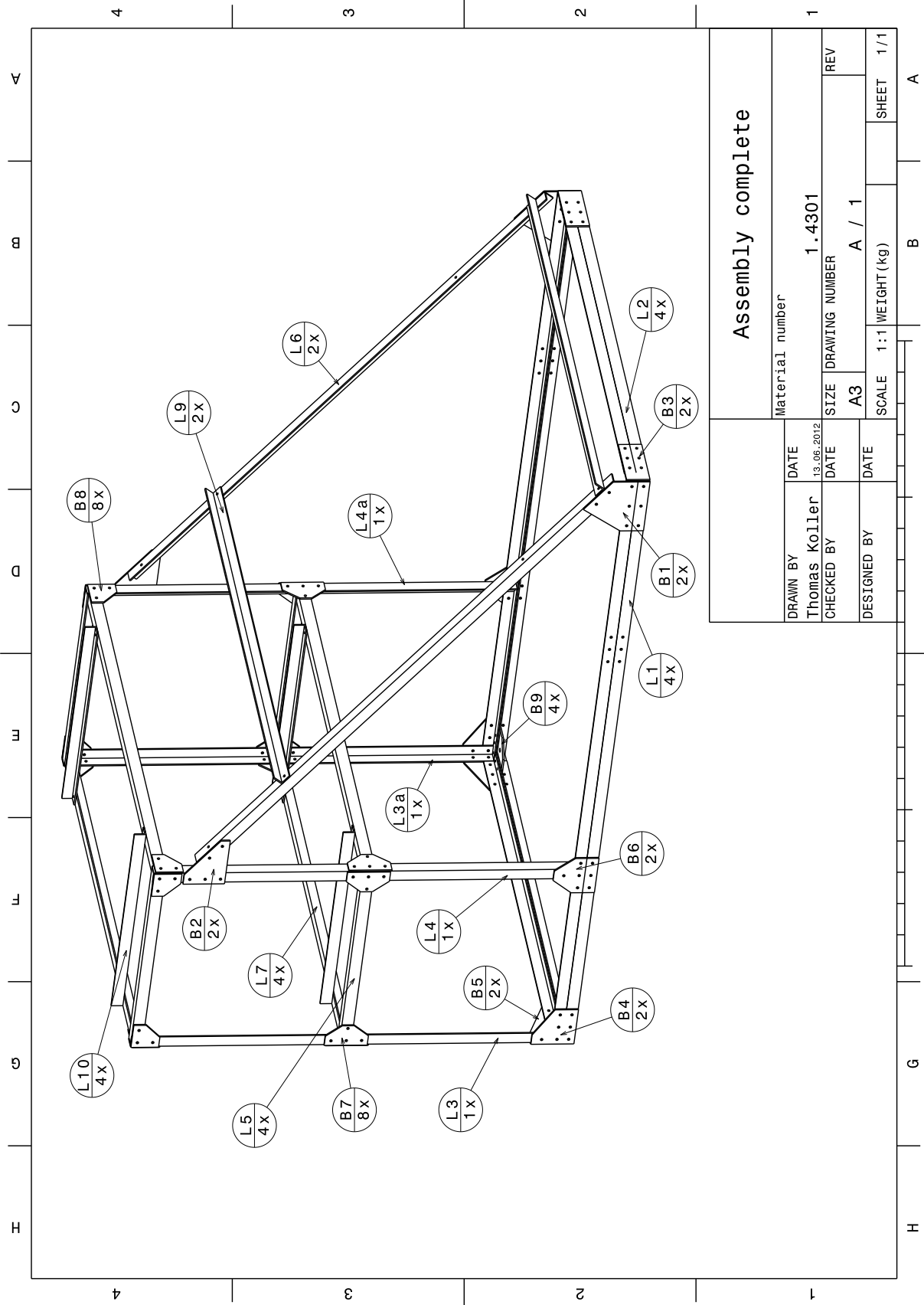
## **C Translation of Portuguese words used in this work**

Horas	-	Hours
Valores	-	Values
Microondas	-	Microwave
TV	-	Television
Lava Roupa	-	Washing machine
Ar Condicionado	-	Air conditioner
Ferro	-	Electric iron
Chuveiro	-	Shower
Geladeira	-	Fridge
Som	-	Speaker
Lampadas	-	Light

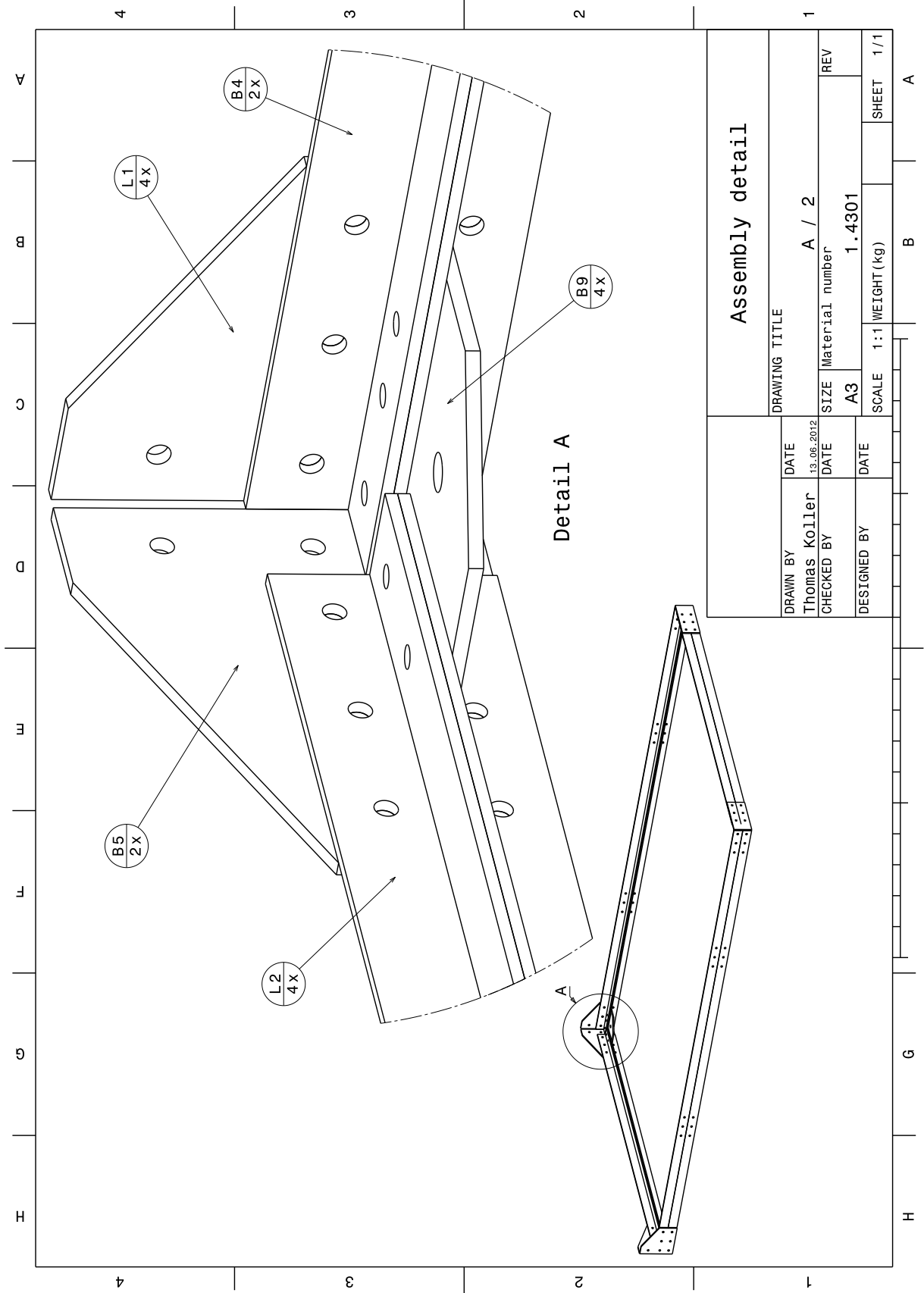
# **D Technical drawing of the designed research facility**

## **D.1 Assembly**

D.1 ASSEMBLY

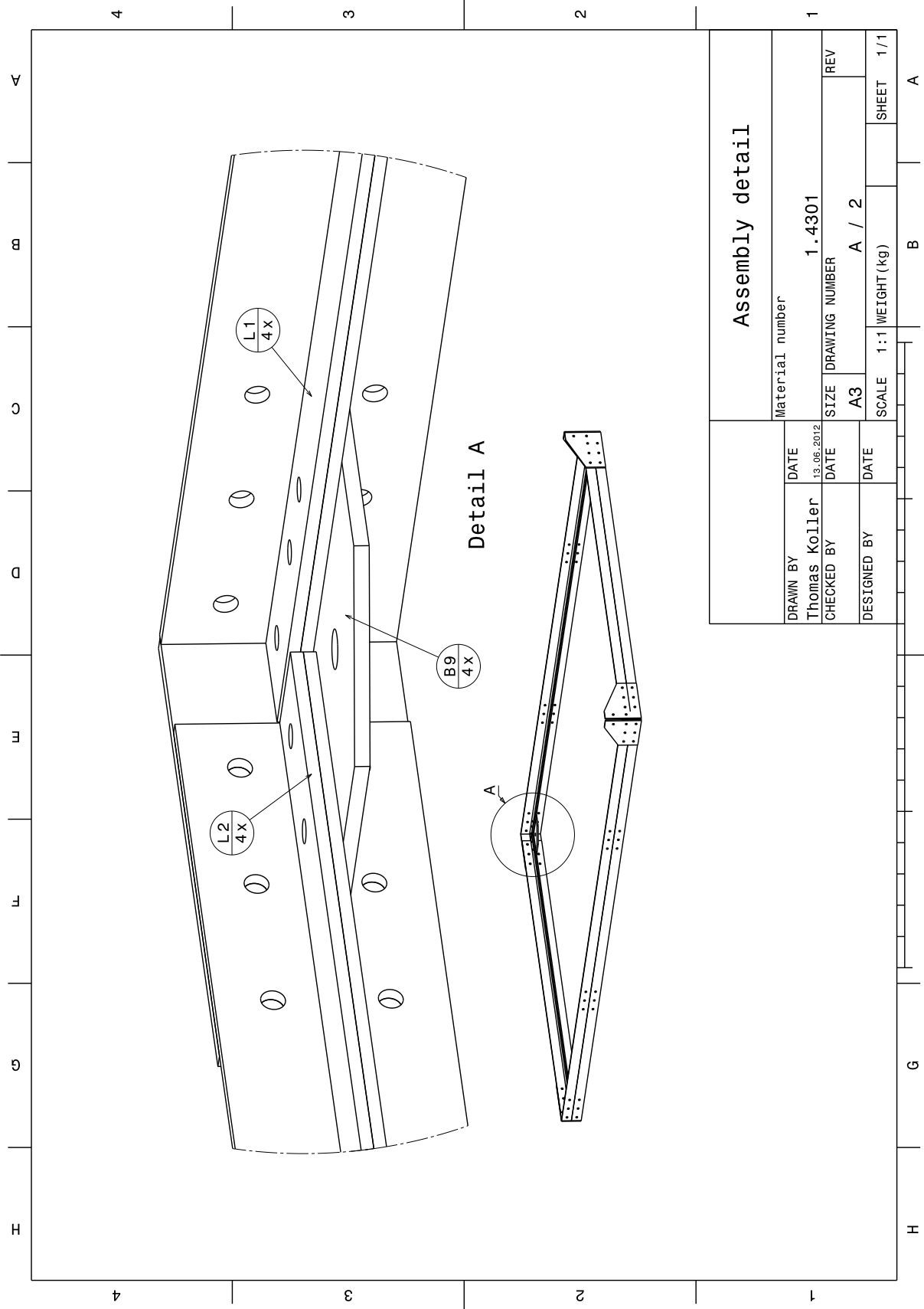


D.1 ASSEMBLY



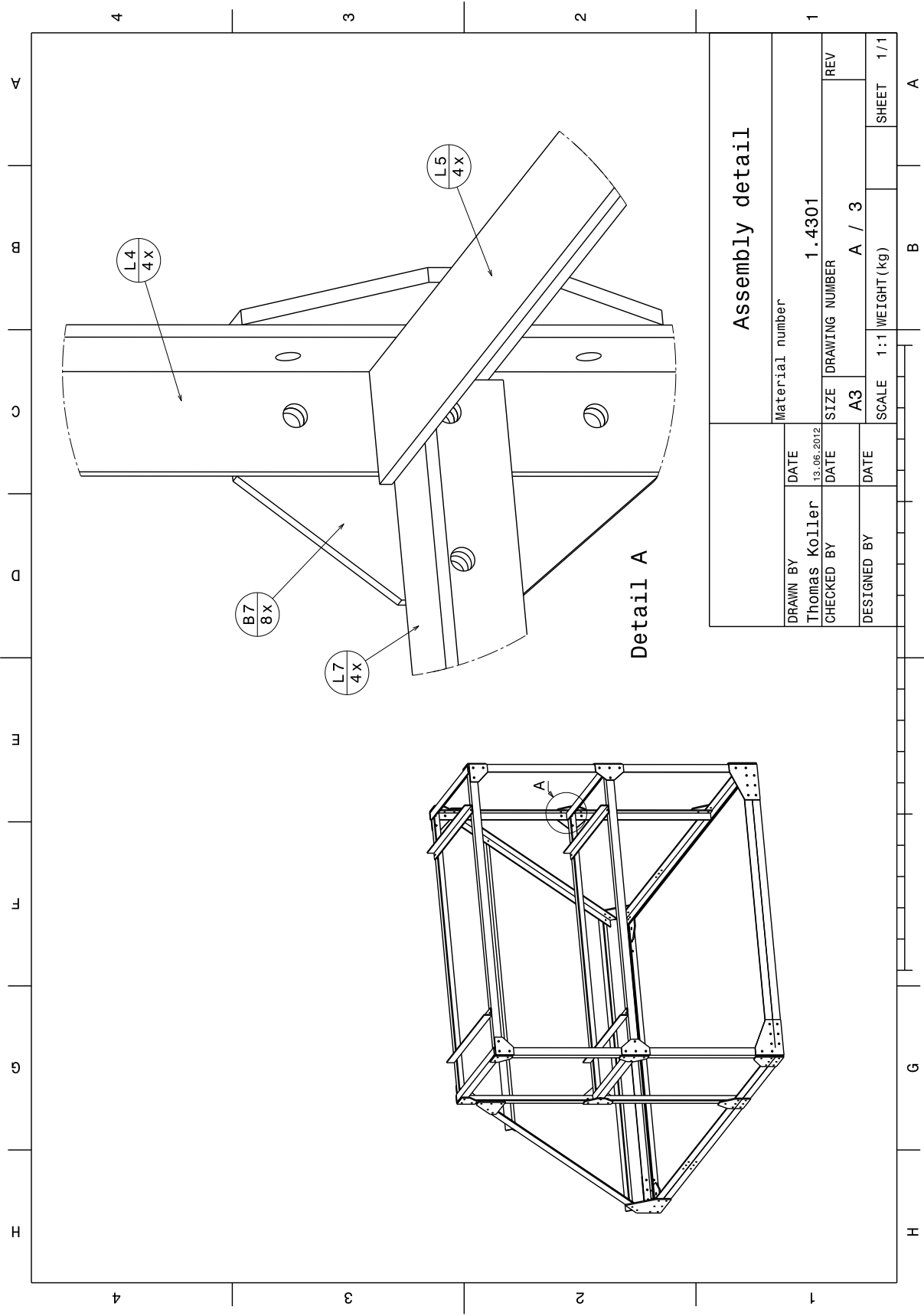
<b>Assembly detail</b>		DRAWING TITLE	
DRAWN BY	DATE	A / 2	
Thomas Koller	13.06.2012	SIZE	Material number
CHECKED BY	DATE	A3	1.4301
DESIGNED BY	DATE	SCALE	1:1 WEIGHT(kg)
			SHEET 1/1

D.1 ASSEMBLY



DRAWN BY		DATE	Material number	
Thomas Koller		13.06.2012	1.4301	
CHECKED BY	DATE	SIZE	DRAWING NUMBER	REV
		A3	A / 2	
DESIGNED BY	DATE	SCALE	WEIGHT(kg)	SHEET
		1:1		1/1

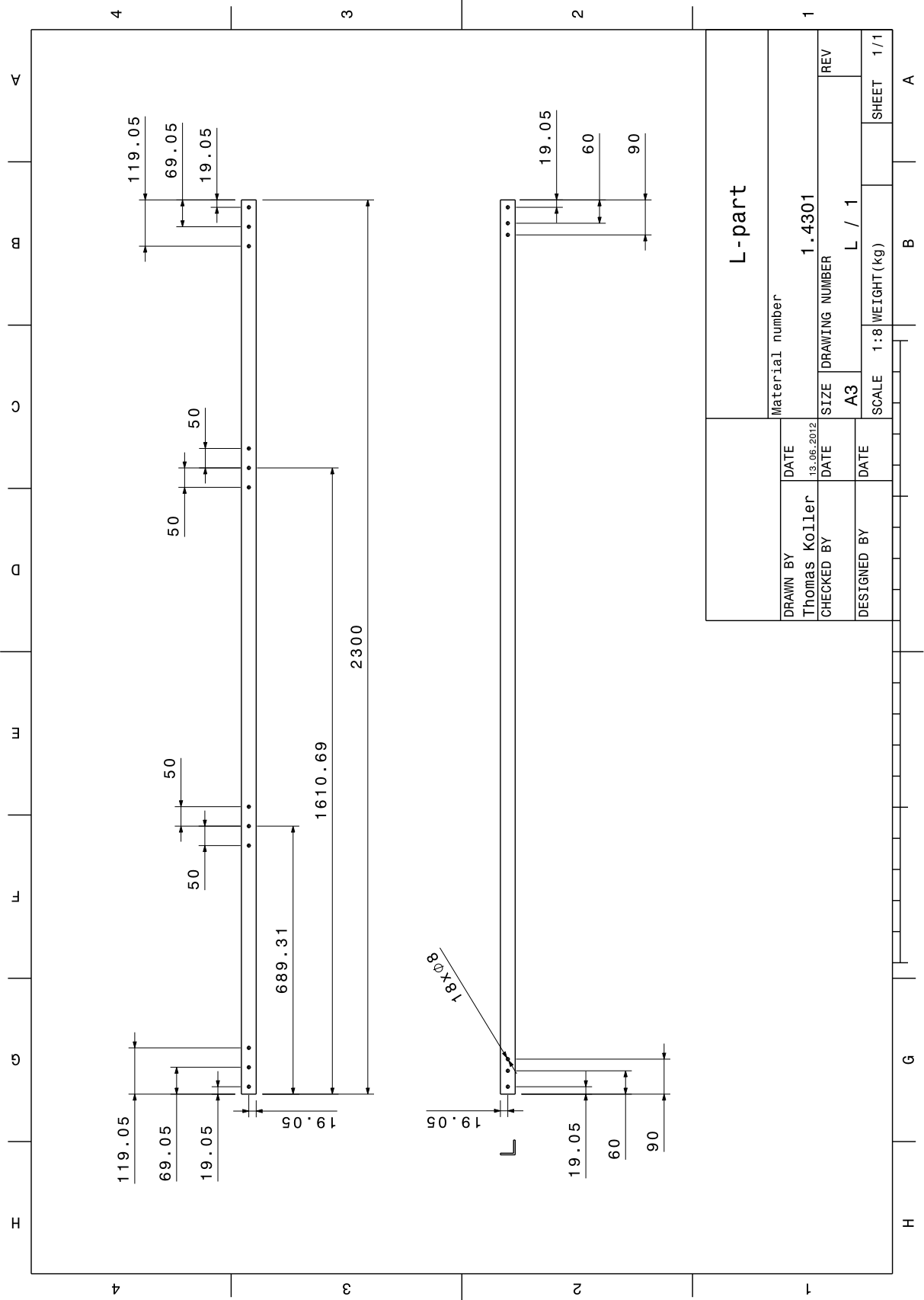
D.1 ASSEMBLY



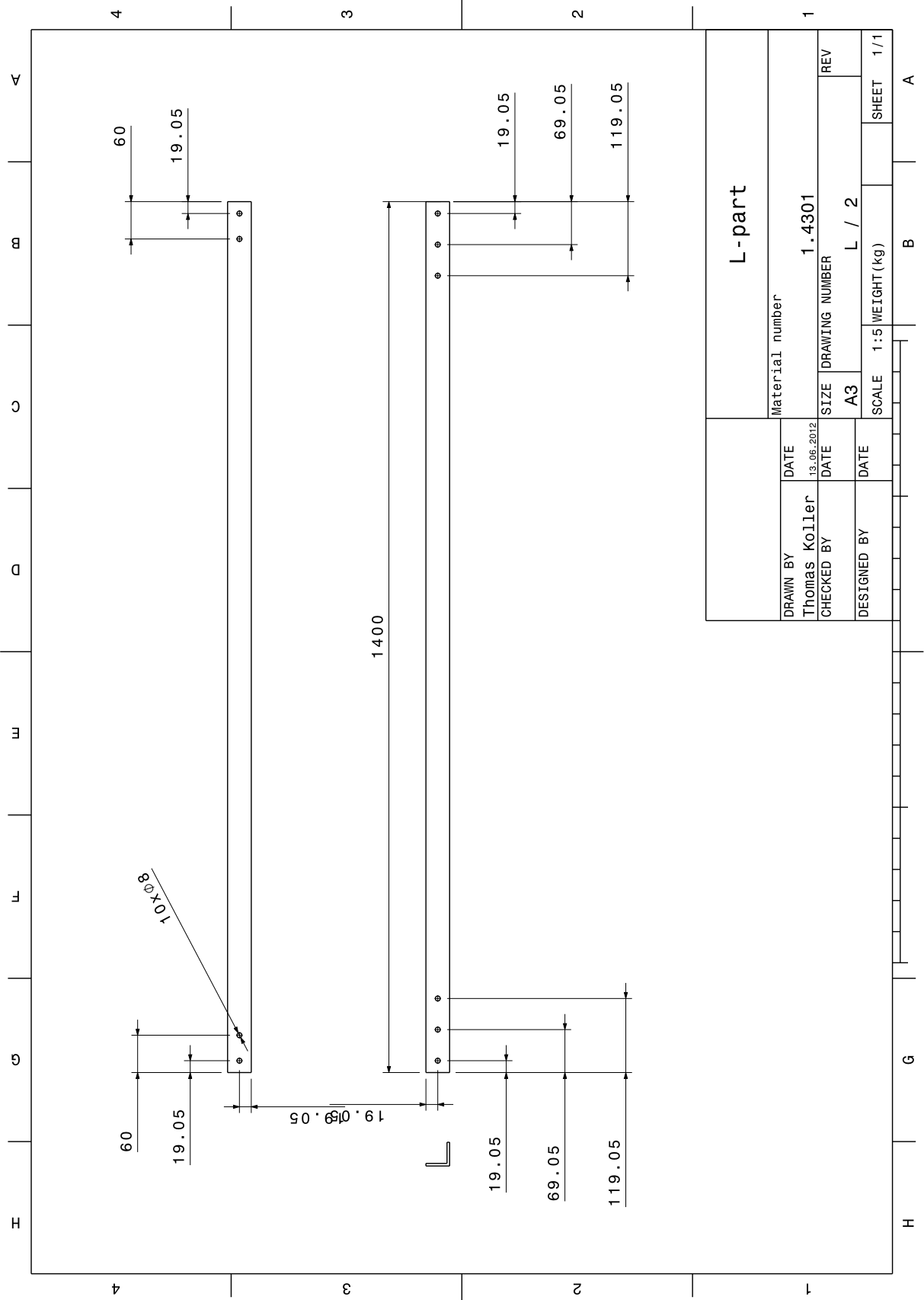
Assembly detail			
DRAWN BY	DATE	Material number	
Thomas Koller	13.06.2012	1.4301	
CHECKED BY	DATE	SIZE	DRAWING NUMBER
		A3	A / 3
DESIGNED BY	DATE	SCALE	1:1 WEIGHT(kg)
			SHEET 1/1

## **D.2 L-parts**

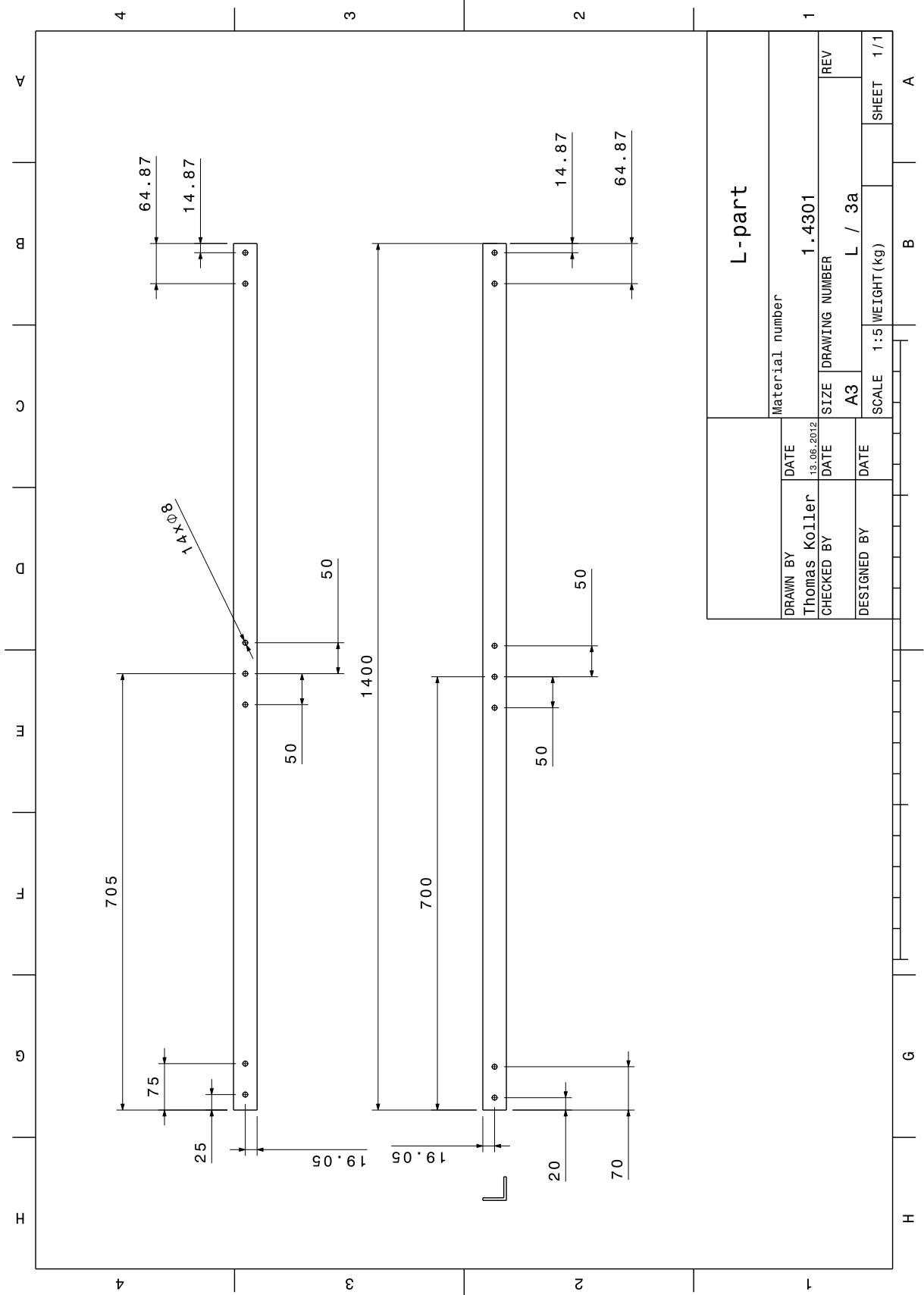
D.2 L-PARTS



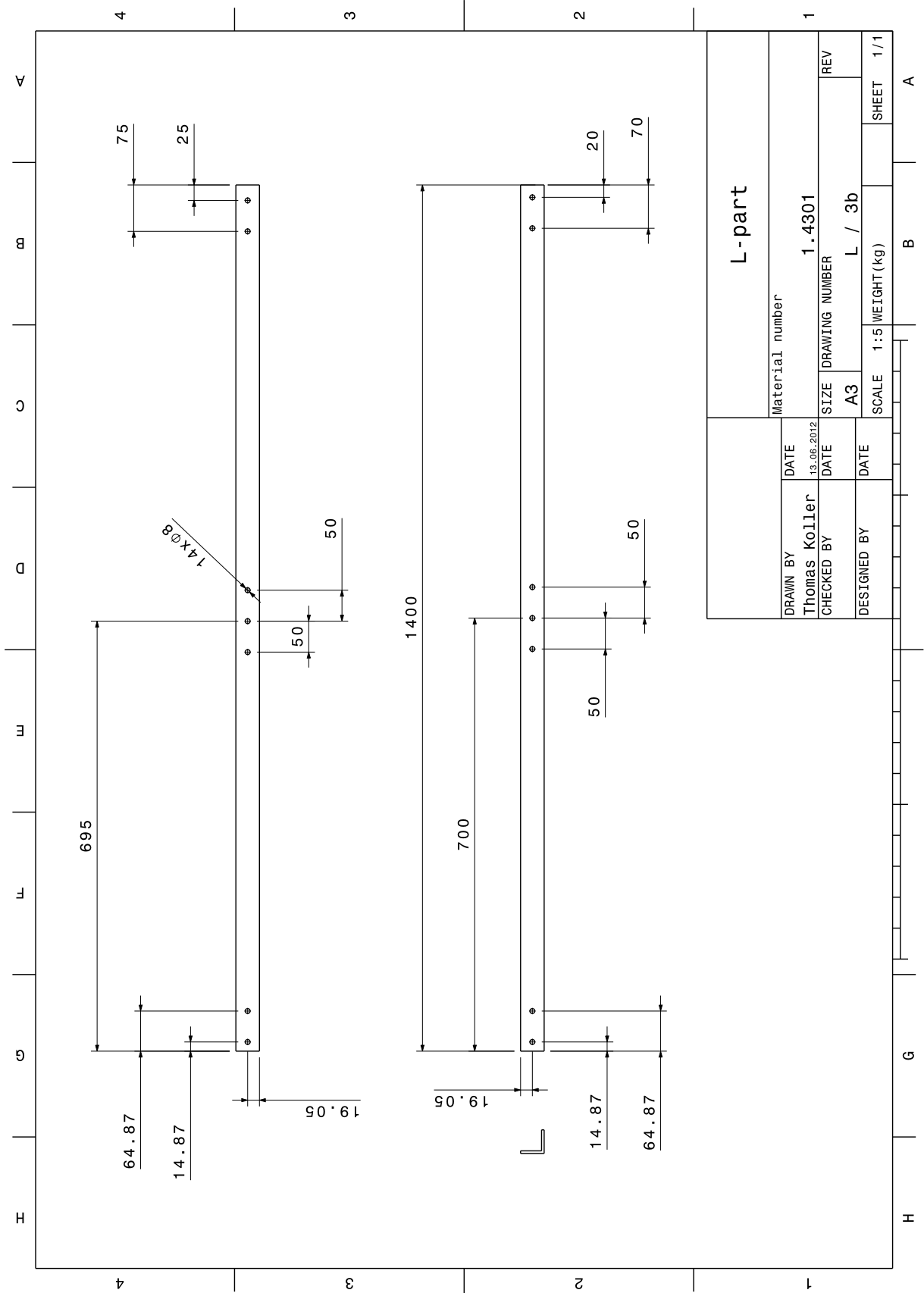
D.2 L-PARTS



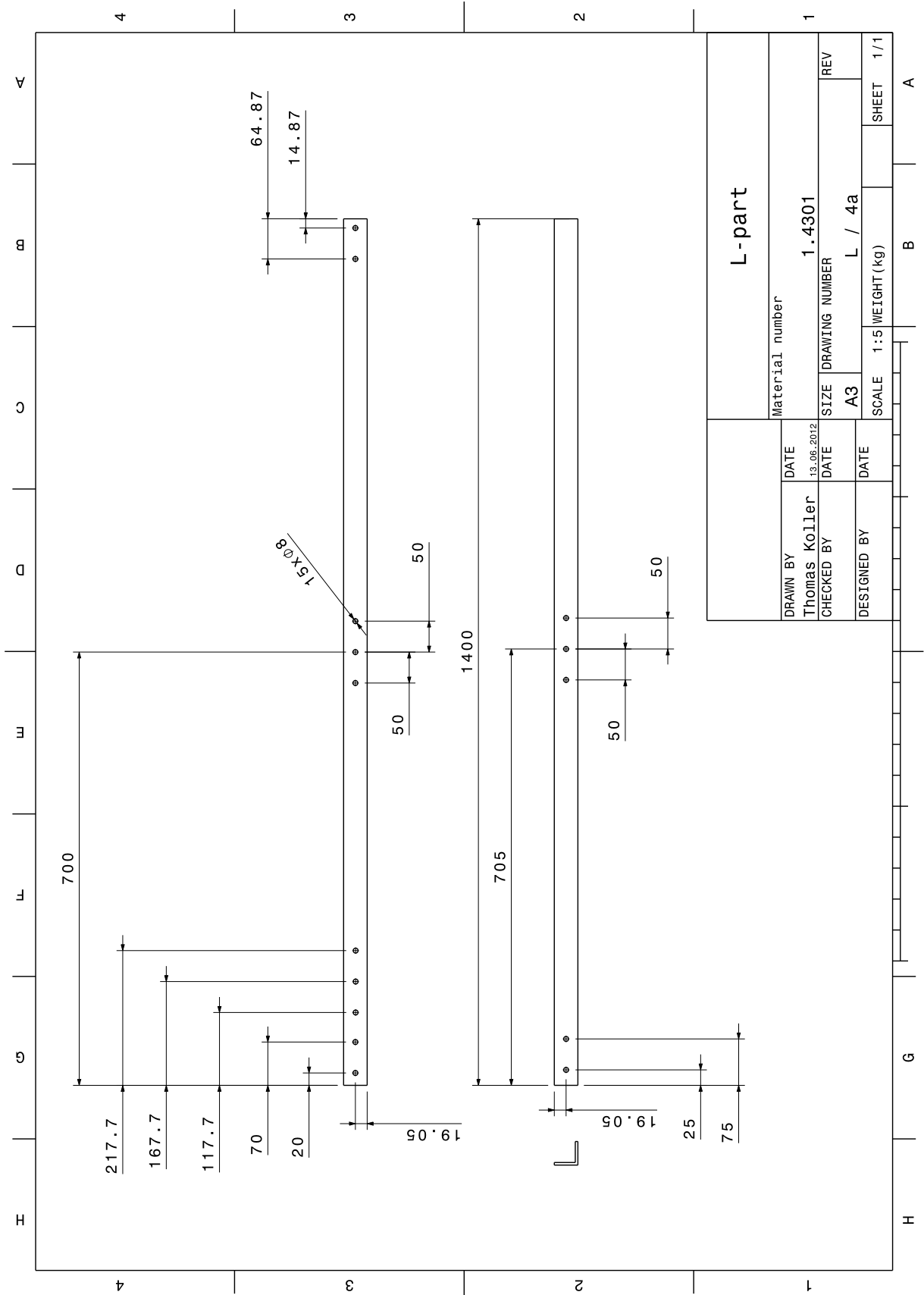
D.2 L-PARTS



D.2 L-PARTS

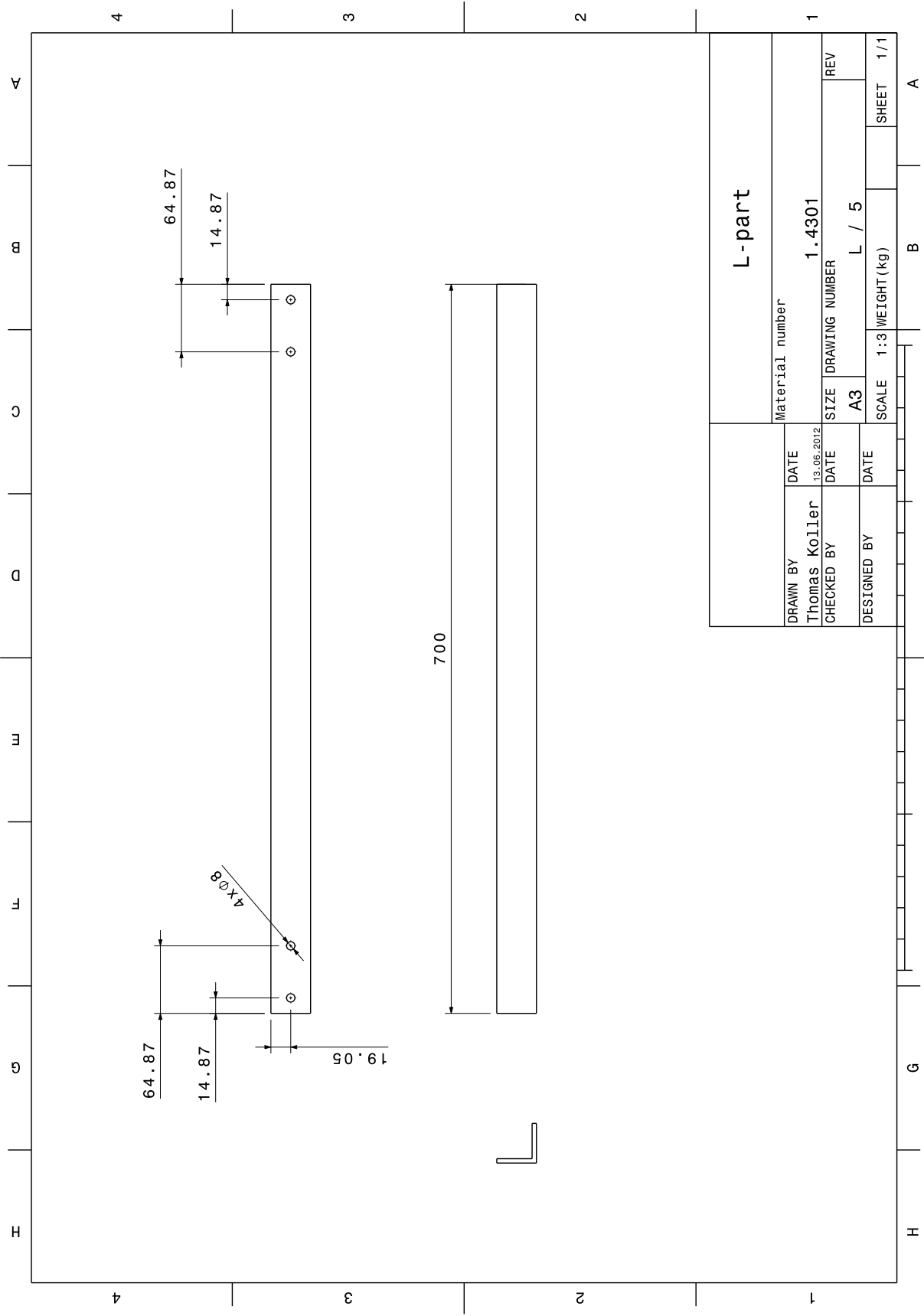


D.2 L-PARTS

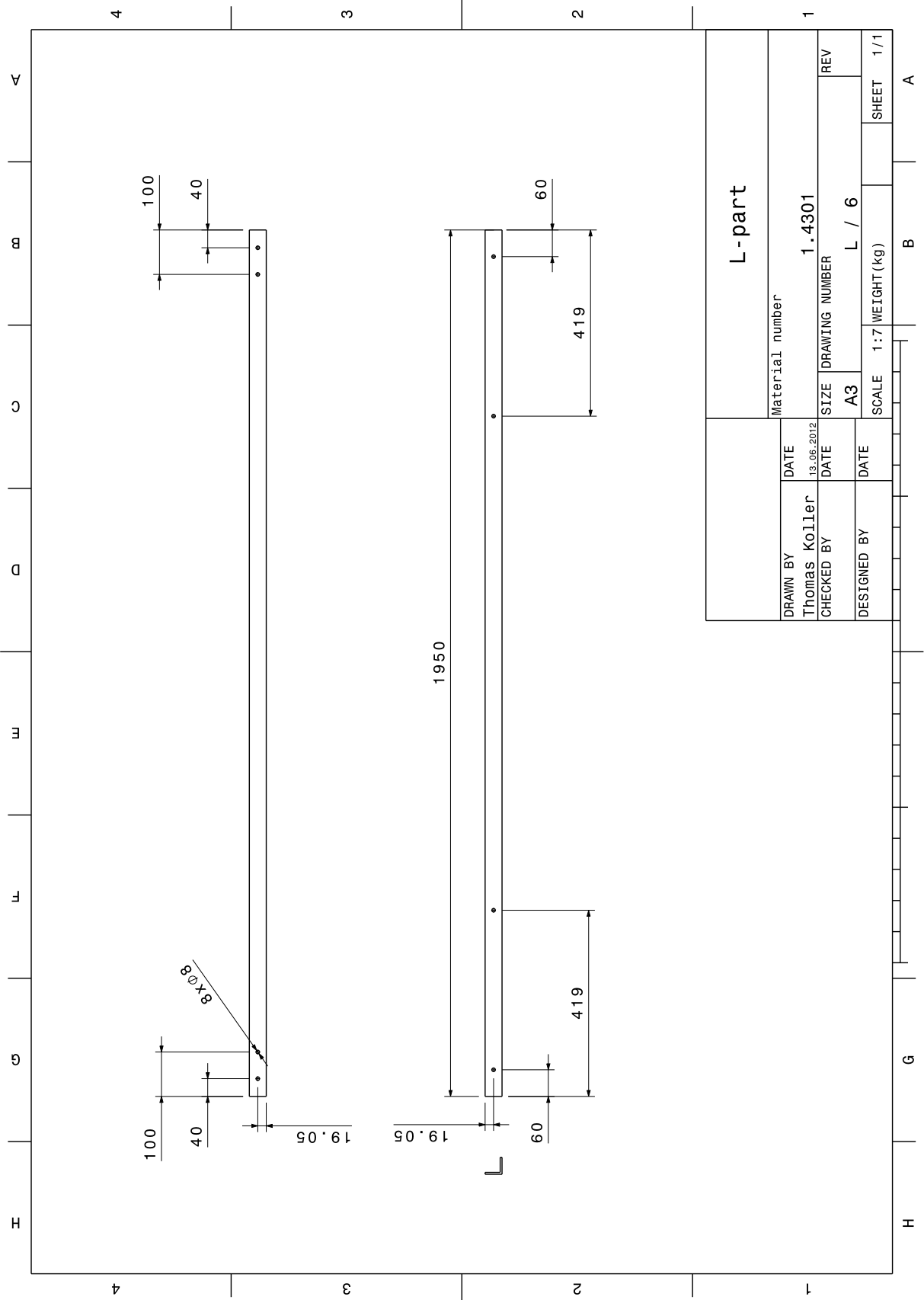




D.2 L-PARTS



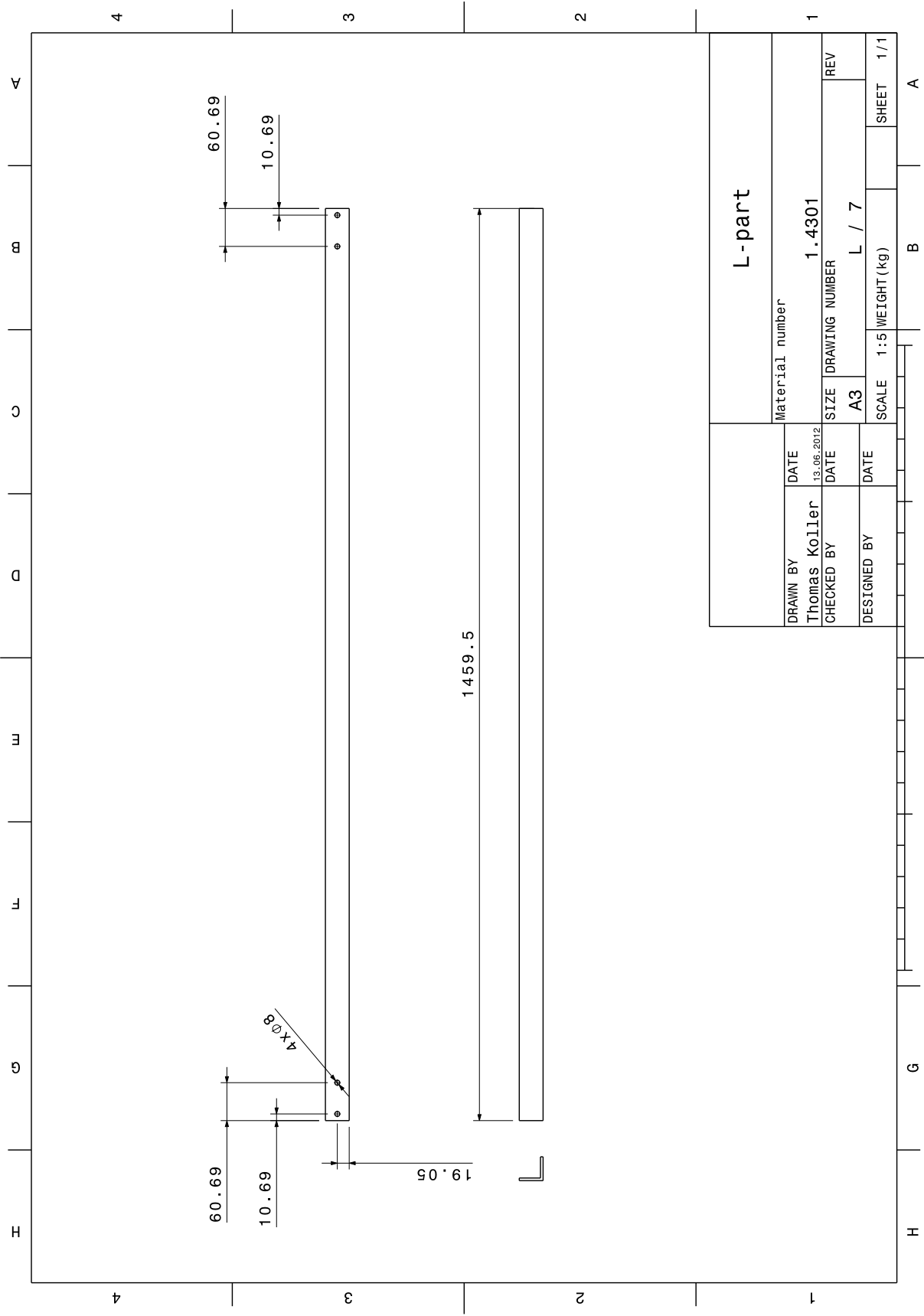
D.2 L-PARTS



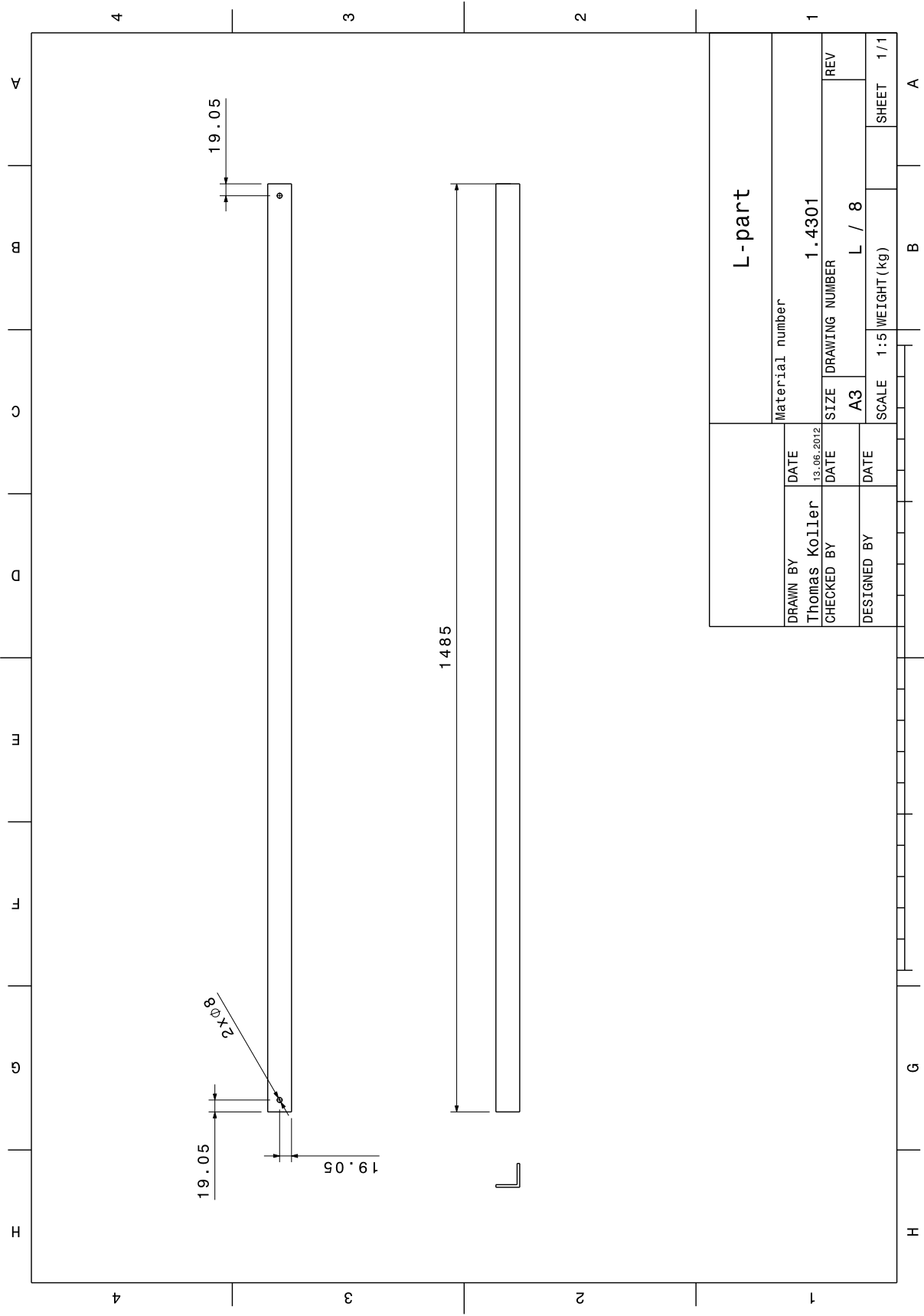
DRAWN BY Thomas Koller		DATE	Material number	
		13.06.2012	1.4301	
CHECKED BY		DATE	SIZE	DRAWING NUMBER
DESIGNED BY		DATE	A3	L / 6
SCALE			1:7	WEIGHT(kg)
SHEET			1/1	

L-part

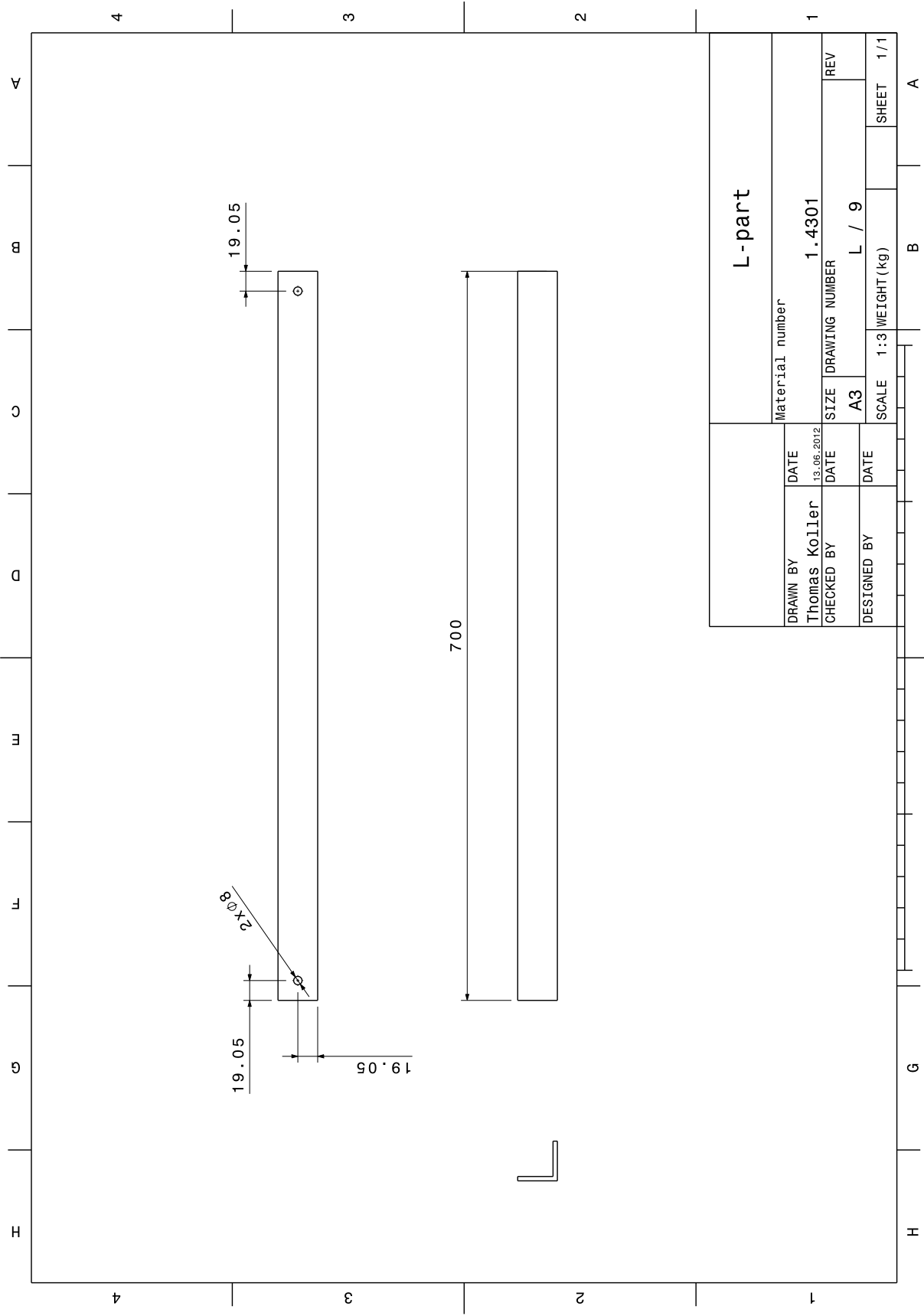
D.2 L-PARTS



D.2 L-PARTS



D.2 L-PARTS



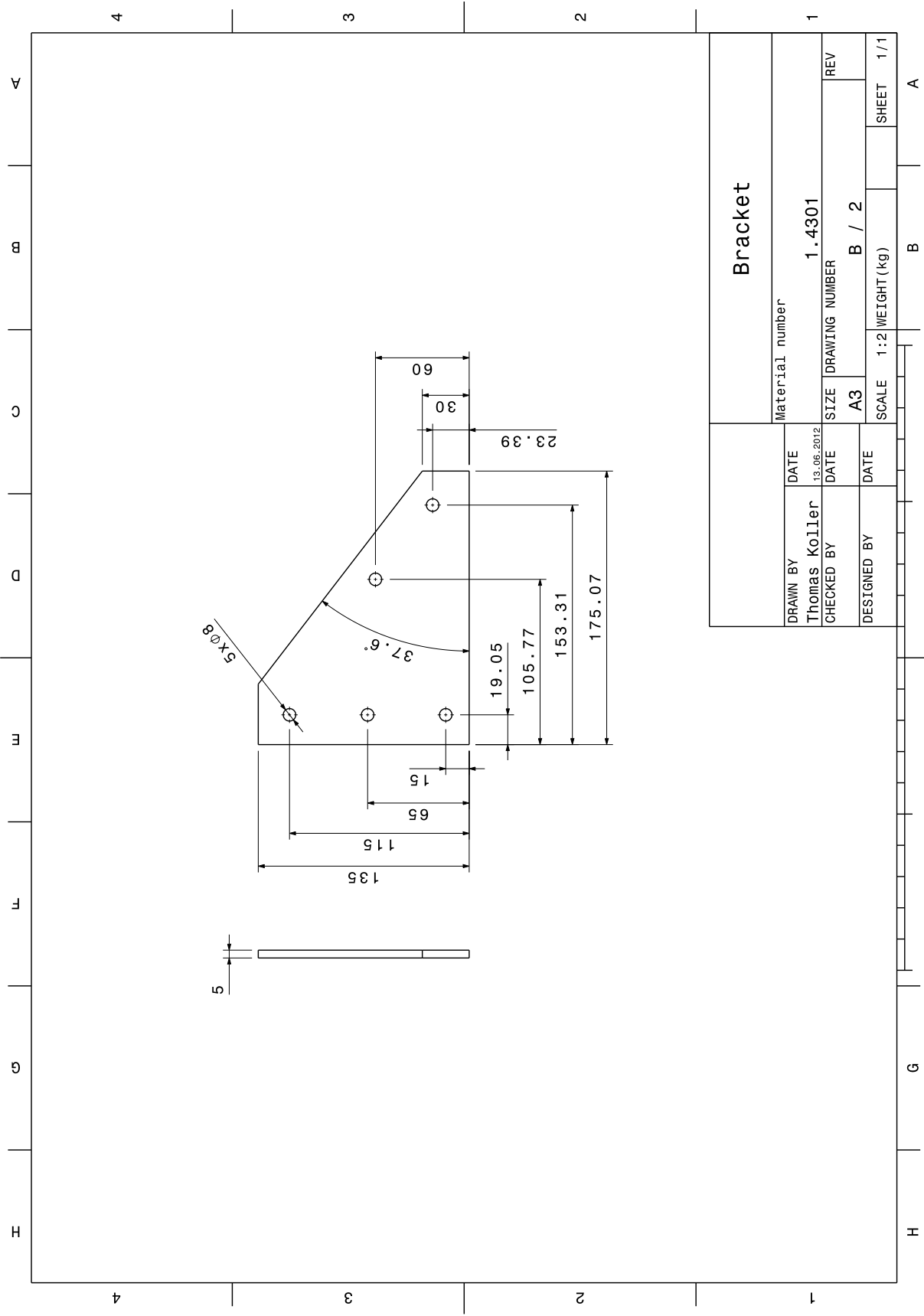
DRAWN BY Thomas Koller		DATE 13.06.2012	Material number 1.4301	
		CHECKED BY	DATE	SIZE A3
DESIGNED BY		DATE	DRAWING NUMBER L / 9	REV
SCALE 1:3			WEIGHT (kg)	SHEET 1/1

L-part

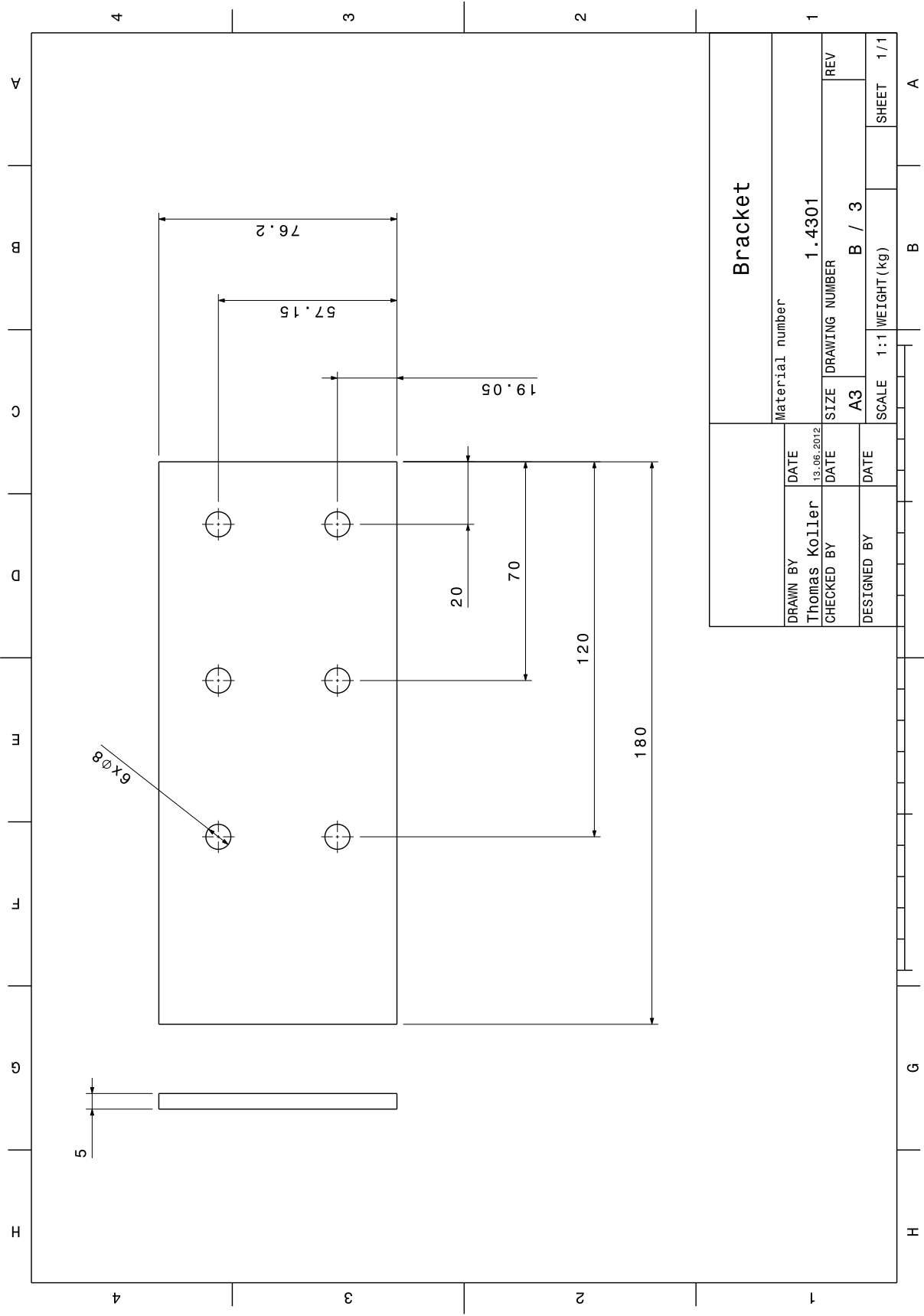
## **D.3 Brackets**



D.3 BRACKETS

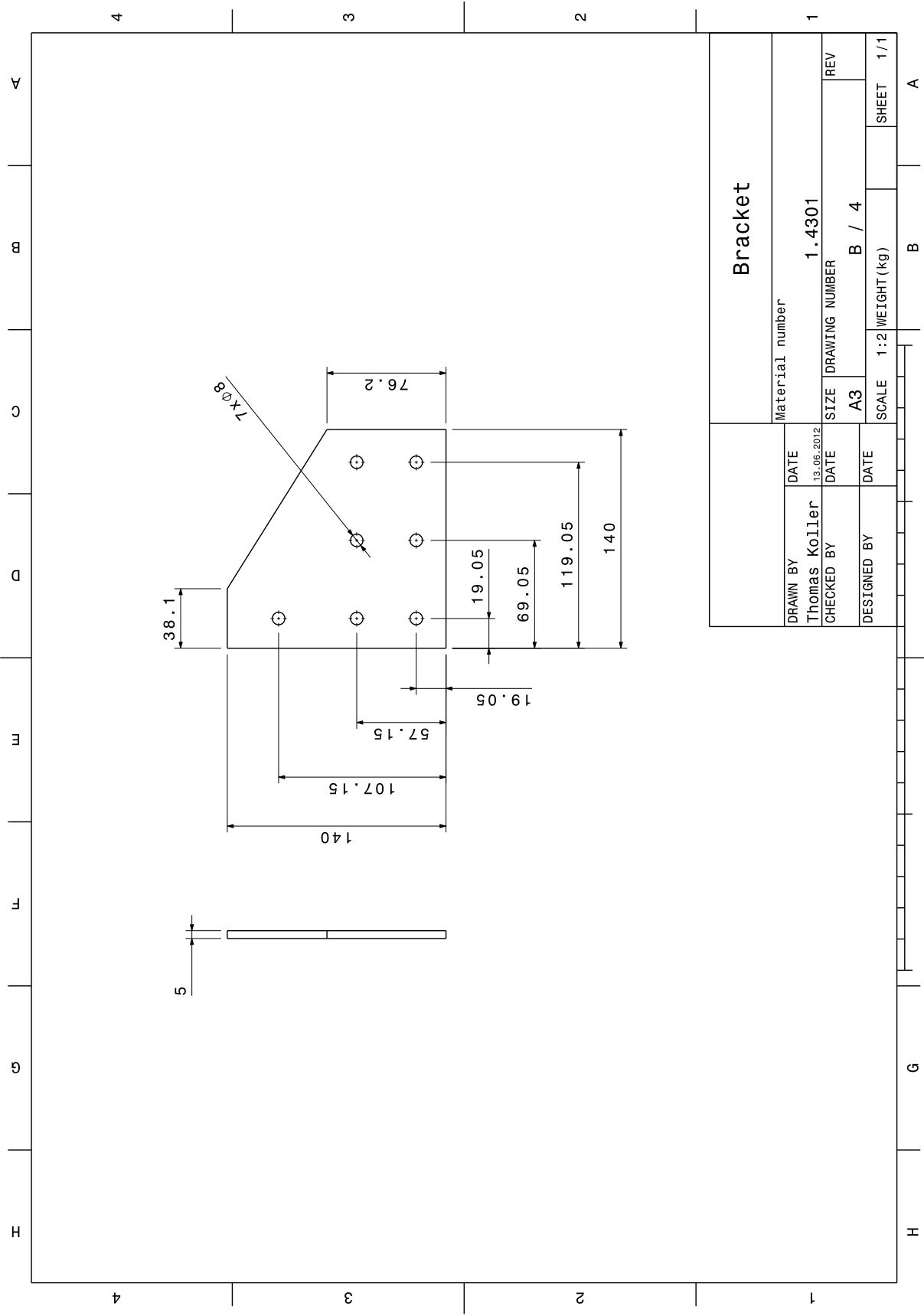


D.3 BRACKETS



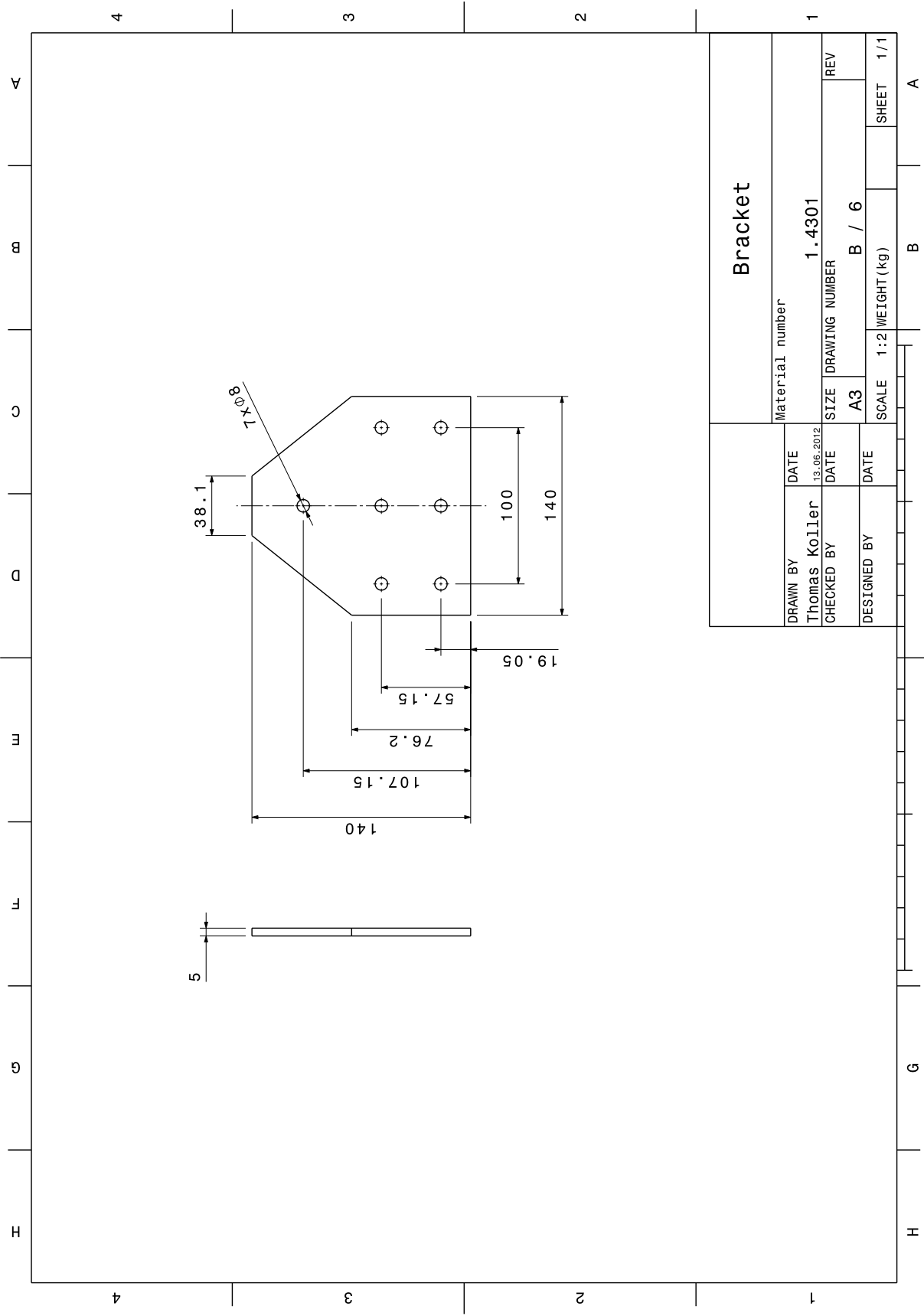
<b>Bracket</b>		Material number		1.4301	
DRAWN BY	DATE	SIZE	DRAWING NUMBER	REV	
Thomas Koller	13.06.2012	A3	B / 3		
CHECKED BY	DATE	SCALE	1:1	WEIGHT(kg)	SHEET 1/1
DESIGNED BY	DATE				

D.3 BRACKETS

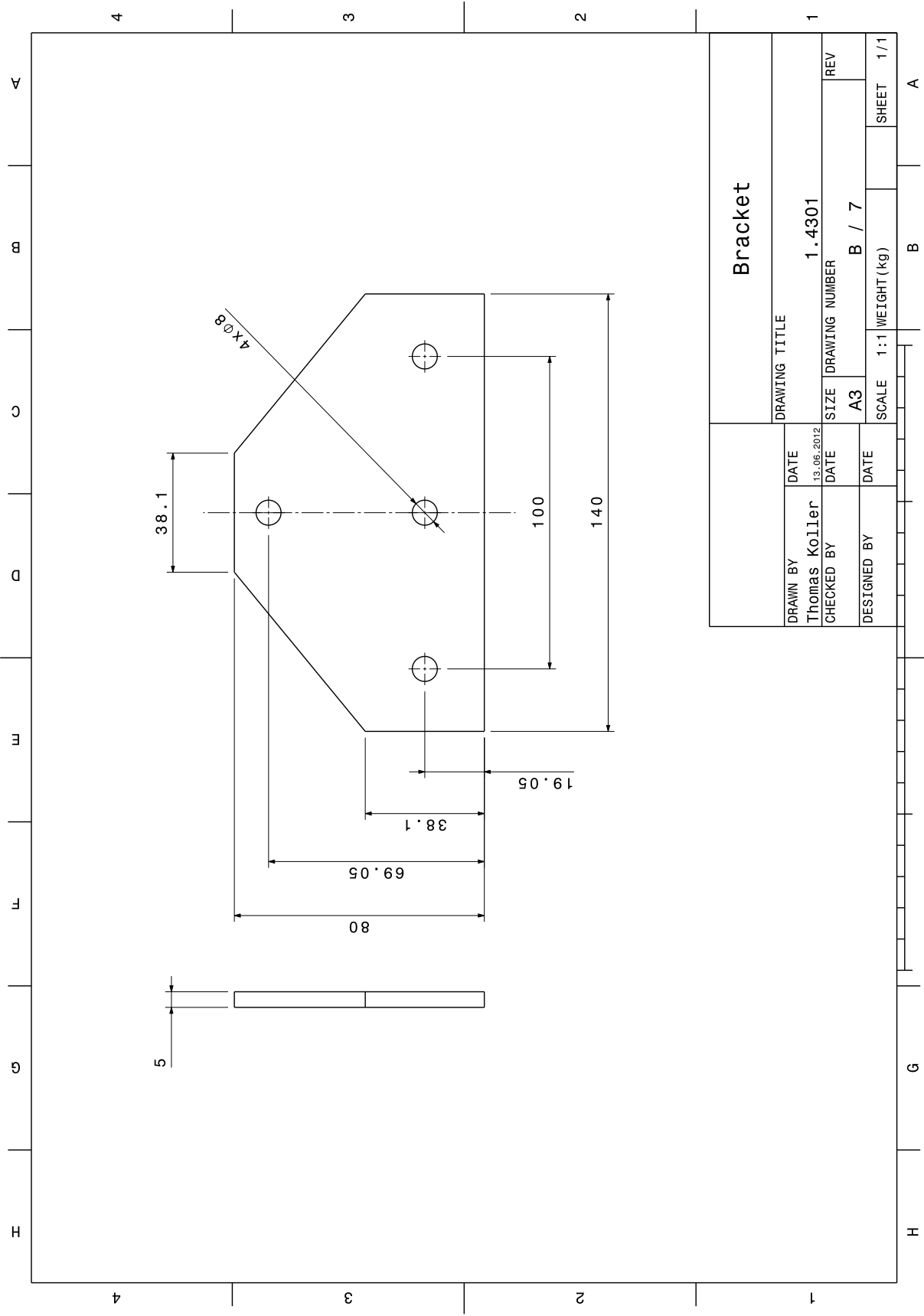




D.3 BRACKETS



D.3 BRACKETS





D.3 BRACKETS

